Vacuum ultraviolet laser spectroscopy of CO molecules in a supersonic jet

C.M. Steinmann

Dissertation presented for the degree of Doctor of Philosophy

at the University of Stellenbosch

Promoter: Dr. E.G. Rohwer, University of Stellenbosch

Co-promoter: Prof. H. Stafast, Friedrich-Schiller Universität, Jena, Germany

December 2003

Declaration

I, the undersigned, hereby declare that the work contained in this dissertation is my own original work and that I have not previously in its entirety or in part submitted it at any university for a degree.

Abstract

Vacuum ultraviolet laser spectroscopy of CO molecules in a supersonic jet

A tunable narrow-bandwidth laser source combined with a supersonic gas jet as sample is well-suited for obtaining high-resolution spectra of cold isolated molecules and complexes. In the present study such a laser source in the vacuum ultraviolet was applied to the spectroscopic investigation of rare carbon monoxide (CO) isotopomers and CO-noble gas van der Waals complexes in supersonic gas pulses seeded with natural CO gas.

Tunable coherent vacuum ultraviolet radiation was generated by two-photon resonant four-wave sum-frequency mixing of two pulsed dye laser beams in a magnesium vapour medium. Laser induced fluorescence excitation spectra of the A(v'=3)-X(v''=0) vibronic band of CO molecules in a noble gas (neon or argon) jet were obtained by measuring the total undispersed fluorescence from the irradiated sample volume in dependence of the excitation wavelength. The dynamics of the flow-cooling process in the supersonic jet were investigated and the experimental parameters optimised using the rotational temperature of $^{12}C^{16}O$ as determined from rotational line intensities. Rotational temperatures as low as 2 ± 1 K were observed.

Spectroscopic detection of the rare $^{12}C^{17}O$ and $^{12}C^{18}O$ isotopomers was facilitated by the low rotational temperature and high spectral resolution. Six rotational lines of $^{12}C^{17}O$ and four of $^{12}C^{18}O$ were detected in the A(v'=3)-X(v''=0) vibronic band. This demonstrates the low detection limit (circa 3 parts per million) obtained in the experiment. The line wavelengths were determined to an accuracy of 0.2 pm using the well-documented $^{12}C^{16}O$ and $^{13}C^{16}O$ lines for calibration. The spectral results on $^{12}C^{17}O$ are, to our knowledge, the first rotationally resolved laboratory measurements published on the A-X band of this isotopomer. Accurate wavelength data of the stable isotopomers of CO is of importance in the interpretation of astrophysical observations of CO in the interstellar medium. The newly determined $^{12}C^{17}O$ wavelengths were successfully applied to a recent problem in astrophysics (Astrophys. J. Lett. 2003).

The conditions in a supersonic jet facilitate the study of weakly bound van der Waals complexes, of which CO-noble gas complexes are prototypes. However, there is no experimental data available on the electronic excitation spectra of the CO-noble gas complexes, lying in the vacuum ultraviolet region. In the present experiment evidence of extensive complexation of the

CO in the noble gas jet has been found, but in the spectral region around the A(v'=3)-X(v''=0) band of CO no distinct spectral features that could be associated with these complexes were observed. Having considered the existing knowledge on CO and CO-noble gas complexes and experimental studies on the excitation and dissociation dynamics of I_2-noble gas complexes, we regard complex induced inter-system crossing or electronic predissociation as the most likely causes for these observations.

The results on the rare CO isotopomers demonstrate the potential of our experimental setup for high-resolution, isotope and state selective spectroscopy in the vacuum ultraviolet with a high sensitivity for fluorescent species. The availability of the now well-characterised experimental setup in our laboratory opens the way for further investigation of molecular or complex species with spectroscopic features in the vacuum ultraviolet region.

Samevatting

Vakuum ultraviolet laser spektroskopie van CO molekules in 'n supersoniese gasstraal

'n Afstembare smal bandwydte laserbron en 'n supersoniese gasstraal as monster is 'n geskikte kombinasie vir hoë-resolusie spektroskopie van geïsoleerde afgekoelde molekules en komplekse. In hierdie studie is so 'n laserbron in die vakuum ultraviolet gebruik in die spektroskopiese ondersoek van skaars koolstofmonoksied (CO) isotopomere en CO-edelgas van der Waals komplekse in supersoniese gaspulse wat 'n klein persentasie natuurlike CO gas bevat.

Afstembare koherente vakuum ultraviolet lig is verkry deur twee-foton resonante vier-golf som-frekwensie vermenging van twee gepulseerde kleurstoflaserbundels in 'n magnesiumdamp medium. Laser-geïnduseerde fluoressensie opwekkingspektra van die A(v'=3)-X(v''=0) vibroniese band van die CO molekules in die edelgasstraal (neon of argon) is uitgemeet deur die totale fluoressensie van die beligte gasmonster, sonder golflengteskeiding, te meet as funksie van die opwekkingsgolflengte. Die dinamika van die vloeiverkoelingsproses in die supersoniese gasstraal is ondersoek en die eksperimentele parameters geoptimeer deur gebruik te maak van die rotasionele temperatuur van $^{12}C^{16}O$ soos bepaal uit die intensiteitsverhoudings van die rotasielyne. Rotasionele temperature tot so laag as 2 ± 1 K is waargeneem.

Spektroskopiese waarneming van die skaars $^{12}C^{17}O$ and $^{12}C^{18}O$ isotopomere is moontlik gemaak deur die lae rotasionele temperatuur en die hoë spektrale resolusie. Ses rotasielyne van $^{12}C^{17}O$ en vier van $^{12}C^{18}O$ is waargeneem in die A(v'=3)-X(v''=0) vibroniese band. Dit demonstreer die lae deteksielimiet (ongeveer 3 dele per miljoen) wat bereik kon word. Die golflengtes van die lyne is bepaal met 'n akkuraatheid van 0.2 pm deur die bekende lyne van $^{12}C^{16}O$ en $^{13}C^{16}O$ vir kalibrasie te gebruik. Die resultate ten opsigte van $^{12}C^{17}O$ is sover vasgestel kon word die eerste rotasioneel-opgeloste laboratorium metings van die A-X band van hierdie isotopomeer. Akkurate golflengte data vir die stabiele CO isotopomere is van belang vir die interpretasie van die astrofisiese waarnemings van CO in die interstellêre medium. Die nuwe $^{12}C^{17}O$ golflengtes is suksesvol aangewend in die oplossing van 'n onlangse interpretasieprobleem in astrofisika (Astrophys. J. Lett. 2003).

Die toestande in 'n supersoniese gasstraal maak die bestudering van swak-gebonde van der Waals komplekse moontlik. Hoewel CO-edelgas van der Waals komplekse as prototipes beskou

word, is daar geen eksperimentele data beskikbaar oor die elektroniese opwekkingspektra van hierdie spesies, wat in die vakuum ultraviolet gebied lê, nie. In hierdie studie is daar eksperimentele getuienis gevind vir uitgebreide kompleksering van CO in die edelgasstraal, maar in die spektraalgebied rondom die A(v'=3)-X(v''=0) band van CO is geen duidelike spektrale kenmerke wat met hierdie komplekse geassosieer kan word, waargeneem nie. Na oorweging van die bestaande kennins oor CO en CO-edelgas komplekse en eksperimentele studies oor die opwekking en dissosiasie-dinamika van I_2-edelgas komplekse, beskou ons kompleksgeïnduseerde intersisteemoorgange of elektroniese predissosiasie as die waarskynlikste redes vir hierdie waarnemings.

Die resultate oor die skaars CO isotopomere toon die potensiaal van ons eksperimentele opstelling vir hoë-resolusie, isotoop- en toestandselektiewe spektroskopie in die vakuum ultraviolet met uitstekende sensitiwiteit vir fluoresserende spesies. Die beskikbaarheid van hierdie nou deeglik gekarakteriseerde eksperimentele opstelling in ons laboratorium maak verdere ondersoek na molekulêre of kompleks-spesies met spektroskopiese kenmerke in die vakuum ultraviolet moontlik.

Acknowledgements

The project presented here was supported by the National Laser Center and would not have been possible without this support. I am grateful to the National Research Foundation for support of my Ph.D. studies in the form of the Henry Dyer Memorial Scholarship. The Laser Research Institute received support from Defencetek during the last two years of this project.

I am sincerely grateful for the promoters I had for my Ph.D. studies. I thank Erich Rohwer for his help and support in so many ways over the six years of my post graduate studies. His initiative and efforts paved the way for this project and for successes still to come. I thank Herbert Stafast for the commitment with which he fulfilled his role as co-promoter amidst his many other responsibilities, and for numerous new ideas and insights.

My research visit to Jena, Germany during my Ph.D. studies was made possible by a travel grant of the Harry Crossley Foundation as well as a Stellenbosch Stipendium. I am grateful for the hospitality of Herta and Erich Glauche and assistance of the staff members of the Institut für Physikalische Hochtechnologie e.V. during my stay in Jena.

Other colleagues whose support was invaluable in the work are Ulli Deutschländer and Trevor Gordon who provided every kind of technical and administrative help needed, Danie Botha and later Marcello Bartolini in the electronics workshop and Mr. Gauernack and the rest of the staff in the mechanical workshop who helped with solutions for numerous mechanical problems. The development of the apparatus would not have been possible without the excellent service of Sparkwell manufacturing who found ways to realise my intricate designs.

Then there is a long list of people – the staff members and fellow students of the Physics Department, especially the members of the Laser Research Group – who contributed each in their own way to make the past four years a time of pleasant collaboration. I cannot name all, but I have to make an exception for Prof. Piet Walters who was always willing to offer advice and help from his extensive experience, Timo Stehmann who was helping me (and others) on a number of occasions in the midst of his own studies, and Anton du Plessis for sharing the laboratory and my enthusiasm.

Last, but perhaps most important, I thank my family and close friends for being there for me. I thank Gayle Loubser for her much appreciated help with the editing of this manuscript on short notice. A special word of thanks goes to my husband-to-be, Niki Steenkamp, and my parents, Dieter and Maretha Steinmann, whose support and care for me mean more to me than I can ever express. I thank God as Creator and Giver of all abilities.

The wonder of nature is that it functions perfectly,

irrespective of our ability to understand it.

Contents

Chapter 1

Introduction

1.1 Motivation

Carbon monoxide[1] is one of the molecules with the widest distribution in the universe. CO has particular significance in astronomy being the second most abundant molecular species (after H_2) in the interstellar space, stellar atmospheres and comet tails [1]. Whereas H_2 cannot be observed directly in radio astronomical observations, CO has dipole allowed spectra in the radio frequency, infrared ranges, as well as the vacuum ultraviolet range of modern satellite based spectrographs. This increases the importance of CO and its isotopomers as tracers to map the distribution of molecular matter in stellar, planetary and cometary atmospheres [2] and the internal structure of interstellar gas clouds ([3] as example). The distribution and ratios of the different isotopomeric species of CO are important parameters in models of stellar evolution and chemistry [4, 5]. On earth CO is a common and toxic waste product of the incomplete combustion of organic material, plays an important role in the reactions during combustion and occurs as impurity in many systems [6]. In atmospheric research CO isotopomers are used as parameters in atmospheric models [7] and the non-stable $^{14}C^{16}O$ serves as an important tracer in atmospheric chemistry [8].

CO has the additional advantages as prototype molecule that its electronic structure is

[1] Wherever the term "carbon monoxide" or "CO" without specification of the isotopic masses is used in this dissertation it refers the CO molecule in general implicitly including all its stable isotopomers, their order of relevance determined by their natural abundance. That means that the particular statement is probably the best known for the most abundant $^{12}C^{16}O$, but is also at least qualitatively applicable to the rarer isotopomers.

simple enough to be analysed by theoretical methods and CO gas can be obtained and handled easily in pure form for experimental studies. It is therefore not surprising that CO and its isotopic variants are some of the molecules most extensively studied by spectroscopic methods and most often employed as prototype molecules.

One of the fields of research where CO serves as an important prototype is in the study of van der Waals complexes containing diatomic molecules. The experimental and theoretical investigation of small van der Waals complexes has been an active research field in the last two decades, aimed at better understanding of the weak but fundamental van der Waals forces binding these complexes, as well as the process of cluster formation. In this field of research CO containing van der Waals complexes such as CO-Ar, CO-Ne, CO-He and CO-CO have been studied extensively. CO-Ar in particular is considered a prototype of the tri-atomic van der Waals complexes not containing He or H atoms [9].

The experimental data available on the isotopomers and van der Waals complexes of CO are extensive, but far from complete, as will be discussed in more detail in chapter 2. Regarding the isotopomers of CO, literature shows that, although the electronic excitation spectrum of $^{12}C^{16}O$ has been investigated extensively up to the high Rydberg levels, the spectroscopic data available on the other isotopomers of CO such as $^{13}C^{16}O$, $^{12}C^{18}O$ and especially $^{12}C^{17}O$ are more limited, as discussed in section 2.3. Regarding the van der Waals complexes there is a complete lack of experimental data on the electronic excitation spectra, as well as dissociation dynamics of CO containing van der Waals complexes, as discussed in section 2.4. In our opinion an experimental study that fully employs the advantages of the combination of high-resolution vacuum ultraviolet laser spectroscopy and extreme sample cooling in a supersonic jet could contribute new experimental data to both these fields of research.

In the present study a natural CO sample under conditions of extreme cooling in a free supersonic noble gas jet was investigated by high-resolution vacuum ultraviolet laser spectroscopy. The potential of our experimental setup results from the combination of a narrow bandwidth tunable vacuum ultraviolet laser source - facilitating high resolution, state selective, time resolved spectroscopy of a well defined sample volume - and a free supersonic noble gas jet optimised to deliver the sample gas at very low temperatures, subject to a controlled level of condensation and practically collisional free conditions at the point of observation.

The work documented here must be considered a pioneer project opening the way for further investigation in our laboratory of (i) the electronic excitation spectra of CO isotopomers such as $^{13}C^{16}O$, $^{12}C^{18}O$, $^{12}C^{17}O$ or others, (ii) the excitation spectra of CO van der Waals molecules and (iii) electronic excitation or ionisation spectroscopy of other scientifically and technologically relevant molecules and complexes.

Chapter 2

State of research

As background to the present study the relevant research on the different isotopomers of CO and CO-noble gas van der Waals complexes is outlined. Considering the aims of the present study the experimental methods are emphasised.

2.1 Basic spectroscopic properties of CO

Carbon monoxide has six stable isotopomers in nature. Their natural abundances on earth, as calculated from the isotopic abundances of carbon and oxygen from reference [10], are given in table 2.1. CO isotopomers containing the unstable ^{14}C isotope also occur in nature, but at concentrations of about 10^{13} times lower and are not considered in this study.

Table 2.1: Natural abundances of the stable CO isotopomers. The relative populations given as percentages are calculated from the natural isotopic ratios of carbon and oxygen on earth.

Isotopomer	**Natural abundance**$^{(a)}$ **(%)**	**Isotopomer**	**Natural abundance**$^{(a)}$ **(%)**
$^{12}C^{16}O$	98.668	$^{13}C^{16}O$	1.100
$^{12}C^{18}O$	1.979×10^{-1}	$^{13}C^{18}O$	2.207×10^{-3}
$^{12}C^{17}O$	3.79×10^{-2}	$^{13}C^{17}O$	4.224×10^{-4}

$^{(a)}$ Calculated from isotopic ratios from Handbook of Chemistry and Physics [10].

The spectroscopic properties of $^{12}C^{16}O$ have been characterised well. The molecule has a relatively high dissociation energy, given in the most recent review as 89592 cm^{-1} for $^{12}C^{16}O$ [11]. As a heteronuclear diatomic molecule, CO has a dipole allowed rotational spectrum in the radio frequency range, a rotation-vibrational spectrum in the infrared, as well as an electronic excitation spectrum of which a significant part (all excitations from the $X^1\Sigma^+$ ground state) lies in the vacuum ultraviolet.

The potential energy curves of most of the known electronic states of $^{12}C^{16}O$ are illustrated in figure 2-1, with the $A^1\Pi(v' = 3) - X^1\Sigma^+(v'' = 0)$ transition that was investigated in our experiment indicated by an arrow. The dissociation energy is indicated by a dotted line. The energies of the electronically excited states of CO relative to the $X^1\Sigma^+(v'' = 0)$ state lie in the vacuum ultraviolet region, from about 206 nm (48474 cm^{-1}) towards shorter wavelengths, although transitions between different electronically excited states such as the Ångstrom bands are found at longer wavelengths. The $A^1\Pi$ state that is of relevance in our experiment is the lowest singlet electronically excited state. It is strongly perturbed by the $a'^3\Sigma^+$, $e^3\Sigma^-$, $d^3\Delta_i$, $I^1\Sigma^-$, $a^3\Pi$ and $D^1\Delta$ states with which it overlaps. These perturbations have been studied in detail for $^{12}C^{16}O$ and for a few bands of $^{13}C^{16}O$ as reviewed by Morton and Noreau [11]. The difference in the perturbations to which $^{12}C^{16}O$ and $^{13}C^{16}O$ are subject respectively illustrates the inaccuracy of using $^{12}C^{16}O$ term values to calculate the term values of any other CO isotopomer.

The rotational and vibrational constants of the $X^1\Sigma^+$ ground state and the $A^1\Pi$ excited states of $^{12}C^{16}O$ used in this work have been taken from the comprehensive compilation of Huber and Herzberg [12]. The vibrational and rotational quantum numbers v and J will be used in the following discussions for all CO isotopomers, with the normal convention that v'' and J'' refer to the vibration and rotation of the lower electronic state whereas v' and J' refer to the upper electronic state in the excitation transition.

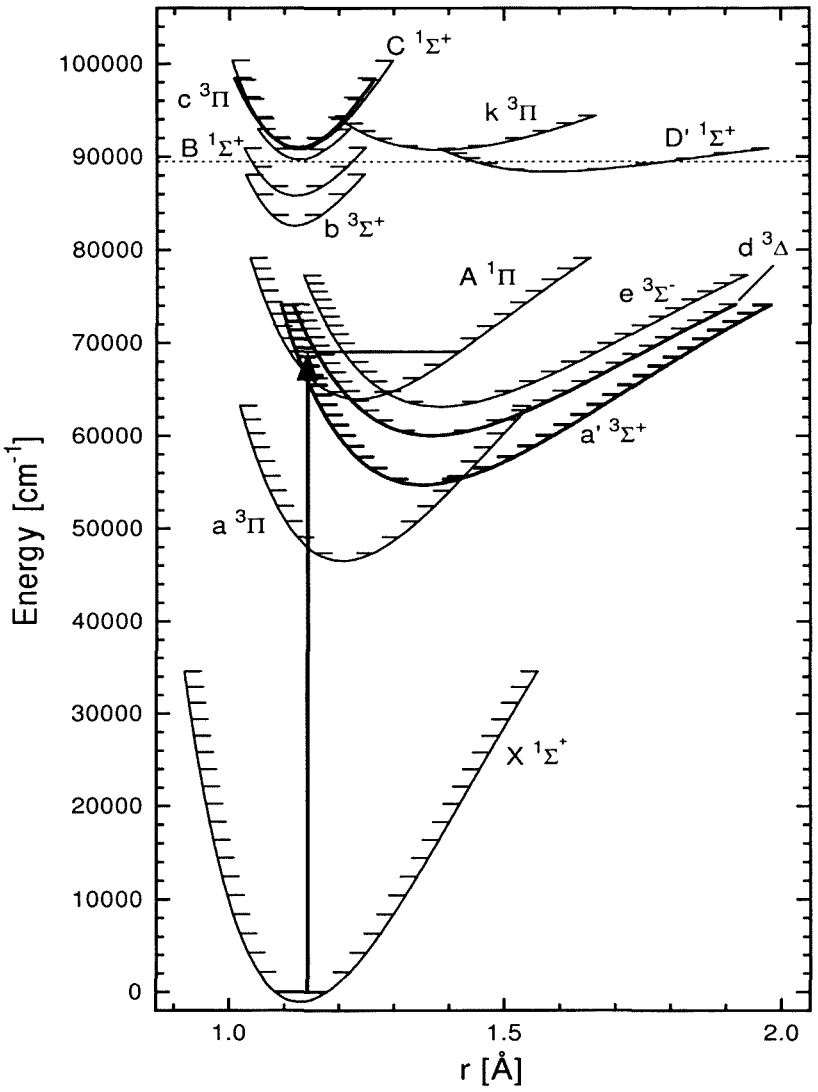

Figure 2-1: Potential energy curves of the electronic states of $^{12}C^{16}O$ up to the dissociation limit, calculated by the RKR procedure, taken from reference [13] with permission of the author. On the x-axis the internuclear C-O distance is plotted. The dotted horizontal line indicates the dissociation energy of CO. The electronic vibrational transition investigated experimentally in the present work is indicated by a vertical arrow.

2.2 Vacuum ultraviolet electronic excitation spectroscopy of $^{12}C^{16}O$

Spectroscopic study of the electronic excitation spectrum of carbon monoxide started in 1875 with the work of Ångstrom and Thalén on transitions in the visible region, followed by the first ultraviolet measurements by Deslandres in 1888 and Lyman shortly after 1900 [6]. The systematic study of the $^{12}C^{16}O$ vacuum ultraviolet spectrum by measuring absorption and emission of gas discharges started in about 1926. The mutual perturbations between the different electronically excited states of $^{12}C^{16}O$ encouraged intensive studies of both the dominant allowed bands as well as forbidden transitions [14].

Although spectroscopic detection of CO definitely has many important applications in environmental science as well as industry, the strongest motivation for the extensive and specialised spectroscopic study of CO, especially its electronic excitation spectrum, has been the astrophysical relevance of the molecule. The astrophysical importance of CO stimulated the laboratory investigation of the vacuum ultraviolet spectra of $^{12}C^{16}O$ and other CO isotopomers in two ways. Firstly, the rate at which interstellar CO molecules are photodissociated by cosmic vacuum ultraviolet radiation is one of the most crucial, but most uncertain parameters in the theoretical models of the gas clouds in the interstellar space [4]. Since it was established that the photodissociation process of CO does not take place by continuum absorption but dominantly via discrete excitations [15, 2] of high Rydberg levels of the molecule, the spectroscopic investigation of the highly excited electronic states of CO became a very active research field. Several groups have participated in extensive investigations of the Rydberg states of $^{12}C^{16}O$ [16, 17]. The properties of the Rydberg states below and above the dissociation limit of CO, as well as mutual perturbations between states that could influence the photodissociation lifetimes of these states, were studied in particular. Secondly, for the interpretation of the vacuum ultraviolet absorption spectra measured in space, accurate laboratory spectra of the relevant electronic transitions of all the different CO isotopomers, also the rare isotopomers, are needed. Such results are available for $^{12}C^{16}O$ as well as $^{13}C^{16}O$ and $^{12}C^{18}O$, but not yet for $^{12}C^{17}O$ as discussed further in section 2.3.

In addition to the continuing absorption and emission spectroscopy (with [18] and [19] as

examples of recent papers) a variety of specialised laser-based methods have been used in the investigation of the electronically excited states of $^{12}C^{16}O$. Optogalvanic spectroscopy (with visible lasers) was employed in the first observations of transitions between some of the highly excited Rydberg states [20, 21]. Different resonantly enhanced multi-photon excitation and ionisation methods have been applied [17, 22, 23, 24, 25, 26, 27]. The group of Vidal was among the first to do state selective laser spectroscopy by multi-step excitation of $^{12}C^{16}O$ using a narrow bandwidth coherent vacuum ultraviolet source based on the method of sum-frequency generation in a gaseous medium [16, 28, 29, 30]. Spectroscopy of $^{12}C^{16}O$ using this type of source has been extended to the extreme ultraviolet (XUV) region [31, 32]. Resonantly enhanced sum-frequency generation in CO gas has also been employed as a spectroscopic method [33, 34]. In our experimental work an experimental setup and coherent vacuum ultraviolet source similar to that of Vidal et al. [30] is used.

The CO samples in the above-mentioned laser based experiments have been stagnant low pressure CO gas or free supersonic expansions of pure CO gas or CO gas mixed with He. Supersonic expansions were used to obtain a high gas density in the sample volume and collision-free conditions for lifetime measurements. The flow-cooling effect was sometimes used to obtain a simplified molecular spectrum - lower temperature increasing the intensities of the low rotational lines and decreasing those of the high rotational lines - but no particular attempt was made to utilise or investigate the extreme cooling that can be obtained with a supersonic expansion. Drabbels et al. [22], using a CO-He jet in their experiment, mention that the low temperatures (about 4 K) in their supersonic expansion did facilitate the detection of lines of the rarer isotopomers of CO ($^{13}C^{16}O$ and $^{12}C^{18}O$) in natural abundance, indicating the potential of flow-cooling.

It is not within the scope of this discussion to give a complete review of the spectroscopic results that were obtained in the above-mentioned and other work on CO. Reviews of the spectroscopic data available on $^{12}C^{16}O$ have been compiled by Herzberg (1950) [35], Krupenie (1966) [6], Simmons et al. (1969) [14], Tilford and Simmons (1972) [36], Huber and Herzberg (1979) [12] and Morton (1994) [11].

2.3 Vacuum ultraviolet electronic excitation spectroscopy of rare CO isotopomers

In astrophysics the detection of different isotopomers of CO and the determination of their densities and density ratios are of great importance in the study of the interstellar medium [37]. The presence of all of the 6 stable isotopomers of CO in the interstellar medium has been confirmed by observation of radio frequency emission [4].

The vacuum ultraviolet absorption spectrum in the radiation from distant light sources is the best method to obtain quantitative column densities of CO isotopomers in the interstellar space along a specific line of sight [18]. Using the spectroscopic results of the less abundant isotopomers of CO, saturation of the absorption lines can be avoided, resulting in more accurate density values. Even more important than determining absolute densities are the observed ratios of the different isotopomeric column densities and their deviation from the ambient interstellar isotopic ratios [4]. This deviation of the CO isotopomer ratios, termed isotopic fractionation [4], yields important parameters in the theoretical models of the physical and chemical evolution of the interstellar gas clouds, and even the stellar evolution in the galactic region under observation [11].

Of relevance to our work is the extent to which the rotationally resolved vacuum ultraviolet spectra of the stable CO isotopomers, in particular their astrophysically important $A^1\Pi(v') - X^1\Sigma^+(v'' = 0)$ progressions, have been recorded both in the interstellar space and in the laboratory.

The vacuum ultraviolet absorption spectra of interstellar $^{12}C^{16}O$ and $^{13}C^{16}O$ were first observed as low resolution spectra in 1971 by Smith and Stecher [38]. The Goddard system on the Hubble Space Telescope facilitated the measurement of the first rotationally resolved vacuum ultraviolet absorption spectra of interstellar CO - the $A^1\Pi(v' = 2, 3) - X^1\Sigma^+(v'' = 0)$ bands of $^{12}C^{16}O$ by Smith et al. [39] in 1991 and the $A^1\Pi(v' = 5, 6) - X^1\Sigma^+(v'' = 0)$ bands of $^{13}C^{16}O$ by Sheffer et al. [40] in 1992. Rotationally resolved bands ($A^1\Pi(v' = 2-5) - X^1\Sigma^+(v'' = 0)$) of $^{12}C^{18}O$ and $^{12}C^{17}O$ have been observed and studied by Sheffer et al. in 2002 [4]. However, the observation of the vacuum ultraviolet absorption spectra of the two least abundant isotopomers, $^{13}C^{18}O$ and $^{13}C^{17}O$, was not possible with the Goddard system's sensitivity limits according to

Morton [11].

Proper interpretation of the observed interstellar vacuum ultraviolet spectra of the CO isotopomers requires accurate laboratory measurements of the wavelengths (as well as oscillator strengths) of the relevant spectral lines. The laboratory wavelength data are necessary to calculate the Doppler shift of the interstellar lines and subsequently the mean velocity of the gas cloud relative to the observer. In contrast to the extensive vacuum ultraviolet spectroscopy done on $^{12}C^{16}O$ there has not been the same systematic investigation of the spectra of the other isotopomers. In particular laboratory data for the $A^1\Pi(v') - X^1\Sigma^+(v'' = 0)$ transitions that have been observed in space are not available yet for all isotopomers of CO. Morton et al. [11] reported in 1994 the lack of rotationally resolved laboratory measured data on a number of astrophysically important transitions of the rarer CO isotopomers. They expressed a particular need for accurate rotationally resolved data on the $A^1\Pi(v' = 0 - 9) - X^1\Sigma^+(v'' = 0)$ vibronic bands of $^{12}C^{18}O$ and the $A^1\Pi(v' = 0 - 7) - X^1\Sigma^+(v'' = 0)$ vibronic bands of $^{12}C^{17}O$. Beaty et al. [41] measured and published the lacking data of the $^{12}C^{18}O$ spectrum in 1997, but in 2002 when Sheffer et al. [4] reported the first interstellar vacuum ultraviolet observation of $^{12}C^{17}O$, the above mentioned data of this isotopomeric species were still not available.

Emission and absorption spectroscopy of ^{13}C and ^{18}O isotopically enriched samples have been the dominant methods used in the investigation of the rarer isotopomers of CO. A hollow cathode lamp filled with isotopically enriched CO samples [42, 43, 44], CO in a discharge lamp [45, 46], as well as an isotopically enriched CO_2-Ar supersonic jet with an electric discharge generating CO [41, 47, 48] have been used for emission spectroscopy of $^{13}C^{16}O$, $^{12}C^{18}O$ and $^{13}C^{18}O$. Absorption spectroscopy of the same species has been done using cyclotron radiation [18], plasma sources [45, 49, 50] and a microwave excited Xe lamp [46] as radiation sources and stagnant isotopically enriched CO gas as sample.

The work of Ubachs, Velchev and Cacciani [51] illustrates the power of high resolution laser spectroscopy (resonantly enhanced multiphoton ionisation) in combination with a flow-cooled sample in a supersonic jet: the chosen $E^1\Pi(v' = 1) - X^1\Sigma^+(v'' = 0)$ vibronic band could be detected and analysed for all six isotopomers using natural CO as well as a ^{13}C enriched sample.

2.4 Spectroscopic and theoretical studies of CO-noble gas van der Waals complexes

Van der Waals complexes have received increasing attention in the last decade. Van der Waals forces are weak intermolecular interactions, but play a fundamental role in chemical and physical processes such as the solvation and folding of large biological molecules, adsorption processes and liquid-gas phase transitions. High resolution spectroscopic studies of weakly bound van der Waals complexes provide the most direct source of information on the intermolecular van der Waals force [52]. Small van der Waals complexes are also studied as the first step towards cluster formation - a research field receiving increased interest [53]. The study of intermolecular van der Waals forces by investigation of van der Waals complexes involves specialised and challenging work in both the fields of experimental spectroscopy and theoretical modeling. The renewed interest and progress in van der Waals molecules in recent years is due both to progress in the experimental techniques of laser spectroscopy and molecular beams and to the increase in computational capacity available for theoretical modeling [54].

CO-noble gas van der Waals complexes serve as important prototypes for the study of weakly bound tri-atomic (diatomic molecule bound to an atom) van der Waals complexes [55]. The CO-noble gas van der Waals complexes CO-He, CO-Ne, CO-Ar, CO-Kr and CO-Xe can be studied as a series of which the binding energy as well as the limitation on the hindered internal rotation of the CO increases with increasing mass and therefore increasing polarisability of the noble gas atom. Of these complexes CO-Ar (referring to its electronic ground state) has been studied most extensively both by experiment and in theoretical work [9].

The electronic ground states of the CO-noble gas species listed above have been characterised to different extents by spectroscopy in the infrared, microwave, mm and sub-mm spectral regions. These are complemented by theoretical studies searching for increasingly accurate potential energy curves, which describe the intermolecular interaction in the ground state. Brookes et al. [55] give an overview of the work on the different CO-noble gas complexes up to 1999 and could be consulted for detail and more references. The CO-noble gas complexes all have essentially T-shaped equilibrium geometries and rotational spectra that are determined by the hindered internal rotation of the CO subunit [55]. In the last decade a large experimental

as well as theoretical effort was made with the aim to characterise all bound vibrational and rotational states of CO-Ar (see Toczylowski et al. [56] and Brookes et al. [55] and their references). The experimental work included spectroscopy in the infrared [9, 57], mm and sub-mm spectral regions [58, 59, 60, 61]. The theoretical effort involved the development of ab initio potential surfaces in order to model the chaotic behaviour of the high energy rotation levels of the semi-rigid system [55]. The papers of Jansen et al. [62], Toczylowski et al. [56], Gianturco et al. [63] and Pedersen et al. [64] represent the most recent theoretical understanding of the CO-Ar molecule. For CO-He all of the 14 bound levels have been studied by infrared spectroscopy and theoretical calculations of which McKellar et al. [65] gives an overview. For CO-Ne the spectroscopic data, although not complete, include results from infrared [66, 67], microwave [68, 69], as well as millimeter wave spectroscopy [70], from which potential energy curves could be constructed [71, 72]. CO-Kr and CO-Xe are the least studied of the CO-noble gas complexes. Brookes et al. [55] and Walker et al. [73] provide a description of the limited spectroscopic results on CO-Kr and CO-Xe. Apparently no purely theoretical papers have been published on CO-Kr and CO-Xe. From these studies important information could be obtained on suitable experimental conditions for the formation of CO-noble gas van der Waals complexes. CO-Ar has been studied both in low temperature gas cells as well as in continuous and pulsed supersonic gas expansions under a variety of expansion conditions. The conditions reported in the literature compared to our experimental conditions will be discussed in section 6.3.

The same research groups doing spectroscopic studies on CO-noble gas complexes are usually also involved in investigations of the CO-CO dimer [74, 75, 76]. The reason is that the CO dimer can be studied with the same experimental setup under similar experimental conditions as the CO-noble gas complexes.

A detailed understanding of the electronic ground state of the prototype complex, CO-Ar, has been obtained by spectroscopic investigations accompanied by theoretical studies. The theoretical calculations of Toczylowski et al. [56] represent the most accurate two-dimensional potential energy surface of CO, those of Gianturco et al. [63] the first calculations where the dependence on the vibrational coordinate of the CO subunit is included, and the work of Pedersen et al. [64] the first three-dimensional potential energy surface. The most important geometric and spectroscopic constants for the CO(X)-Ar ground state, resulting from recent

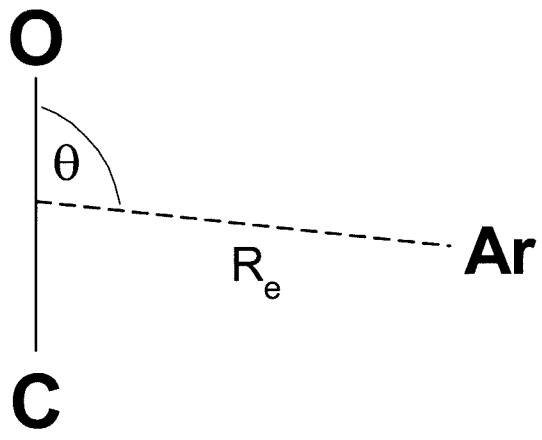

Figure 2-2: Schematic illustration of the CO-Ar van der Waals complex. The angle θ is measured with respect to the centre of mass of the CO molecule. The bond lengths of the C-O molecular bond and the CO-Ar van der Waals bond are not drawn to scale.

work, are given in table 2.2. The labeling of the quantum numbers in table 2.2 and further discussions are done according to Xu and McKellar [9]. For the complete quantum mechanical description of the CO-Ar van der Waals complex a full set of quantum numbers is needed, the nature of which depends on whether a semirigid molecule or a free internal rotor approach is followed as discussed by Xu and McKellar [9]. In the present work only the different vibrational quantum numbers in the complex need to be distinguished. As the symbol v is already used for the quantum number of the stretching vibration of the molecular CO, the symbol v_2 will be used for the bending vibration and v_3 for the stretching vibration of the van der Waals bond, as in table 2.2. In the geometry of the CO-Ar van der Waals complex, the symbol R_{CO-Ar} will be used for the length of the van der Waals bond in general and R_e more specifically for the equilibrium length of the van der Waals bond. Θ is used for the angle between the van der Waals bond and the molecular axis of the CO molecule. Θ is chosen in such a way that $\Theta = 180°$ denotes the linear Ar-CO geometry and $\Theta = 0°$ the linear Ar-OC geometry, as illustrated in figure 2-2.

In contrast to extensive studies of the ground states of the CO-noble gas van der Waals complexes, especially CO-Ar, no experimental data are available on the electronic excitation of

Table 2.2: Geometric and spectroscopic constants of the CO(X)-Ar ground state and some predicted values for the CO(A)-Ar electronic state of the CO-Ar complex.

$\mathbf{D_e}$ $\mathbf{(cm^{-1})}$	$\mathbf{R_e}$ **(Å)**	Θ (degrees)	v_2 $\mathbf{(cm^{-1})}$	v_3 $\mathbf{(cm^{-1})}$	Reference
			$CO(X^1\Sigma^+)$-Ar		
103.0	3.721	93 [a]	...	31.6	[81], ab initio
98.6	3.82	99	11.894	18.175	[56], ab initio
105	3.73	93	11.712 [b]	18.823 [b]	[63], ab initio
102	3.72	93	11.729 [b]	18.004 [b]	[64], ab initio
104.68	3.714	92.88	12.014	18.110	[60], experimental
			$CO(A^1\Pi)$-Ar		
115.5	3.65	93 [a]	...	34.4 [c]	[81], ab initio

[a] This value of Θ was a fixed input value for the calculation.
[b] These values are calculated for $CO(X, v'' = 0)$-Ar. The values calculated for $v'' = 1$ differ slightly.
[c] This value was calculated assuming that the CO bond length in the $CO(A^1\Pi)$-Ar complex is the same as in the ground state.

any of the CO-noble gas van der Waals species. Electronic excitation of a CO-noble gas complex generally refers to a transition in which the CO subunit of the complex makes a transition to an excited electronic state while the noble gas atom remains in its ground state.

Although numerous spectroscopic studies of the electronic excitation spectrum of $^{12}C^{16}O$ have been published - including measurements in supersonic noble gas expansions where CO–noble gas van der Waals complexes were likely to be present - no experimental observation of any electronic excitation lines of any CO-noble gas complex have been reported to my knowledge. The only reports published to my knowledge on the electronic excitation spectrum of a CO-noble gas van der Waals complex are two theoretical test studies on the use of ab initio methods to calculate the electronic excitation spectra of CO-He that have been published by Salazar and Hernández [77, 78]. Their method on CO-He involves ab initio calculations (using Møller-Plesset perturbation theory including perturbations to all orders) of the potential energy curves of the ground as well as excited states of CO-He as a function of the van der Waals bond length. From these potential energy curves dissociation energies and the energies of the vibrational levels can be predicted. They reported a lack of experimental data to compare with the theoretical results on the excited state [77].

On learning of our attempt to obtain experimental measurements of the electronic excitation spectrum for CO-Ar, Salazar and Hernández initiated ab initio modeling of CO-Ar similar to their work on CO-He [79]. Initial results were obtained using second order Møller-Plesset perturbation theory to calculate the interaction energies [80]. The most recent results were obtained using the CCSD(T)[1] correlation method [81]. Potential energy surfaces as function of the van der Waals bond distance were obtained for both the ground state and the lowest singlet excited state, assuming fixed values for the angle Θ and the C-O bond length in the calculation of each potential energy surface. In the calculations done up to date the potential energy surface of the excited $CO(A, v = 3)$-Ar complex was calculated by using the C-O bond length of the ground state $CO(X, v'' = 0)$ molecule and also the angle Θ as determined for the ground state complex. These assumptions limit the accuracy of the results of the calculations. Some numerical values from the results of Salazar and Hernández [81] that are relevant to the

[1] CCSD(T) refers to Coupled-Cluster theory with iterative treatment of single and double excitations and non-iterative treatment of triple excitations.

further discussion are reproduced with their permission in table 2.2, in comparison with the data of higher correlated calculations of Toczylowski et al. [56], Gianturco et al. [63] and experimental data of Hepp et al. [60] in the case of the ground state. The equilibrium well depth D_e and bond length R_e of the ground state CO-Ar complex calculated by Salazar and Hernández correspond well with the higher correlated calculations of Gianturco et al. [63], but the ground state vibrational constant v_3 predicted by Salazar and Hernández differs significantly from the experimental values and other theoretical values. For the excited $CO(A, v' = 3)$-Ar state we currently consider the predicted values of D_e and R_e of Salazar and Hernández [81] to be reasonably accurate, but the predicted values for the vibrational constant v_3 to be only an upper limit.

Chapter 3

Physical principles of applied methods

In this chapter the three main physical processes applied in the experimental work are discussed. An understanding of the physical principles is crucial to understand the behaviour of the processes and to optimise the experimental conditions for each of these processes.

3.1 Cooling and condensation in a supersonic jet

The advantages of a supersonic jet were first recognised in 1951 by Kantrowitz and Grey [82]. Since the 1960s the method developed rapidly and was increasingly applied to facilitate spectroscopy of isolated cold molecules [83]. Supersonic jets offer uniquely favourable conditions for the study of single molecules as well as weakly bound complexes: low translational temperatures combined with collision-free conditions (no matrix effects), as well as a relatively high sample density. The non-equilibrium conditions in the jet, that cause the cooling of the internal degrees of freedom and especially the condensation of the gas to lag behind the translational temperature, can be very useful in experiments.

A pulsed[1] free gas jet consists of a gas reservoir containing gas at a certain stagnation

[1]Models of the conditions in supersonic jets, including the mathematical relations in the discussion below, generally refer to continuous jets. The conditions in a pulsed jet, as used in our experiment, can be described by the same models as long as the gas pulse period is long relative to the time needed for the jet flow to develop fully [84].

pressure, a pulsed valve allowing gas to expand into a low pressure volume, and adequate pumping capacity to maintain the pressure difference. No skimmers or other means to influence the beam path after the valve orifice are used. A supersonic jet develops, contrary to an effusive molecular beam, if the mean free path length of the gas in the reservoir is much smaller than the size of the orifice. In this case the flow through the orifice and for some distance downstream of the orifice is hydrodynamic flow [85]. In this part of the expansion, by means of collisions, the enthalpy of the random motion of the gas particles in the reservoir is converted into directed mass flow. As a result the mean mass flow velocity u increases while the velocity distribution of the gas particles narrows significantly, causing the translational temperature T_{tr} to decrease, the speed of sound a in the gas to decrease and the Mach number $M_a = a/u$ to increase from $M_a = 1$ at the narrowest point of the nozzle to supersonic values $M_a > 1$ as expansion progresses. The maximum mass flow velocity reached in the jet (at infinite Mach number) is limited by the finite amount of random energy contained in the stagnant gas prior to expansion and is given by $\sqrt{\frac{5}{3}}u_p$ where u_p is the most probable speed of particles in the stagnant gas. The mass flow velocity approaches this maximum value (asymptotically) relatively early in the jet at a Mach number of about 4 [86], after which it remains practically constant while the density of the gas and temperature continue to decrease, resulting in a decrease in the local speed of sound and increase in M_a. For positions further than 4 nozzle diameters from the nozzle along the jet axis the dependence of M_a on distance is approximated by the expression[2] [87]

$$M_a = A\left(\frac{X}{D}\right)^{(\gamma-1)} \tag{3.1}$$

where X is the axial distance from the nozzle, D the nozzle diameter, γ the ratio of heat capacities C_p/C_v of the expanding gas and A is a constant depending on γ. The local temperature, the pressure and the density in the beam also change, being related[3] to the changing Mach

[2] This expression holds under the condition that the flowing gas in the hydrodynamic flow zone can be treated as a continuous medium.

[3] The assumptions in deriving this relation are that the conditions of adiabatic reversible flow holds and the expansion is isentropic.

Table 3.1: Physical gas properties of carbon monoxide, argon and neon.

Property [a]	**Carbon Monoxide** $T_{ref} = 193\ K$	**Argon** $T_{ref} = 180\ K$	**Neon** $T_{ref} = 21\ ^{\circ}C$
C_P (kJ/kmol) at T_{ref}, 1.013 bar	7.01	20.99	~21 [b]
C_V (kJ/mol) at T_{ref}, 1.013 bar	5.01	12.52	~12 [b]
γ at T_{ref}, 1.013 bar	1.40	1.68	1.65 [b]
T_{boil} (K) at 1.013 bar	81.60	87.27	27.09
Δ_{vap} (kJ/mol) at T_{boil},1.013 bar	6.05	6.519	1.84

[a] All data in this table were obtained from reference [88] except for the specific heat capacities of neon indicated by the superscript [b]. Of the available data lowest temperature data were selected.
[b] Values obtained from website of Airliquide (21 May 2003), reference [89].

number by [85, p. 141]

$$\frac{T_{tr}}{T_{tr0}} = \left(\frac{P}{P_0}\right)^{(\gamma-1)/\gamma} = \left(\frac{\rho}{\rho_0}\right)^{(\gamma-1)} = \frac{1}{1+\frac{1}{2}(\gamma-1)M_a^2} \tag{3.2}$$

where T_{tr0}, P_0, ρ_0 and T_{tr}, P, ρ are the translational temperature, pressure and density of the gas in the reservoir and in the expansion, respectively.

In flow cooling experiments, as in the present experiment, monatomic gases are usually chosen as carrier gases since these gases only have translational energy and do not store extra energy in internal degrees of freedom. For monatomic gases $\gamma \approx \frac{5}{3}$ and $A \approx 3.26$ in the equations above. Empirical values of γ, as well as other gas properties, for the gases used in the present experiment are given in table 3.1.

The cooling process in a monatomic gas supersonic expansion, that is the result of collisions, cannot continue infinitely. With increasing distance from the orifice the density of the gas decreases and the flow becomes increasingly directed. Therefore the number of collisions per time interval decreases rapidly until the expansion can be regarded as free molecular flow. Under this condition the Mach number, as well as temperatures associated with all degrees of freedom, are "frozen" [90], although the density continues to decrease with the square of the

distance[4]. The terminal Mach number according to the calculations of Anderson and Fenn [86] is given by equation 3.3[5] in terms of the mean free path length of the gas particles in the stagnant gas λ_0 and an empirical parameter termed the collisional effectiveness constant ϵ.[6]

$$\begin{aligned} M_{aT} &= 2.05\epsilon^{(\gamma-1)/\gamma}\left(\frac{D}{\lambda_0}\right)^{(\gamma-1)/\gamma} \\ &= 133\,(P_0 D)^{0.4} \quad \text{(for argon gas with } P_0 \text{ in bar and } D \text{ in cm)} \end{aligned} \tag{3.3}$$

Combining equations 3.3 and 3.2 a relation between the stagnation pressure P_0 and the terminal temperature T_T reached in the jet is obtained:

$$\frac{T_0}{T_T} = 1 + \frac{1}{2}(\gamma - 1)\,\alpha^2\,(P_0 D)^{2(\gamma-1)/\gamma} \tag{3.4}$$

where α is a parameter depending on the collisional effectiveness ϵ and the collisional diameter σ of the gas ($\sigma = 3.67 \times 10^{-8}$ cm for argon). For any noble gas the exponent $2\,(\gamma - 1)\,/\gamma$ is equal to 0.8 and for argon gas with P_0 in bar and D in cm the relation [91] reduces to

$$\frac{T_0}{T_T} = 1 + 5896\,(P_0 D)^{0.8}\,.$$

The condition of free molecular flow in an undisturbed free supersonic expansion in theory continues up to the Mach disk. The position of the Mach disk depends on the background pressure P_B in the vacuum chamber into which the gas expands, and can be calculated for most gases by the expression 3.5 [87] where X_M is the distance from the nozzle to the Mach disk and D the nozzle diameter, and P_0/P_B is within the limits $15 \leq P_0/P_B \leq 17000$.

$$\frac{X_M}{D} = 0.67\left(\frac{P_0}{P_B}\right)^{0.5} \tag{3.5}$$

In an experimental setup, care should be taken to ensure that the free molecular flow part of the beam is used as probe volume without interference of the Mach disk. The practical aspects

[4]Note that the substitution of equation 3.1 into equation 3.2 for the case $M_a \gg 1$ yields an inverse square dependence of the density on the axial distance $\rho \propto 1/X^2$ as expected for flow from a point source [90].

[5]This equation does not hold for He where quantum statistical effects cause a deviation.

[6]The collisional effective3ness is a measure of the change in the mean random velocity per gas particle per collision. For argon $\epsilon = 0.25$ [86].

are discussed in more detail in section 4.2.

In this experiment a seeded expansion is used with the molecules of spectroscopic interest (CO in the present work) mixed into the monatomic gas expansion as a small percentage. The final state that these molecules reach in the expansion (regarding their rotational and vibrational degrees of freedom as well as condensation) depends on the rate at which these processes yield equilibration with the translationally cold carrier gas bath. The rotation-translation equilibration is rapid and typically extensive rotational cooling is observed. The rate of vibration-translation equilibration is generally slower so that the vibrational cooling is not complete [92]. The phase equilibration in general is slow so that the extent of condensation is limited in spite of the low translational temperature. The first step of condensation is the formation of van der Waals complexes with a single van der Waals bond - either between two of the molecules or between a molecule and a carrier gas atom - but larger clusters will also form under suitable experimental conditions.

The extent of cluster formation is influenced by and can be controlled by experimental parameters such as the stagnation pressure and reservoir temperature, the nozzle geometry, the carrier gas and the sample gas-carrier gas ratio in the expanding gas mixture [93]. The optimal conditions seem to be very setup-specific and only general rules of thumb exist.

In principle the cooling process and the formation of condensation products are competing processes in the sense that the binding energy that is released during condensation (see Δ_{vap} values in table 3.1) reheats the gas and in the case of extensive condensation limits the minimum translational temperature that can be reached. The rate of cooling which depends on the rate of two-body collisions in the jet is proportional to $P_0 D$ [91]. In the special case of a pure noble gas jet it is proportional to $(P_0 D)^{0.4}$ as seen in equation 3.3. The rate of condensation, or more specifically the formation of van der Waals complexes in such an expansion, depends on the number of three-body collisions [94, p. 124] which is proportional to $P_0^2 D$ or D/λ_0^2 [91]. If an extremely low translational temperature with minimum condensation is required, a larger nozzle cross section D and lower stagnation pressure P_0 are advisable. If a measure of condensation is desired, as in our experiment, the optimisation could be done towards larger D and especially higher stagnation pressure P_0 in order to advance both cooling and condensation processes. From experimental results a conical nozzle geometry and a lower temperature T_0 in

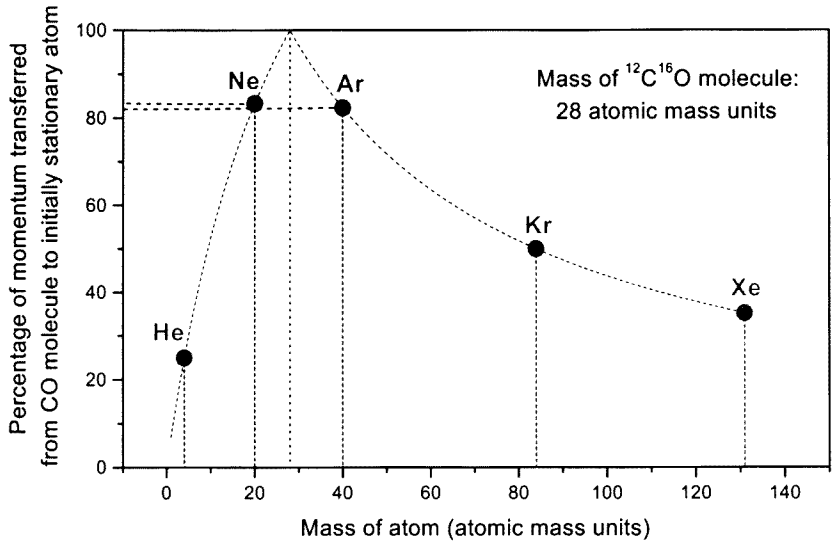

Figure 3-1: Illustration of the efficiency of different noble gas species as carrier gases with respect to the cooling of $^{12}C^{16}O$ molecules seeded into the expansion. The curve was obtained by calculating the percentage of momentum transferred from the $^{12}C^{16}O$ molecule to an initially stationary noble gas atom during an elastic two-body collision.

the gas reservoir generally advances cluster formation [93].

Two other practically important parameters influencing the cooling are the percentage of sample molecules added to the carrier gas and the choice of the carrier gas. If the percentage of the molecular gas added to the carrier gas expansion is increased beyond trace amounts, it will increasingly influence the behaviour of the expansion. It can be understood in terms of a change of the effective heat capacities and heat capacity ratio of the gas mixture [94, p. 125] as the fraction of molecular gas to carrier gas is increased. Molecules with internal degrees of freedom have lower specific heat capacities than that of the argon or neon carrier gases, as illustrated by the γ-values listed in table 3.1.

The choice of carrier gas is another parameter of practical significance. The efficiency of collisional cooling of any molecule, and particularly CO, in different noble carrier gases varies. If it is assumed that the translational degrees of freedom of the CO molecule seeded into the noble gas expansion are cooled mainly by two-body collisions with the noble gas atoms and that

the cross section is the same for the different noble gases[7], then according to the classical theory of elastic two-body collisions (a simple "billiard-ball" model assessed for head-on collisions) the efficiency of momentum transfer in a collision depends on the mass ratio $M_{CO}/M_{noble\ gas}$. The closer this ratio is to 1 the more completely the momentum is transferred from the hot CO molecule to the cold carrier gas atom. Figure 3-1 illustrates this effect. It can be seen that Ar and Ne are the two noble gases that should be most efficient for cooling CO.

3.2 Generation of tunable coherent vacuum ultraviolet light

Since the development of lasers in the early 1960s the advances in high-sensitivity high-resolution spectroscopy have benefited greatly from tunable narrow bandwidth lasers as ideal sources of radiation. Nonlinear optical processes[8], facilitated by the high intensities of laser beams, provide methods to extend the range of high-resolution laser spectroscopy to regions of the spectrum where no suitable laser sources are available. Nonlinear crystals are employed to extend the range over which continuous tuning is possible in the near infrared, visible and near ultraviolet range, but these crystals become opaque at wavelengths below about 200 nm. For generation of narrow bandwidth (typically of the order of 0.1 cm^{-1}) tunable coherent radiation in the vacuum ultraviolet region (below 200 nm), four-wave mixing processes in gaseous nonlinear media have to be used [95]. Metal vapours and/or noble gases are generally employed as gaseous nonlinear media. For the generation of wavelengths shorter than the 105 nm cut-off of window materials, noble gases combined with a windowless setup and frequency doubled dye lasers are used (for example [96] and [32]). To generate wavelengths in the range $105 - 200$ nm, metal vapours generally yield better conversion efficiencies due to higher nonlinear susceptibilities and the possibility of phase matching by the addition of a noble gas [13].

In every experimental application of four-wave mixing the challenge is to choose the most appropriate gaseous medium and to optimise the experimental conditions to yield optimal out-

[7] This is only a rough estimate since the difference in the collisional cross sections of a collision of a CO molecule with different noble gas atoms will certainly influence the result.

[8] Nonlinear frequency conversion processes become even more dominant in work with modern high power ultrashort pulse picosecond and femtosecond solid state lasers. However for high-resolution spectroscopy, such as the work documented here, a narrow bandwidth as provided by a nanosecond pulsed laser source is crucial. This discussion only refers to frequency conversion processes applicable in work with narrow bandwidth nanosecond laser sources of moderate power, of which dye lasers are still the prototype.

put in the desired wavelength range. Wallace and Zdasiuk [97] first investigated magnesium vapour, mixed with helium gas but not phase matched, as a nonlinear medium for two-photon resonant third-harmonic and sum-frequency generation. They reported a wide continuous tuning range (140 – 160 nm) in the vacuum ultraviolet and a high power conversion efficiency. McKee et al. [98] extended the range of wavelengths generated in magnesium vapour to shorter wavelengths (121 – 129 nm) and Yamanouchi et al. [99] used a magnesium vapour medium to obtain longer wavelengths (160 – 174 nm). In an experimental investigation of magnesium vapour as nonlinear medium, Junginger et al. [100] presented magnesium vapour prepared in a heat pipe oven and phase matched by the addition of krypton gas as an efficient low-loss, high density medium for third-harmonic generation around 144 nm. Vidal and collaborators demonstrated in their extensive excitation spectroscopy of CO that sum-frequency generation in such a medium serves as a suitable source of narrow bandwidth vacuum ultraviolet radiation for high resolution spectroscopy [16, 28, 29, 30].

3.2.1 Sum-frequency generation in a magnesium vapour medium

The nonlinear processes relevant in this work are the sum-frequency generation process, where two incident fields at frequencies ω_1 and ω_2 in the visible interact with the medium to generate the sum-frequency $\omega_s = \omega_1 + \omega_1 + \omega_2$ in the vacuum ultraviolet and the degenerate third-harmonic generation process where $\omega_1 = \omega_2$ and $\omega_s = 3\omega_1$. Both of these are third order nonlinear processes and are generally described as four-wave mixing processes. In a gaseous nonlinear medium, third order processes constitute the lowest order nonlinear processes that can be employed for frequency conversion.

In the current section the physical principles underlying the experimental requirements for efficient sum-frequency generation are discussed using results from the theoretical description. A concise description of the theory of sum-frequency generation in a gaseous medium, as applicable to the present experiment, is found in appendix 8.1 and references thereof.

Four-wave mixing can be described most generally as the coupling of four electromagnetic waves due to their interaction with a nonlinear optical medium, resulting in the transfer of energy between the different electromagnetic fields [101, p. 90]. The interaction is characterised by the nonlinear polarisation of the medium which is expressed in terms of the electric fields

and the nonlinear susceptibilities characteristic of the medium (equation 8.15).

The theoretical description of sum-frequency generation yields an expression for the generated sum-frequency intensity (equation 8.17) from which it can be deduced that the intensity of the generated vacuum ultraviolet depends on the intensities of the incident beams, the square of the medium density, the square of the medium length, the square of the nonlinear susceptibility of the medium and the phase matching factor. These last two factors yield the characteristic medium requirements for efficient sum-frequency generation in an experimental vacuum ultraviolet source.

For efficient sum-frequency generation the gaseous medium must have a sufficiently large third order nonlinear susceptibility for the sum-frequency generation process. The susceptibility tensor $\chi^{(3)}(-\omega_s;\omega_1,\omega_1,\omega_2)$ is characteristic of the medium, but as shown by the quantum mechanical expression 8.12 it is subject to fundamental selection rules and influenced by resonances - factors that must be considered in an experimental setup. The first aspect to consider is that the nonlinear susceptibilities of the even orders vanish in centrosymmetric gaseous media leaving four-wave mixing (a third order process) as the lowest order frequency up-conversion process. Secondly the angular momentum selection rule applied to the nonlinear susceptibility determines the polarisation of the incident laser beams that can be employed for the generation of a sum-frequency or third-harmonic output (equation 8.14 and the discussion thereof). Thirdly the susceptibility for sum-frequency generation can be enhanced by suitable resonances with the atomic magnesium energy levels. There are three possible resonances to be employed for resonant enhancement as illustrated in figure 3-2: a one-photon resonance of an incident frequency, a two-photon resonance of ω_1 or a three-photon resonance of the incident frequencies which is associated with a one-photon resonance of ω_s. The one and three-photon resonances (figure 3-2 (a) and (c)) have the disadvantage that these resonances inevitably bring along strong one-photon absorption of either an incident or the generated sum-frequency wave by a dipole allowed transition. The two-photon resonance (figure 3-2 (b)) is the method of choice as it enhances the nonlinear susceptibility without causing enhanced one-photon absorption. Magnesium vapour provides both a large intrinsic third order nonlinear susceptibility [97] as well as suitable two-photon resonances with low two-photon absorption coefficients [100] for the generation of sum-frequencies in the vacuum ultraviolet.

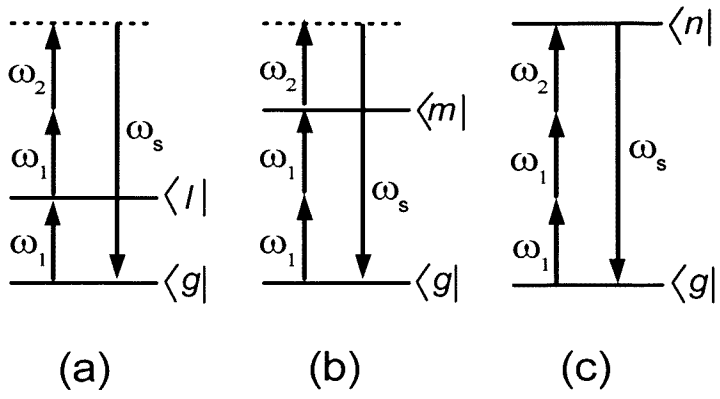

Figure 3-2: Schematic illustration of the three possibilities for resonant enhancement: a one-photon resonance of ω_1 (a), a two-photon resonance of ω_1 (b) and a three-photon resonance (c). The solid horizontal lines represent atomic energy levels labeled g, l, m, n. The dotted line indicates a virtual energy level.

In an experimental vacuum ultraviolet source, where the macroscopic output in terms of energy is important, efficiency on the quantum mechanical level is insufficient. The second medium requirement is that the contributions to the sum-frequency wave, generated in different volume elements of the medium, must interfere constructively - a condition called phase matching. Phase matching is equivalent to the fundamental physical requirement for the conservation of linear momentum in the interaction of four electromagnetic fields. For collinear beams, the phase matching condition can be expressed as a relation between the indices of refraction of the medium at the incident and generated frequencies

$$2\omega_1 n_1 + \omega_2 n_2 = \omega_s n_s. \tag{3.6}$$

A magnesium vapour medium can be phase matched by the addition of a positively dispersive gas such as krypton. The index of refraction of a mixture of two gases depends on the number densities of both gases and in the case of magnesium and krypton [100] the difference in their dispersive behaviour can be used to adjust the indices of refraction of the medium by adjusting the krypton-magnesium pressure ratio in the medium, until the phase matching condition,

equation 3.6, is satisfied[9].

In an experimental setup the requirement for phase matching sets stringent requirements for the conditions in the two-component nonlinear medium. To obtain and maintain phase matching in such a medium, the noble gas-metal vapour mixture must be homogeneous and extremely stable. For a sufficiently large metal vapour density, a high temperature is needed and to obtain phase matching, this temperature must be homogeneous over the medium length as well as stable over time. The partial pressures of the magnesium vapour and the krypton gas must be well defined and independently adjustable to facilitate fine-tuning of the pressure ratio. These stringent requirements can be met if the medium is prepared in a crossed concentric heat pipe oven [103]. The principles of operation and characteristics of such a heat pipe oven are discussed briefly in section 3.2.2.

Thirdly, in any medium there are other linear and nonlinear optical processes competing with sum-frequency generation that have to be taken into account and suppressed if possible. One-photon absorption of the incident frequencies ω_1 and ω_2 can be minimised by avoiding one-photon resonance conditions. Two-photon absorption of the two-photon resonant frequency ω_1 that causes saturation at high intensities cannot be avoided, but magnesium vapour has been reported to have a favourably small two-photon cross-section [100]. The absorption of the generated sum-frequency radiation in the medium due to photo-ionisation cannot be avoided, since the sum-frequency energy typically lies above the ionisation threshold of the metal. The enhanced absorption of the sum-frequency radiation near auto-ionisation bands of the metal vapour often causes dips in the conversion efficiency in such wavelength regions [99]. The generation of the third harmonic of the resonant incident frequency competes strongly with sum-frequency generation being enhanced in the same way by the resonance. However, it can be suppressed by appropriate polarisation of the incident beams. Other third and higher order nonlinear processes may cause saturation at high input laser intensities.

3.2.2 Principles of operation of a crossed concentric heat pipe oven

The crossed concentric heat pipe oven facilitates the preparation of a magnesium vapour-krypton gas medium meeting the stringent phase matching requirements without any special

[9] Sections 3.5 and 3.6 of reference [102] can be consulted for more detail.

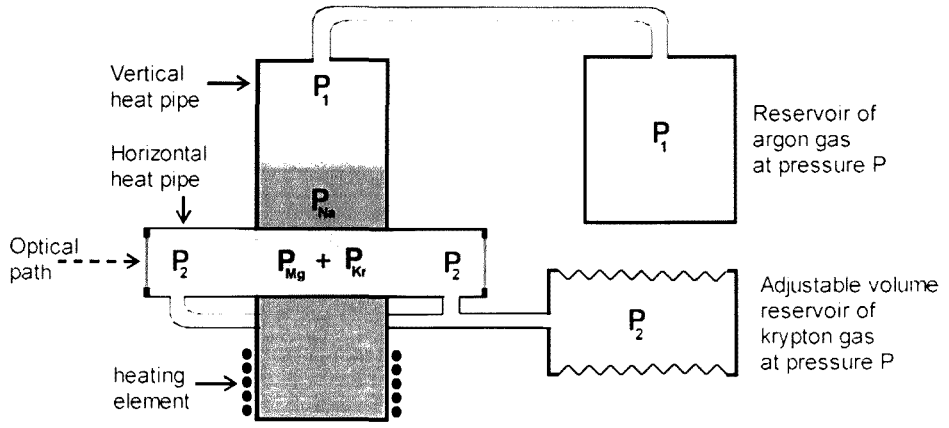

Figure 3-3: Schematic illustration of a crossed concentric heat pipe oven as used in our experiment.

thermal design or active temperature control.

The crossed concentric heat pipe oven used in the present work has originally been developed by Vidal and collaborators. The specific model used here was originally described by Scheingraber and Vidal [103] and a slightly modified version by Steffes et al. [104]. A comprehensive description and experimental characterisation of our heat pipe oven can be found in chapter 4 of reference [102]. Only a short description of the principles of operation has been considered necessary here.

A crossed concentric heat pipe oven consists of two separate heat pipes - a vertical heat pipe of larger diameter with a heat pipe of smaller diameter inserted horizontally into it - see figure 3-3. There is only thermal contact between the two heat pipes. The vertical heat pipe has sodium as working material and is filled with argon gas to pressure P_1. It is heated near the bottom by a heating coil with constant heating power, and the sodium vapour column that forms in it serves as a mechanism to obtain and maintain a very homogeneous and stable temperature in the middle zone of the horizontal heat pipe, which is in thermal contact with the vapour. The horizontal heat pipe contains the two components of the nonlinear medium: magnesium metal as working material and krypton gas at pressure P_2 as gas load. In both of the heat pipes, the working material (sodium and magnesium respectively) is continuously

evaporating at the heated zone of the pipe, flowing as vapour towards the colder zone(s) in the heat pipe where it condenses. A metal mesh lining the inside acts as wick to return the liquid phase working material from the condensation region to the evaporation region by capillary action. Both heat pipes are connected to gas reservoirs with relatively large volumes kept at room temperature to ensure that the fluctuations in P_1 and P_2 are negligible once the heat pipe is at operating temperature.

The homogeneous magnesium vapour-krypton gas mixture and the stability needed for phase matching are provided by the properties of the liquid-vapour phase equilibria in the heat pipe system. In the vertical heat pipe the externally regulated argon pressure P_1 determines the sodium vapour pressure P_{Na} ($P_{Na} = P_1$) and therefore the temperature of the sodium vapour. This constant and stable temperature facilitates the establishment of a well defined and stable magnesium vapour pressure P_{Mg} in the middle section of the horizontal heat pipe. The middle section of the horizontal heat pipe therefore contains a homogeneous mixture of magnesium vapour (at partial pressure P_{Mg}) and krypton gas (at partial pressure $P_{Kr} = P_2 - P_{Mg}$). P_{Mg} and P_{Kr} only depend on the stable pressures P_1 and P_2 respectively and are not influenced by fluctuations in the heating power. Both P_{Mg} and P_{Kr} can be adjusted independently by adjusting P_1 and P_2 respectively.

3.3 Electronic excitation spectroscopy by laser-induced fluorescence measurements

The detection of fluorescence upon irradiation of a sample with a laser, generally called laser-induced fluorescence spectroscopy, has been the dominant method in laser spectroscopy of molecules in supersonic expansions according to the review of Levy [105]. The two types of laser-induced fluorescence spectra are fluorescence excitation spectra and dispersed fluorescence spectra.

In the work described here fluorescence excitation spectroscopy was the method of choice. In fluorescence excitation spectroscopy, the laser wavelength is tuned while measuring the total fluorescence, using for example a photomultiplier tube. The resulting spectrum of the total fluorescence as function of the excitation wavelength is essentially the product of the absorption

spectrum and the fluorescence quantum yield of the molecule [106, p. 386]. Under collision-free conditions the fluorescence quantum yield is in most cases near to 1 for all excited levels so that fluorescence excitation spectroscopy serves as a highly sensitive method to obtain the absorption spectrum [105]. The lowest detection limit is usually imposed by either the background stray light signal or the electronic noise in the detection system, depending on which is the greater of the two.

If additionally the absorption cross-sections for the investigated fluorescent states are either similar or known, as for the rovibronic transitions of a single vibronic band, the relative line intensities of the spectrum obtained by fluorescence excitation spectroscopy can further be used to obtain the relative populations in the ground states $N(v'', J'')$ from which the transitions originate.

In the dispersed fluorescence method the excitation laser wavelength is set at a specific absorption wavelength of the sample and the emitted fluorescence is analysed using a monochromator or polychromator. This method has not been employed in the work described here, but could serve well as a complementary technique in future work - see chapter 7.

Chapter 4

Experimental setup and methods

The experimental setup used in the present work consists of the pulsed source of coherent narrow bandwidth vacuum ultraviolet radiation (section 4.1), a pulsed free supersonic jet as spectroscopic sample (section 4.2) and a computerised system for control, detection of laser-induced fluorescence and data acquisition (section 4.3). Figure 4-1 gives a schematic overview of the components of this experimental setup.

4.1 Vacuum ultraviolet laser source

Tunable coherent vacuum ultraviolet radiation is generated by two-photon resonant four-wave sum-frequency mixing in a medium of magnesium vapour and krypton gas inside a crossed concentric heat pipe oven. The setup for the generation of tunable coherent vacuum ultraviolet is illustrated in figure 4-2 (see reference [102] for additional details).

The incident beams are provided by two pulsed dye lasers (both Lambda Physik, FL 3001X with Coumarin 440 dye) pumped by a XeCl excimer laser (Lambda Physik, EMG 203 MSC). The two beams are combined collinearly in a polarising beam combiner (Halbo Optics, PBC 10 M) and focussed by a $f = 800$ mm biconvex quartz lens into the magnesium vapour medium. Good temporal overlap of the ca. 25 ns long laser pulses is guaranteed by pumping the two dye lasers by the same excimer laser and arranging the optical path lengths through the two lasers to be roughly the same. Optimal spacial overlap of the beams at their focal point in the nonlinear medium is done in this setup by having mirror M1 as well as the polarising beam combiner BC

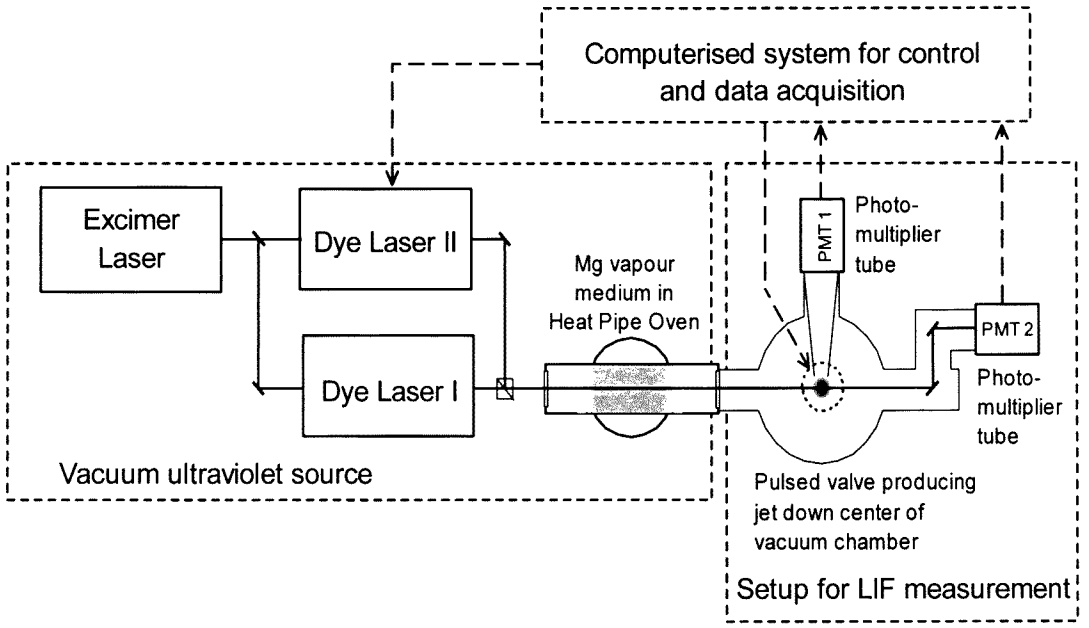

Figure 4-1: Schematic illustration of the main components of the experimental setup. The dotted lines distinguish the part of the setup constituting the vacuum ultraviolet source from the vacuum system containing the supersonic jet. The dashed arrows indicate connections with the control and data acquisition system. The vacuum pumps, voltage sources and equipment of the control and data acquisition systems are not shown here.

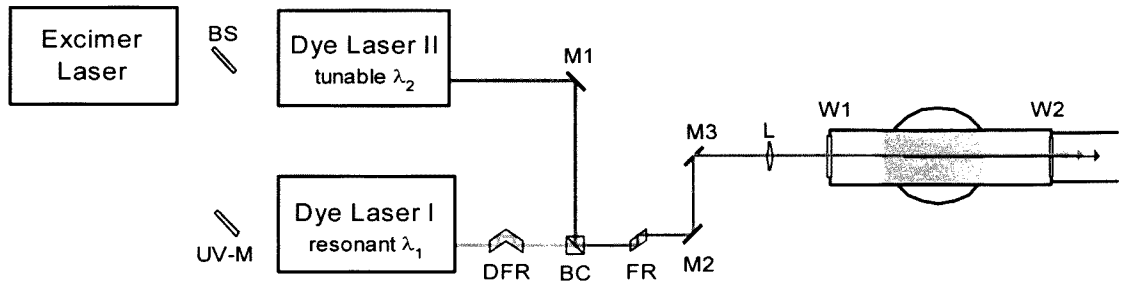

BS Beamsplitter for 308 nm (Sirah)
UV-M 45 degree mirror for 308 nm (CVI, XECL-2037-45-UND)
DFR Double Fresnel rhombus (Halbo Optics, FRH 10 M)
BC Polarising beam combiner (Halbo Optics, PBC 10 M)
FR Fresnel rhombus (Karl Lambrecht Cormporation, FRS4-10-BB580)
M1, M2, M3 Beam stearing mirrors for visible (Linos Photonics LBSM-VIS 38 3079 050)
L Biconvex quartz lens, f = 800 mm
W1 Quartz window
W2 MgF2 window

Figure 4-2: Schematic illustration of the experimental setup for the generation of tunable narrow bandwidth vacuum ultraviolet light.

mounted on stands that allow accurate rotation around horizontal and vertical axes through the reflecting surface. After visual pre-alignment, the beam overlap can be optimised further by small adjustments to the orientation of BC while monitoring the sum-frequency signal. Due to the importance of the spacial (lateral) overlap it was found that the internal alignment of the dye lasers had to be optimised for good beam quality rather than maximal output energy.

The heat pipe oven (see figure 3-3) is operated with a total pressure of ca. 250 mbar in the outer vertical heat pipe, setting the temperature of the central heated zone of the horizontal heat pipe oven to typically 750 °C. In this heated zone of the horizontal heat pipe oven, a homogeneous gas mixture of magnesium vapour (circa 20 mbar) and typically around 260 mbar krypton gas is prepared, serving as the nonlinear optical medium with an optical path length of circa 60 mm. The horizontal heat pipe has a quartz entrance window and a vacuum ultraviolet transmitting MgF_2 window on the exit side between the heat pipe and the vacuum system. The krypton gas effectively confines the magnesium vapour and with the additional measures of water cooling of the end caps of the horizontal heat pipe and the insertion of baffles with 5 mm apertures inside both the windows of the horizontal heat pipe, no problems with window contamination have been encountered.

The four-wave mixing process is enhanced both by a two-photon resonance and by phase matching of the medium. Resonant enhancement is achieved by fixing the wavelength of dye laser I at 430.878 ± 0.002 nm corresponding to a two-photon resonance with the $3s^2\ ^1S_0 - 3s3d\ ^1D_2$ transition of atomic magnesium, as illustrated in figure 4-3. The wavelength of the sum-frequency radiation is tuned by tuning the wavelength of the dye laser II. Phase matching of the magnesium vapour-krypton gas medium is obtained by optimising the krypton pressure by adjusting the volume of the krypton reservoir. Figure 4-4 shows typical phase matching curves. Phase matching is usually obtained with a Kr:Mg vapour pressure ratio of about 12 : 1. It was not found necessary to re-adjust the Kr:Mg pressure ratio during scans up to ca. 50 cm^{-1}.

In this vacuum ultraviolet source enhancement of the sum-frequency generation process and suppression of the competing third harmonic of the resonant dye laser were achieved by applying both circular polarisation of the incident laser beams and optimisation of the phase matching. Due to angular momentum selection rules (as explained in more detail in appendix 8.1) optimal third-harmonic generation requires linearly polarised incident laser beams, whereas

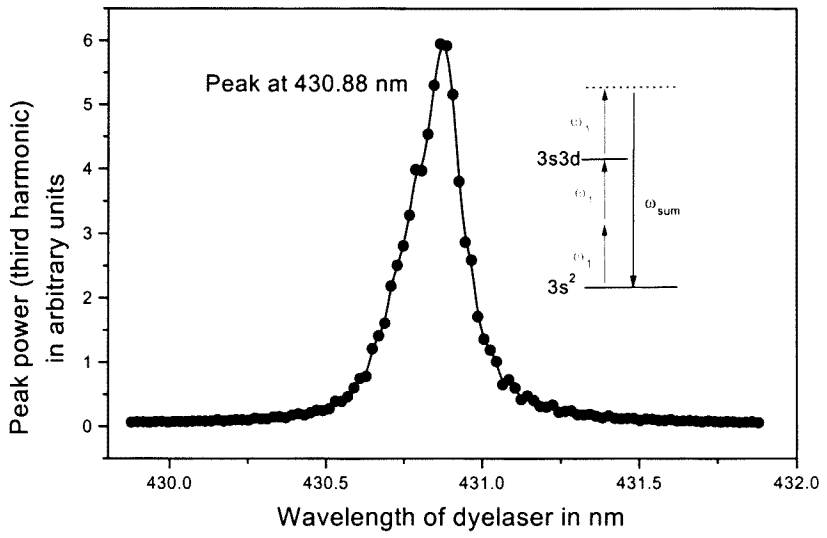

Figure 4-3: Illustration of the resonant enhancement of the four wave mixing process as the incident laser wavelength ω_1 is tuned to a two-photon resonance of magnesium vapour. As illustrated here for the case of third harmonic generation the peak power of the generated sum-frequency increases by about two orders in magnitude by the resonance condition.

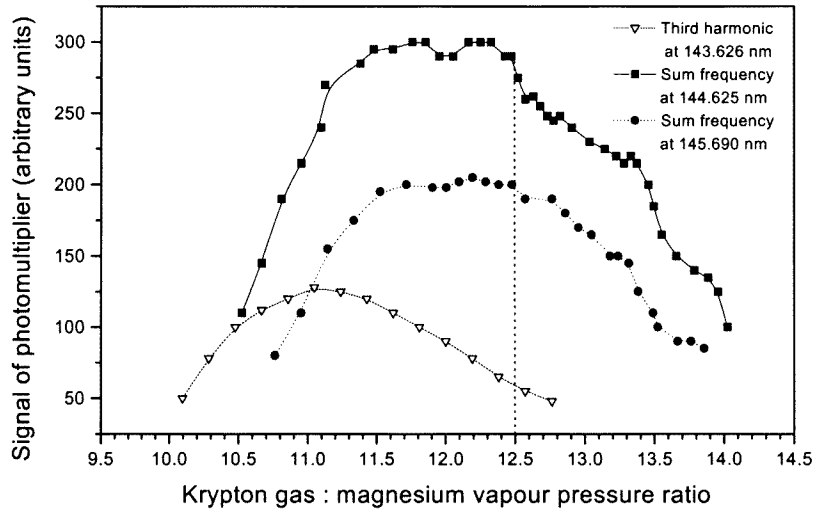

Figure 4-4: Phase matching curves for the generation of vacuum ultraviolet at three different wavelengths: the third harmonic of dye laser I at 143.626 nm and the sum-frequency at 144.625 nm and 145.690 nm. The dotted vertical line indicates a suitable magnesium vapour-krypton gas pressure ratio where the phase matching suppresses third harmonic generation while enhancing sum-frequency generation.

optimal sum-frequency generation with suppressed third-harmonic can be achieved by employing incident beams polarised circularly in opposite senses. The outputs of the dye lasers are about 95 % vertically polarised. Propagating the beam of dye laser I through a double Fresnel rhombus (DFR) changes its polarisation to about 85 % horizontally polarised. Opposite circular polarisation is achieved by propagating the two dye laser beams, now polarised perpendicularly, through a Fresnel rhombus (FR) functioning as a quarter-wave retarder to produce dominantly circularly polarised light in opposite senses. The polarisation is, however, not complete enough to suppress the third harmonic fully. The difference in phase matching conditions for the third-harmonic and sum-frequency generation processes was used to discriminate further against the third-harmonic. As illustrated in figure 4-4 the phase matching peak for third-harmonic generation (yielding 143.63 nm) occurs at a slightly lower Kr:Mg pressure ratio than the peak for the longer wavelength sum-frequency (typically 144.6 – 145 nm). By choosing a Kr:Mg pressure ratio on the high pressure side of the sum-frequency peak the third harmonic is suppressed, at the cost of having lower sum-frequency intensity as well. The third method used to promote the sum-frequency generation relative to third-harmonic generation was to ensure that the non-resonant dye laser produced a higher energy output than the resonant dye laser. Using these methods, it was always possible to ensure that the amplitude of the third-harmonic signal, measured when allowing only the resonant beam into the heat pipe oven, was not more than 50 % of the amplitude of the vacuum ultraviolet signal measured with both beams unblocked. It could then be assumed that at least 50 % of the vacuum ultraviolet signal[1] measured with both beams unblocked should be of the sum-frequency wavelength.

The characteristics of the generated sum-frequency radiation are closely related to that of the incident dye laser beams. The dye lasers provide moderate pulse energies of about 1 – 2 mJ per pulse with a 25 ns full width half maximum, and pulse-to-pulse energy fluctuation of roughly 10 %. The bandwidth of the dye lasers depending on the wavelength in the 7th grating order is about 0.2 – 0.3 cm^{-1}. The peak power of the generated sum-frequency radiation is estimated from the signal amplitude on the photomultiplier to be in the order of a few mW or

[1] Measurement of the third-harmonic signal by blocking the nonresonant dye laser beam provides an upper limit for the contribution of the third harmonic to the total vacuum ultraviolet signal. When the nonresonant dye laser beam is unblocked, the third-harmonic contribution should decrease due to competition between the third-harmonic and the sum-frequency generation processes. The true percentage of sum-frequency radiation is therefore expected to be higher than 50 %.

about 10^{15} photons per second. This corresponds to a typical power conversion efficiency in the order of 10^{-7}. The bandwidth of the generated sum-frequency radiation, as estimated from the line widths of the CO spectra, is about 0.25 cm^{-1} (0.5 pm at 144.7 nm).

The continuous tuning range of the sum-frequency wavelength is determined by the tuning range of the laser dye in dye laser II. Coumarin 440 was used in dye laser II throughout this work. The sum-frequency signal could be observed to follow the efficiency profile of Coumarin 440 over its tuning range, as illustrated in figure 4-5 (b). On closer investigation, broad dips in the vacuum ultraviolet intensity at specific wavelength ranges that are not due to changes in the dye laser energy but rather to autoionisation bands in the magnesium ionisation continuum are observed. The vacuum ultraviolet wavelength region that is of interest for probing the $A^1\Pi(v' = 3) - X^1\Sigma^+(v'' = 0)$ band of CO lies on the short wavelength side of such a broad dip in the spectrum of the vacuum ultraviolet source as illustrated in figure 4-5 (a). This had the result that the vacuum ultraviolet power that was used in the scans showed a steady decrease towards the red in all scans.

The laser beam emerging from the heat pipe oven consists of the two incident frequencies ω_1 and ω_2, the tunable sum-frequency $\omega_{SF} = \omega_1 + \omega_1 + \omega_2$ and the third harmonic $\omega_{TH} = 3\omega_1$ of the resonant dye laser frequency. No separation of the sum-frequency, third-harmonic and incident beams was done in the present work. From a spectroscopic viewpoint it was not considered necessary since neither the fundamental visible wavelengths nor the third harmonic of the resonant wavelength were expected to have a significant interaction cross section with CO or the CO van der Waals molecules. Although the visible incident wavelengths and the third-harmonic vacuum ultraviolet wavelength in the experimental laser beam did not interact with the sample molecules, their presence had to be taken into account when considering the measurement of the vacuum ultraviolet intensity, scattered light and fluorescence. This is discussed in the section 4.3.

4.2 Vacuum system and pulsed supersonic jet

The pulsed free supersonic jet apparatus consists of a gas reservoir (adjustable volume, 2.2 to 2.9 liter) containing gas mixtures at pressures up to 7 bar, connected to a vacuum chamber

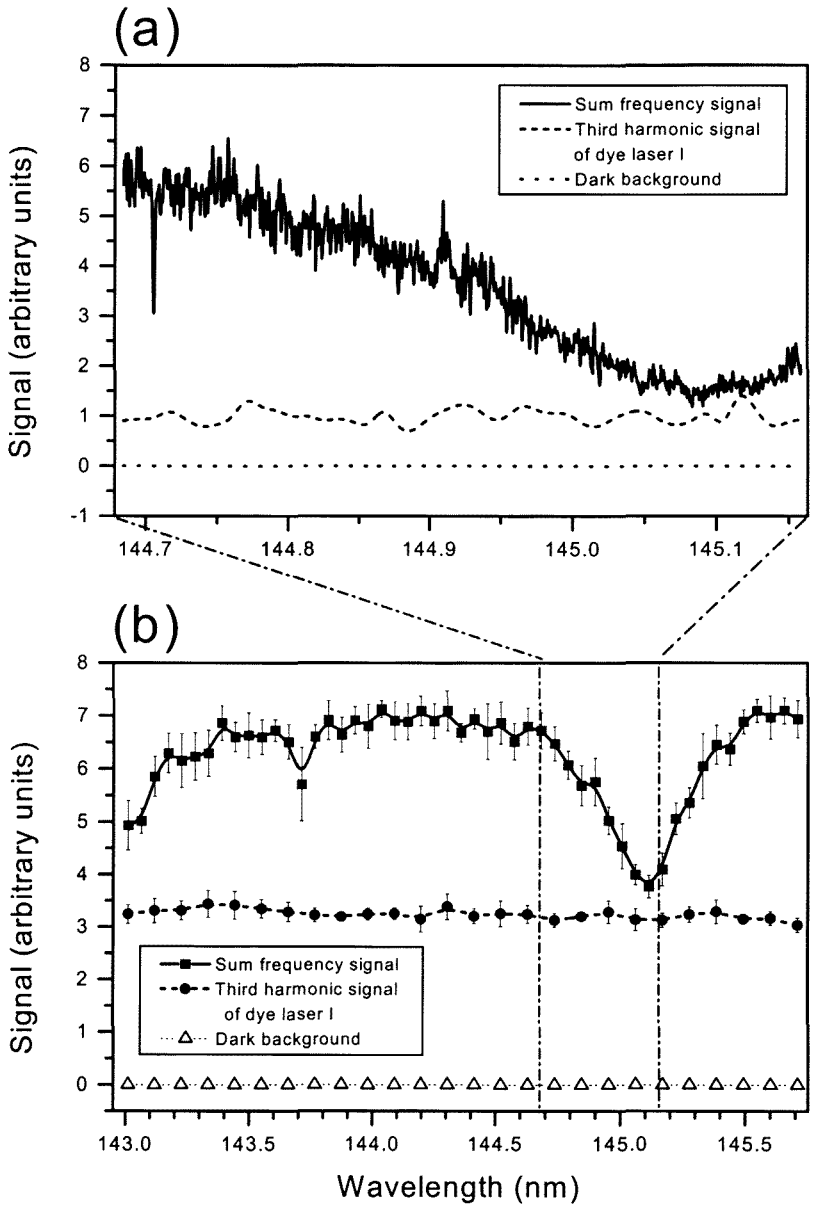

Figure 4-5: Plots of the spectrum of the tunable vacuum ultraviolet source - sum frequency peak power versus vacuum ultraviolet wavelength. The part of the spectrum of interest for investigating the $A^1\Pi(v' = 3) - X^1\Sigma^+(v'' = 0)$ band of CO is shown in (a) whereas (b) shows the vacuum ultraviolet spectrum over the greatest part of its useful range using Coumarin 440 dye in dye laser II.

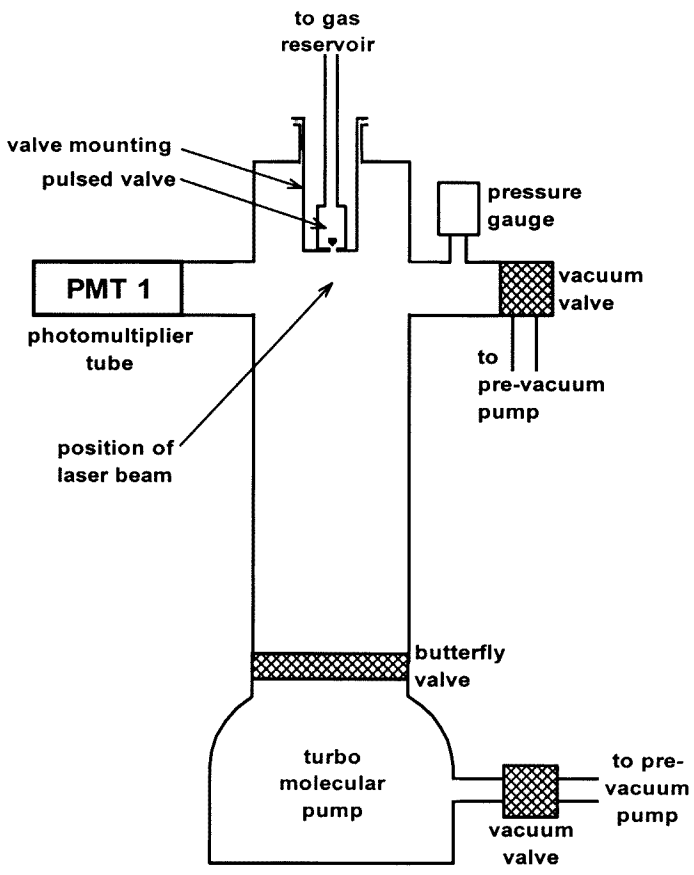

Figure 4-6: Schematic illustration of the vacuum chamber and mounting of the pulsed valve.

through a pulsed valve. As illustrated in figure 4-6, the pulsed valve is mounted in the top of the cylindrical vacuum chamber (diameter 100 mm, length 700 mm, provided with four KF-40 flanges 95 mm from the top). The vacuum chamber is evacuated by a turbo molecular pump (Pfeiffer TPH 200, 190 l/s) positioned at the bottom of the chamber, with a rotation pump (Vacuubrand, model RS-15, 15 m^3/h) as pre-vacuum pump. The pressure transducers (pirani, Leybold-Heraeus, model 162 02 B3 and penning, Leybold-Heraeus, model 172 85 B1) and a bypass to the pre-vacuum pump to assist quick evacuation are positioned at the top of the chamber, on the same height as the laser beam. A background pressure of ca. 5×10^{-6} mbar could be maintained in the vacuum chamber, also during extended measurements. Using a repetition rate of 1 Hz[2], as normally used during the experimental work, the pressure recorded by the pressure transducers could be seen to increase momentarily during each gas pulse and decrease again to the background pressure before the next gas pulse. Under the pressure conditions of the experimental work the position of the Mach disk, as calculated by equation 3.5 in section 3.1, was never closer than approximately 0.5 m from the nozzle. Therefore interference of the Mach disk with the sample volume was not expected or observed.

The valve that was used in this experiment is a solenoid valve (General Valves series 9, Part nr. 9-181-900) driven by a home-built pulsed voltage source. The valve exhibits an opening time of ca. 0.4 ms and could provide gas pulses with minimum duration of ca. 1.5 ms. Attempts to obtain shorter gas pulses failed, possibly partly due to the pulsed voltage source providing only ca. 75 % of the driving voltage that is specified for the valve.

The temporal development of the gas pulse could be investigated in two ways. Initially general testing of the valve was done using a custom fast ionisation gauge as described by Gentry and Giese [107]. The fast ionisation gauge ionises the gas passing through its grid and produces a current signal proportional to the gas density, with a rise time of a few microseconds [107]. Figure 4-7 illustrates a few good fast ionisation gauge measurements as displayed on an oscilloscope. The results as illustrated in figure 4-7 showed that the valve does not open completely when trying to obtain a pulse duration shorter than about 1.3 ms. Another useful result obtained by this method was the time delay between the voltage pulse of the pulsed valve

[2]The low repetition rate of 1 Hz was used to ensure that the vacuum chamber was evacuated sufficiently between two gas pulses so that a slowly rising background pressure in the chamber would not desturb the gas expansion during long measurements.

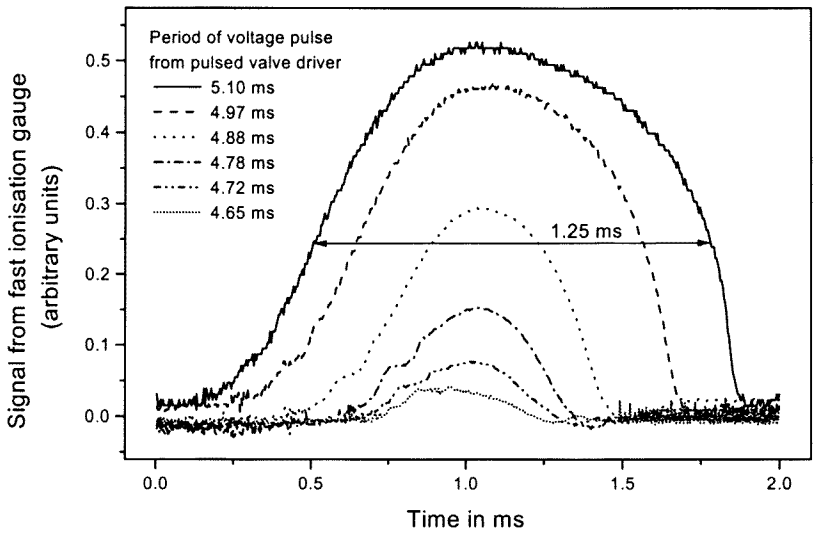

Figure 4-7: Fast ionisation measurements of the gas pulse from the pulsed valve measured at a distance of 40 mm from the nozzle. The expansion gas was nitrogen expanding from a stagnation pressure of 1.6 bar; the background pressure was 5×10^{-5} mbar. Note that the period of the gas pulse (full width half maximum) is not necessarily equal to that of the voltage pulse - it greatly depends on the stagnation pressure and mechanical forces in the valve. These curves confirm that when the gas pulse period is decreased below ca. 1.3 ms the peak gas density decreases with the period indicating that the valve does not open completely any more. The valve takes ca. 0.5 ms to open completely.

driver and the gas pulse. The disadvantage of the fast ionisation gauge that made it impractical for general use during the experiment is that the home-built model only yielded useful results in a very limited range of conditions (stagnation pressures) due to arcing problems.

The second method to investigate the gas pulse behaviour was by measuring the fluorescence signal of a chosen $^{12}C^{16}O$ line while scanning the laser pulse ($\tau_L \sim 25$ ns) in time over the gas pulse ($\tau_G \sim 2$ ms) by changing the delay time between the gas pulse trigger and the laser trigger. These so-called "delay scans" could be employed under all relevant experimental conditions. The profile of the gas pulse as recorded in a delay scan contains additional information on the temperature of the gas during the pulse as the fluorescence of a specific excitation transition is influenced by the population of the ground state rotational level which is influenced by the gas temperature.

The delay scan method was used to determine the merit of changing to an elongated vacuum

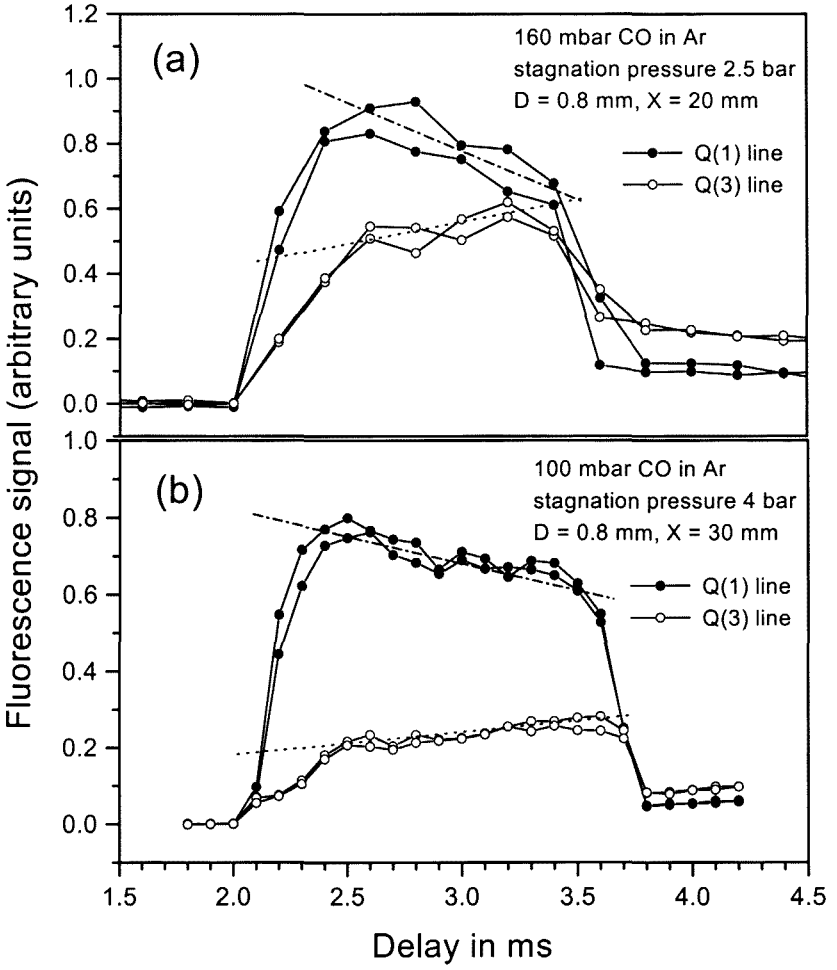

Figure 4-8: Time scans over the gas pulse at the $Q(1)$ and $Q(3)$ wavelengths of $^{12}C^{16}O$ (a) with the short (200 mm) vacuum chamber that was initially tested and (b) with the 700 mm long vacuum chamber that was used in the experiment. The rates with which the signal amplitudes of the $Q(1)$ and $Q(3)$ signals changed during the gas pulse (indicated by the dotted lines) were relatively fast in the shorter vacuum chamber (a): -290 units/s and 120 units/s for the $Q(1)$ and $Q(3)$ signals respectively, corresponding to a temperature rise of 13 K/ms. Using the longer chamber (b) the rates of change were significantly smaller: -110 units/s and 60 units/s respectively, corresponding to a temperature rise of 3 K/ms.

chamber in an early stage in the experiment - the results illustrated in figure 4-8. Initially a shorter vacuum chamber was used in the setup giving a free path length of only 130 mm between the pulsed valve and the butterfly valve in the bottom of the chamber and a volume of 1.6 dm^3. Delay scans with the shorter chamber (figure 4-8 (a)) indicated a relatively steep increase in the rotational temperature of approximately 12 K/ms of the gas sample during the pulse period. This temperature increase is due to the fast increase in the background pressure during the gas pulse period in the small volume of the chamber. After the vacuum chamber had been enlarged to provide an unobstructed space of about 630 mm along its axis before reaching the butterfly valve and a volume of 5.5 dm^3, the delay scans (figure 4-8 (b)) showed a much slower temperature increase of approximately 3 K/ms during the gas pulse, even at a higher stagnation pressure. The enlarged vacuum chamber has been used in all experiments of which the data are presented here.

Having a fixed vacuum chamber geometry, pumping capacity and a specific pulsed valve with its typical pulse duration, there are several parameters that can still be adjusted to influence the conditions in the sampled gas volume in the supersonic jet (i.e. in the volume in the jet irradiated by the vacuum ultraviolet beam). The basic parameters are the nozzle geometry, orifice diameter of the nozzle, the distance from the nozzle to the laser beam, the stagnation pressure, the percentage CO molecules in the expanding gas and the noble gas species used as carrier gas.

In our experiment, the nozzle geometry was fixed by the geometry of the available valve and the need for a vacuum tight seal around the orifice. The resulting geometry is illustrated in figure 4-9. The smallest orifice diameter in the nozzle (D) and the nozzle-to-laser distance (X) could be adjusted, although by rather cumbersome methods. The diameter of the orifice of the valve itself is 0.8 mm. The effective orifice diameter could be decreased by inserting a small disk with a smaller hole in front of the valve orifice as illustrated in figure 4-9. Since the position of the laser beam and the photomultiplier PMT 1 detecting the fluorescence signal were fixed and the length of the valve mounting was not adjustable, the nozzle-to-laser distance could only be changed to predetermined values (X = 14 mm, 20 mm and 30 mm) by interchanging valve mountings of different lengths. Suitable values of D and X were established by experimental measurements early in the project, using argon as carrier gas and measuring the rotational

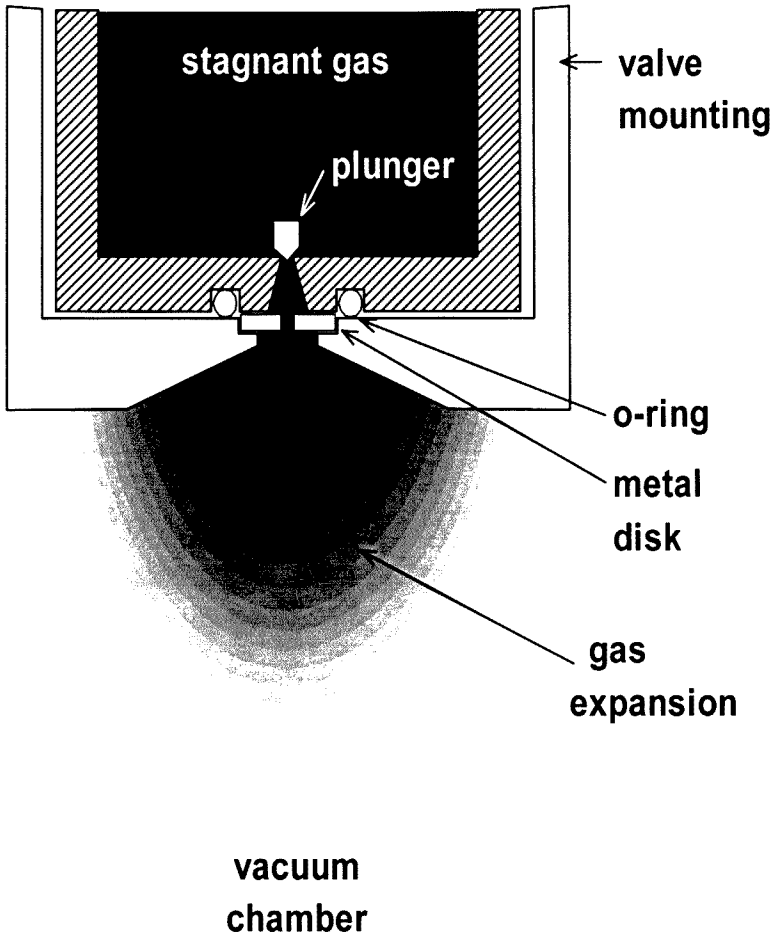

Figure 4-9: Schematic illustration of the geometry of the nozzle of the pulsed valve used in the present work. A thin metal disk (grey shaded) was inserted in front of the valve to decrease the effective orifice of the nozzle arrangement.

temperature[3] and the fluorescence signal amplitude that could serve as a measure of the gas density with different setups. The values $D = 0.8$ mm and $X = 20$ mm were found to provide a suitable compromise between lowest temperature and sufficient gas density. The choice of the value for X corresponds with the experimental rule of thumb [108] that cooling is practically complete at a distance of about 10 orifice diameters from the nozzle. This setup was then used throughout the work, employing the remaining gas-related parameters for further optimisation of the conditions as discussed under the experimental results in section 5.1.

4.3 Laser-induced fluorescence detection and data acquisition

The system responsible for the detection of the laser-induced fluorescence, data acquisition and control of the experiment is illustrated schematically in figure 4-10. The experiment is controlled and the data are acquired by a personal computer (a PC 486 that runs Windows 3.1) running a custom programme in HP VEE (Hewlett Packard Visual Engineering Environment). The computer is connected via an interface card (HP82335) and parallel port to the dye laser II, the delay generator and a computer interface with analog-to-digital functionality (Stanford Research Systems, SR 245) in order to set the laser wavelength, to set the delay between the laser pulse and the gas pulse and to retrieve data automatically at every step of a scan. Each data point in a scan is the average of a user-set number of laser pulses (usually 10) in order to reduce the influence of shot-to-shot fluctuations in vacuum ultraviolet power. All experiments were done at a repetition rate of 1 Hz. The delay generator triggers the pulsed valve driver and the excimer laser with the appropriate delay between them. The trigger for the data acquisition system (boxcars and computer interface) originates from a photodiode detecting the excimer radiation, making it independent of any time-jitter the excimer discharge might show.

The vacuum ultraviolet fluorescence of the molecules in the illuminated region of the supersonic jet is measured by a solarblind photomultiplier PMT 1 (EMR Photoelectric, model 542G-08-18-03900, Cs-I cathode) positioned perpendicular to both the laser beam and the supersonic jet. The relative power of the transmitted vacuum ultraviolet beam is measured by splitting ca. 8 % of the beam off with a MgF_2 window and reflecting this radiation with a

[3]The method of determining the rotational temperature is discussed in detail in section 5.1.

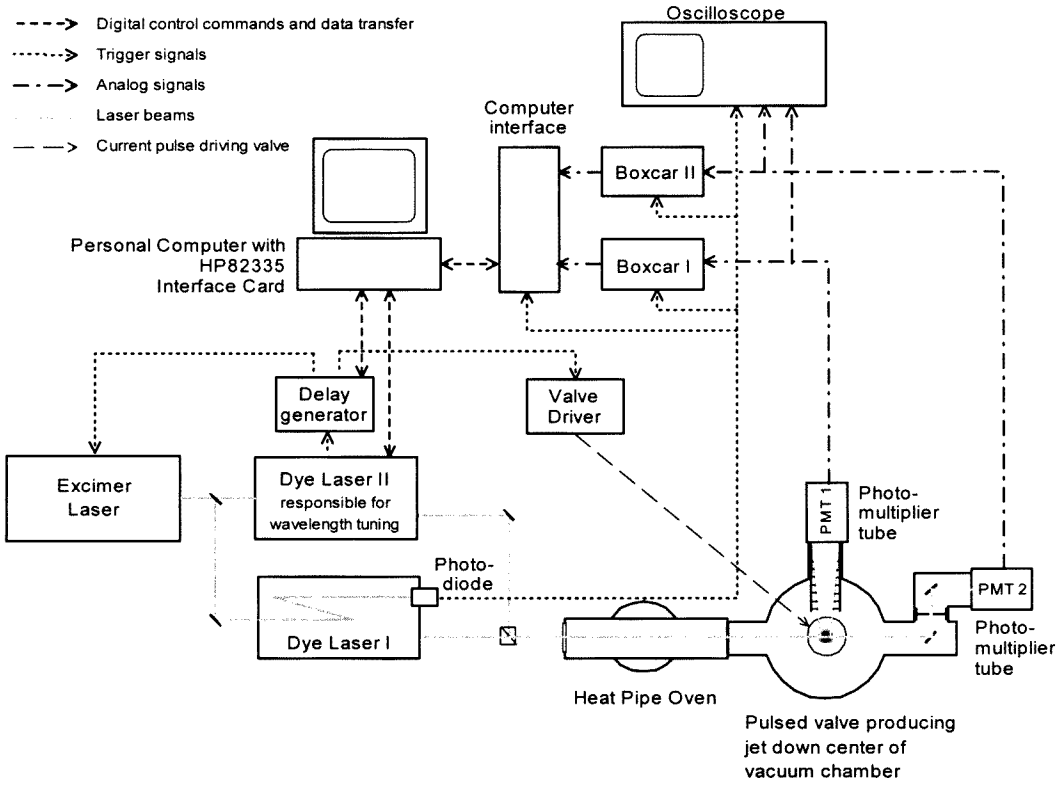

Figure 4-10: Schematic illustration of the computerised data acquisition and control system.

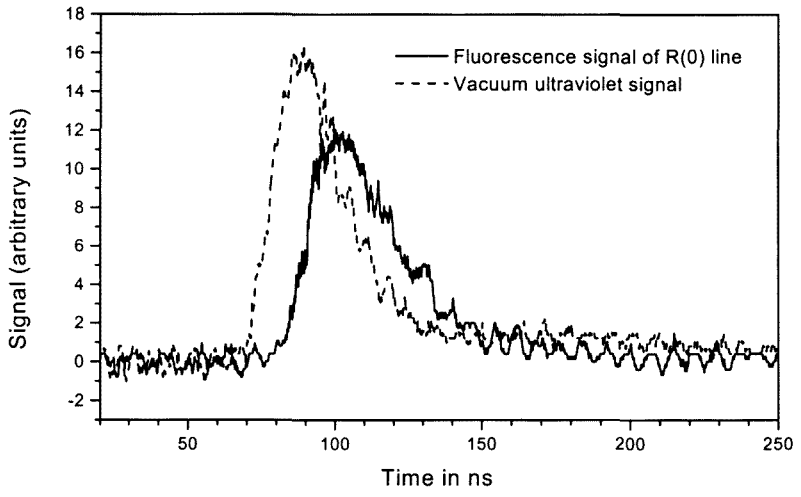

Figure 4-11: The fluorescence signal of the strong R(0) CO line as well as the signal of the transmitted vacuum ultraviolet beam as displayed on the oscilloscope.

convex polished aluminium surface onto the photocathode of a second solarblind photomultiplier PMT 2 (Hamamatsu, model R973, Cs-I cathode). The signals of the two photomultipliers are integrated by two boxcar integrators (Stanford Research Systems, model SR250) and the analog values transferred to the computer interface where they are digitised. Simultaneously the photomultiplier signals can be viewed on a 500 MHz oscilloscope (Hewlett-Packard, model 54616B) as illustrated in figure 4-11.

The laser beam emerging from the vacuum ultraviolet source contains not only light at the desired vacuum ultraviolet sum-frequency $\omega_{SF} = \omega_1 + \omega_1 + \omega_2$, but also the vacuum ultraviolet third-harmonic frequency $\omega_{TH} = 3\omega_1$ of the resonant laser as well as the two visible incident frequencies ω_1 and ω_2. The peak powers of the sum-frequency and the third-harmonic are of the same order whereas the incident visible light has an intensity of roughly 6 orders of magnitude larger. The presence of the visible incident light, as well as the vacuum ultraviolet third-harmonic had to be taken into account in the design of the detection system for the vacuum ultraviolet laser-induced fluorescence. The visible incident wavelengths in the beam do not disturb the detection system, provided that the photomultipliers that are used are truly solar blind. It was found that only photomultipliers with Cs-I photocathodes are truly blind for visible light of high intensities, whereas tubes with Cs-Te as photocathode material do register

signals when illuminated with relatively high intensities of visible light (around 440 nm), despite being classified as solarblind in most catalogues[4]. To avoid this problem, only photomultiplier tubes with Cs-I photocathodes were used. On the contrary, the third-harmonic frequency of the resonant dye laser lying near the sum-frequency in the vacuum ultraviolet is detected by the photomultiplier tubes. This has the disadvantage that (without beam separation) the power of the sum-frequency radiation could not be measured separately. In the results presented here the measurements of the vacuum ultraviolet power are measurements of both the power of the sum-frequency and the power of the third harmonic of the resonant dye laser I simultaneously. These vacuum ultraviolet power measurements therefore provide only a qualitative (or, at best, a relative) measure of the power of the sum-frequency radiation that is the quantity of interest. For this reason the experimental spectra were not normalised with respect to the sum-frequency power.

The vacuum ultraviolet signal has usually been measured beyond the vacuum chamber where the experiment takes place. Measured in this way, the vacuum ultraviolet signal was a useful diagnostic tool. It indicates that the vacuum ultraviolet beam is aligned correctly and without obstructions through the experimental volume. It clearly shows unexpected dips in the generated vacuum ultraviolet due to magnesium crystals momentarily obstructing the optical path. Its absorption in the experimental volume when tuned to a strong CO absorption line. The latter serves as indication of the presence of CO in the supersonic jet even if no fluorescence is detected.

As the detection of small signals from rare isotopomers and van der Waals complexes was the aim, the reduction of stray light and other noise on the fluorescence signal was important. For the reduction of stray light, a tailor-made baffle with multiple apertures was inserted in front of the photomultiplier PMT 1. This baffle reduces the solid angle observed by the photomultiplier so that it receives only the light coming from the irradiated region (ca. 10 mm cross section) in the centre of the supersonic jet. A single aperture was inserted in the beam before the reflector in front of the second photomultiplier PMT 2 to reduce reflections from that region back into the vacuum chamber. As far as possible all inner surfaces of the vacuum chamber and light

[4]This observation is verified by the same observation by Mellinger [13, p. 29] (working in the group of Vidal then) who attributed this sensitivity to high intensity visible light to two-photon absorption in the Cs-Te.

baffles have been painted with black absorptive polyurethane low outgassing paint (Aeroglaze Z306). Since the absorptivity of this paint in the vacuum ultraviolet range was not specified, it was tested experimentally in comparison with a clean aluminium surface and commercial mat black spraypaint. With the reflection of the vacuum ultraviolet beam from the clean aluminium taken as 100 % the Aeroglaze paint reduced the reflection to 33 %, whereas commercial black spraypaint still showed 55 % reflection. With these measures implemented, the stray light signal was below the detection limit of the apparatus.

The remainder of the noise on the signal was found to be electronic noise originating mainly from the electronics of the boxcar integrators. It could be reduced somewhat by optimising the position of the gate over which the signal is integrated and by avoiding a gate width smaller than ca. 10 ns. The remaining noise consists of a data-point-to-data-point variation as well as a slow apparently random drift in the dark background level.

4.4 Optogalvanic setup for wavelength calibration

Accurate wavelength calibration of the experimental spectra was very important in the results presented here. Calibration was done in the present experiment using either the vacuum ultraviolet fluorescence lines of CO or the visible optogalvanic lines of neon.

General calibration of the dye laser wavelengths, independent of the sum-frequency generation process, was done by acquiring the optogalvanic spectrum of neon as illustrated in figure 4-12. The setup consists of a see-through hollow cathode lamp filled with neon and the recorded signal is simply a measure of the lamp current measured over a large resistor. The discharge volume inside the hollow cathode is irradiated by a fraction of the beam of the dye laser II split off with a glass window. In the hollow cathode lamp a sustained neon gas discharge exists. The lamp current is a function of the electron density in the discharge which is determined by the total collisional ionisation rate from all atomic energy levels [109]. Whenever the wavelength of the laser irradiating the discharge corresponds to a transition between any two populated atomic or ionic energy levels of neon, the optical pumping perturbs the steady state populations of two or more levels. This causes a temporal change in the ionisation rates leading to a perturbation in the electron density and subsequently in the lamp current. The temporal

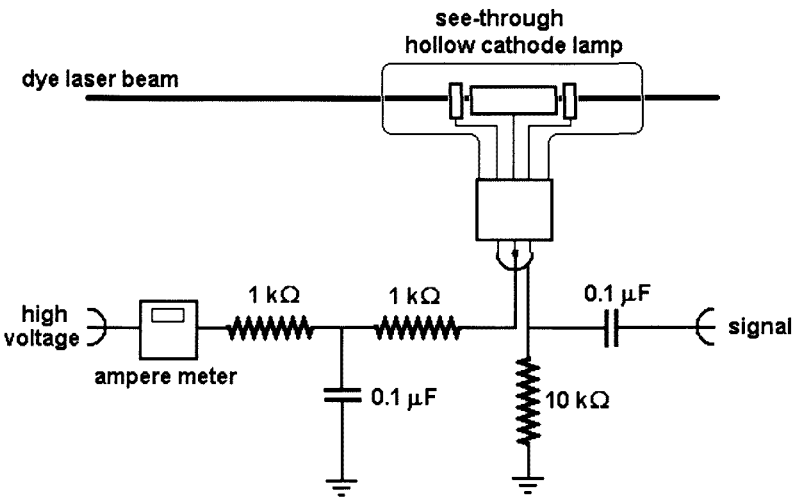

Figure 4-12: Experimental setup for the measurement of an optogalvanic spectrum of neon as the wavelength of the laser irradiating the discharge volume in the hollow cathode lamp is tuned.

increase (or decrease) in the lamp current is integrated by choosing an appropriate boxcar gate (illustrated in figure 4-13) and processed in the same way as the photomultiplier signals. The atlas of optogalvanic transitions of neon of Ashworth and Brown [110] is extremely useful for identifying lines in the optogalvanic spectrum of neon.

The optogalvanic neon spectra could in principle be used to calibrate vacuum ultraviolet laser-induced fluorescence excitation spectra if the fixed resonance wavelength is accurately known and an optogalvanic spectrum of the tuned dye laser is recorded simultaneously with the vacuum ultraviolet spectrum, as illustrated in figure 4-14. This was, however, not done routinely since with only two boxcars available the vacuum ultraviolet power had to be neglected if the optogalvanic spectrum was recorded and secondly the well known $^{12}C^{16}O$ and $^{13}C^{16}O$ lines that were present in all spectra could be used for accurate calibration, as discussed in section 5.2.

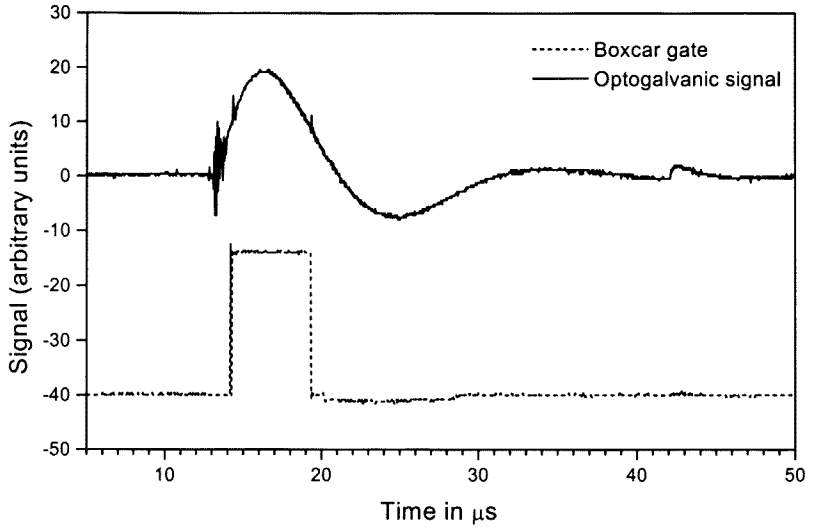

Figure 4-13: A strong optogalvanic signal of neon as displayed on the oscilloscope as well as the boxcar gate over which integration is performed to record the peak height.

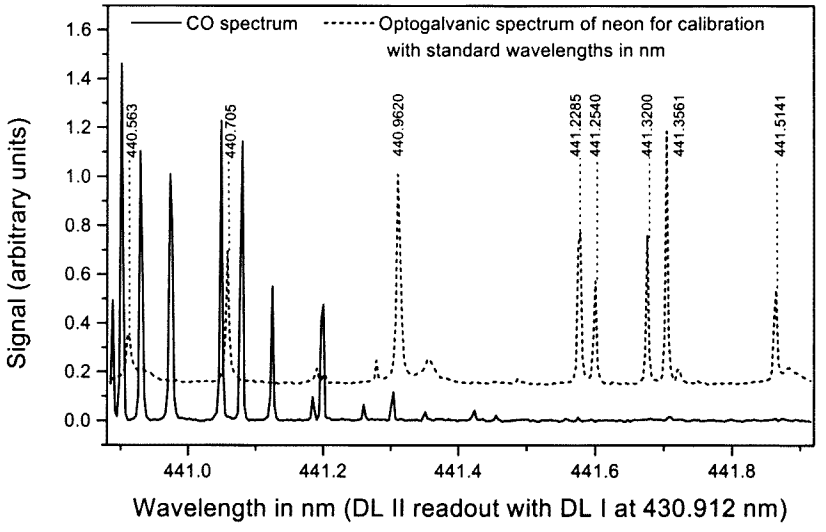

Figure 4-14: Illustration of a part of the CO $A - X$ $(3 - 0)$ band as well as the optogalvanic spectrum of neon as recorded for calibration purposes. The two spectra are recorded simultaneously as function of the dye laser wavelength as given by the readout of the dye laser that is tuned. The known wavelengths of the optogalvanic lines of neon can be used to calibrate the wavelengths of the tuned dye laser. If the fixed resonance wavelength of the other dye laser is known the vacuum ultraviolet wavelength scale can be calibrated from this data.

Chapter 5

Experimental results

The useful and scientifically interesting results that were obtained from the experimental work presented here are as diverse as the physical processes that are combined in this setup. They include general experimental results on flow-cooling in the supersonic jet and the laser-induced fluorescence spectra of CO that were measured under these conditions, the detection of rare isotopomers of CO as well as results on the formation of CO-noble gas van der Waals molecules in the setup.

5.1 Flow cooling in the pulsed supersonic jet

Extensive flow cooling of the CO molecules in the supersonic jet was obtained in the experiment, using either argon or neon as carrier gas. The flow-cooling process in the supersonic jet was investigated, characterised and optimised to yield the desired experimental conditions by analysing the laser-induced fluorescence spectrum of $^{12}C^{16}O$.

In the analysis of the measured spectra, it was assumed that the laser-induced fluorescence excitation spectra represent the absorption spectrum of the molecule well, also in terms of line intensities. Therefore the relative line intensities $I(J', J'')$ of the $A^1\Pi(v' = 3, J') - X^1\Sigma^+(v'' = 0, J'')$ rovibronic lines of the laser-induced fluorescence spectra, each corrected for the degeneracy of the lower level $g(J'')$ and the Hönl-London factor of the transition $S_{J'J''}$ according to

the relation

$$N(v''=0,J'') \propto \frac{I(J',J'')g(J'')}{S_{J'J''}} \tag{5.1}$$

present a good measure of the relative populations of the ground state rotational levels from which they originate [111]. The $A^1\Pi - X^1\Sigma^+$ transition of CO is characterised by $\Delta\Lambda = +1$ and $\Lambda'' = 0$. Substituting these values into the Hönl-London factors taken from Herzberg [35, p. 208], and using $g(J'') = 2J'' + 1$ the expressions for the populations of the R, Q and P branches become

$$\begin{aligned} N^R(v'' &= 0,J'') \propto 4\frac{I^R(J',J'')(2J''+1)}{(J''+2)} \\ N^Q(v'' &= 0,J'') \propto 4I^Q(J',J'') \\ N^P(v'' &= 0,J'') \propto 4\frac{I^P(J',J'')(2J''+1)}{(J''-1)} \end{aligned} \tag{5.2}$$

Under conditions of thermal equilibrium, these relative populations of the rotational levels are related by the Boltzmann relation

$$\frac{N_{J''}}{N_{J''=0}} = (2J''+1)\exp(-\frac{E_{J''}-E_{J''=0}}{kT_{rot}})$$

defining the rotational temperature T_{rot} of the ensemble of molecules. The energy differences $E_{J''} - E_{J''=0}$ between the rotational levels of the $X^1\Sigma^+(v''=0)$ ground state were calculated for $^{12}C^{16}O$ using the molecular constants of the $^{12}C^{16}O$ $X^1\Sigma^+$ state published by Herzberg [35, p. 522], and for the other isotopomers by correcting these constants for the difference in reduced mass according to the relations describing the isotope effect [35, p. 141-145]. The rotational temperature was obtained by plotting the natural logarithm of $N_{J''}/(2J''+1)$ versus $E_{J''} - E_{J''=0}$ (this type of graph will be called a "Boltzmann plot" in the text following). The gradient of the least squares fit through the data points on such a plot is equal to $-1\backslash kT_{rot}$, from which T_{rot} was determined. In the case of a rotational thermal equilibrium among the $v''=0, J''$ manifold the plot is a straight line.

The "typical Boltzmann" plot of a large number of rotational lines from the $A^1\Pi(v'=3) - X^1\Sigma^+(v''=0)$ band of $^{12}C^{16}O$, as illustrated in figure 5-1, clearly deviates from a straight

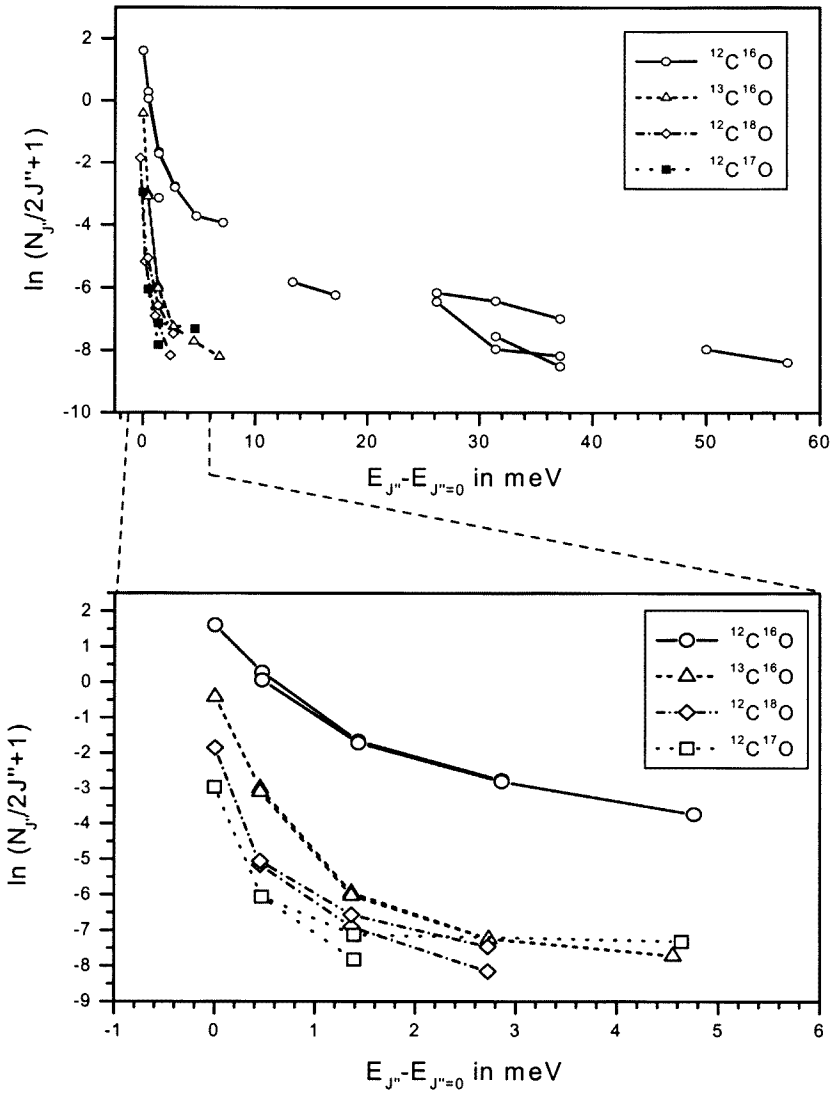

Figure 5-1: Boltzmann plots of the spectroscopically determined relative populations $N_{J''}$ of the lower J'' rotational level, weighed by the $2J''+1$ degeneracy versus the rotational energy of the J'' level.

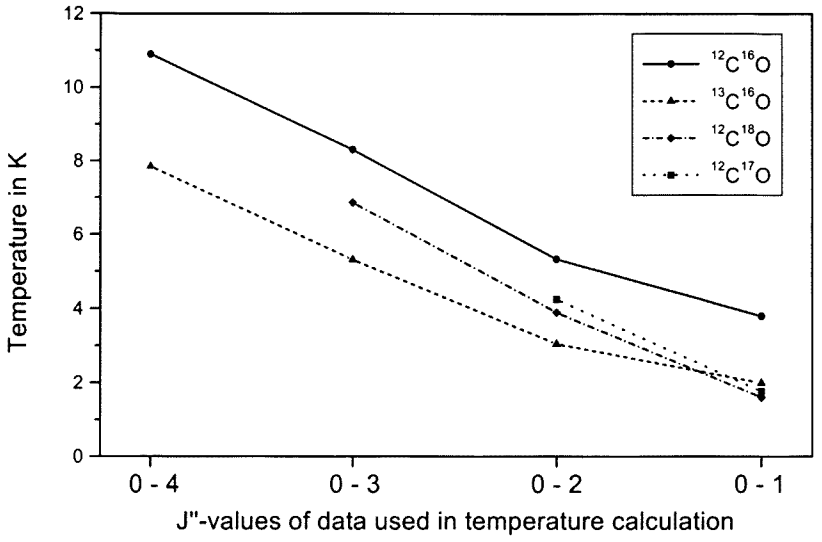

Figure 5-2: Plot of the derived rotational temperatures of 4 CO isotopomers versus the J''-values of the rotational lines from the $A^1\Pi(v' = 3) - X^1\Sigma^+(v'' = 0)$ band that were used to determine each temperature.

line. The populations in the higher rotational levels are in excess compared to the populations expected in these levels when extrapolating the Boltzmann distribution of the lowest few rotational levels. In spite of the fact that strictly speaking no true rotational temperature can be assigned to this non-equilibrium system, it is convenient to assign an estimated experimental rotational temperature even in this case, for the sake of comparing the extent of cooling of different spectra. The experimental rotational temperatures that are referred to in this document are obtained by doing a least squares fit through the data points of the Boltzmann plot belonging to the lowest few rotational levels (as done elsewhere in literature [85]). Usually the data points of lines with $J'' = 0 - 4$, or as many of these as available, have been used in the temperature calculation. At very low temperatures the $J'' = 3$ and 4 line intensities are often too low to yield accurate populations and are then neglected. Even this selection influenced the rotational temperature obtained as illustrated in figure 5-2, showing the general trend that omission of the data with the highest J'' yields a temperature that is lower by about 2 K. Therefore only temperature values calculated from data with the same J'' values can be compared.

An additional factor that has to be considered when calculating temperatures is that the

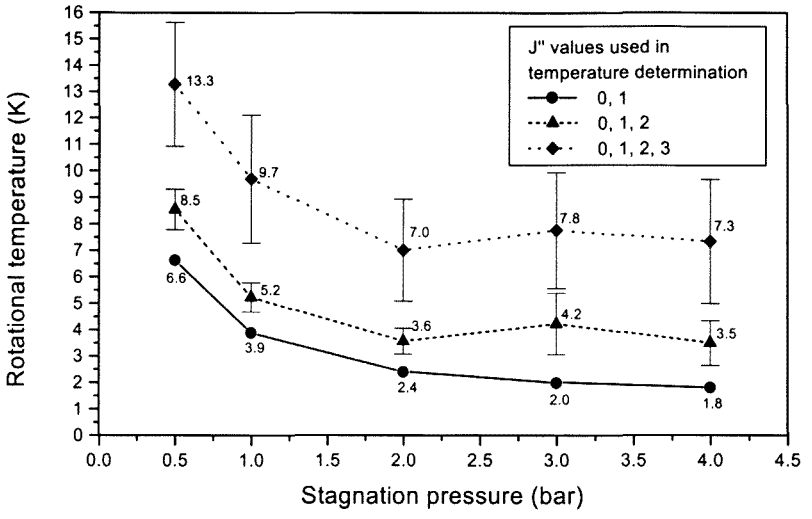

Figure 5-3: Rotational temperature as function of stagnation pressure for a mixture of 0.5 % CO in Ne.

fluorescence of the strongest $^{12}C^{16}O$ lines easily saturates the photomultiplier tube. The onset of saturation could not be seen from the line profiles except for a broadening of the spectral lines, but it influenced the peak heights yielding false (usually too high) temperatures. The absolute CO concentration at which saturation occurred differed for different stagnation pressures, occurring at lower CO concentrations when the stagnation pressure was higher and therefore the temperature lower and the low-J'' transitions very strong. In the experiments, care had been taken to avoid saturation in spectra from which temperatures were determined.

The rotational cooling of the CO molecules in the supersonic jet was controlled by varying the stagnation pressure, the percentage CO in the gas mixture and the carrier gas species.

The effect of the stagnation pressure, illustrated in figure 5-3, is a decreasing rotational temperature in the jet with increasing stagnation pressure. In the plot of the temperatures calculated using only the $J'' = 0, 1$ data, a decrease in the rotational temperature with every increase in stagnation pressure can be seen up to 4 bar. In the plots where higher J'' data were included in the temperature calculation, the same trend can be seen up to about 2 bar, but a further temperature decrease for stagnation pressures higher than 2 bar is not clearly observable. It is obscured by the effect of the non-equilibrium rotational population distribution: the excess

populations in the higher J'' levels have an increasing influence on the modeled experimental temperature the lower the actual temperature is.

The percentage CO[1] in the expanding gas mixture has been found to influence the rotational temperature reached in the jet. The results illustrated in figure 5-4 for two different stagnation pressures shows a trend that the rotational temperature in the jet increases with an increasing percentage CO in the gas mixture. The maximum percentage CO of which the experimental rotational temperature could be obtained with reasonable accuracy was limited by the onset of saturation of the strongest CO lines.

The third parameter that could be used to control the extent of flow cooling of the CO molecules in the jet is the choice of the carrier gas species. For $^{12}C^{16}O$ significantly lower rotational temperatures were observed when using neon as carrier gas: the rotational temperature of the $^{12}C^{16}O$ molecules with neon as carrier gas was on average about $7 - 10$ K lower than in an argon expansion at $3 - 4$ bar stagnation pressure. This effect was smaller for the heavier CO isotopomers, as illustrated in figure 5-5. The relative temperatures of the different CO isotopomers flow-cooled in neon and argon are discussed further in section 6.1.

Important results on the temporal characteristics of the pulsed jet were obtained from the so-called delay scans described in section 4.2. A delay scan shows the temporal development of the fluorescence signal of a single rovibronic transition over the period of the gas pulse. It contains not only information on the temporal changes in the gas density as the valve opens and closes, but also on the changes in the rotational temperature of the CO over the period of the gas pulse. If delay scans are measured at a series of CO rovibronic lines (for example the $Q(1)$, $Q(2)$, $Q(3)$, $Q(4)$ lines of the $^{12}C^{16}O$ isotopomer) the average temperature profile of the gas pulse can be calculated in the usual manner for each data point on the delay scan. Figure 5-6 illustrates the typical results of a set of delay scans. Figure 5-6 (a) shows the development of the fluorescence signals of four Q lines of $^{12}C^{16}O$ and figure 5-6 (b) the rotational temperatures calculated from these fluorescence signals at 0.1 ms time intervals. The rotational temperature is found to decrease rapidly as the expansion develops and reaches its minimum value about $0.3 - 0.4$ ms after the valve started to open. The temperature gradually increases again towards

[1] The percentage CO was based on partial pressures at room temperature: percentage CO = (partial CO pressure)/(total stagnation pressure)

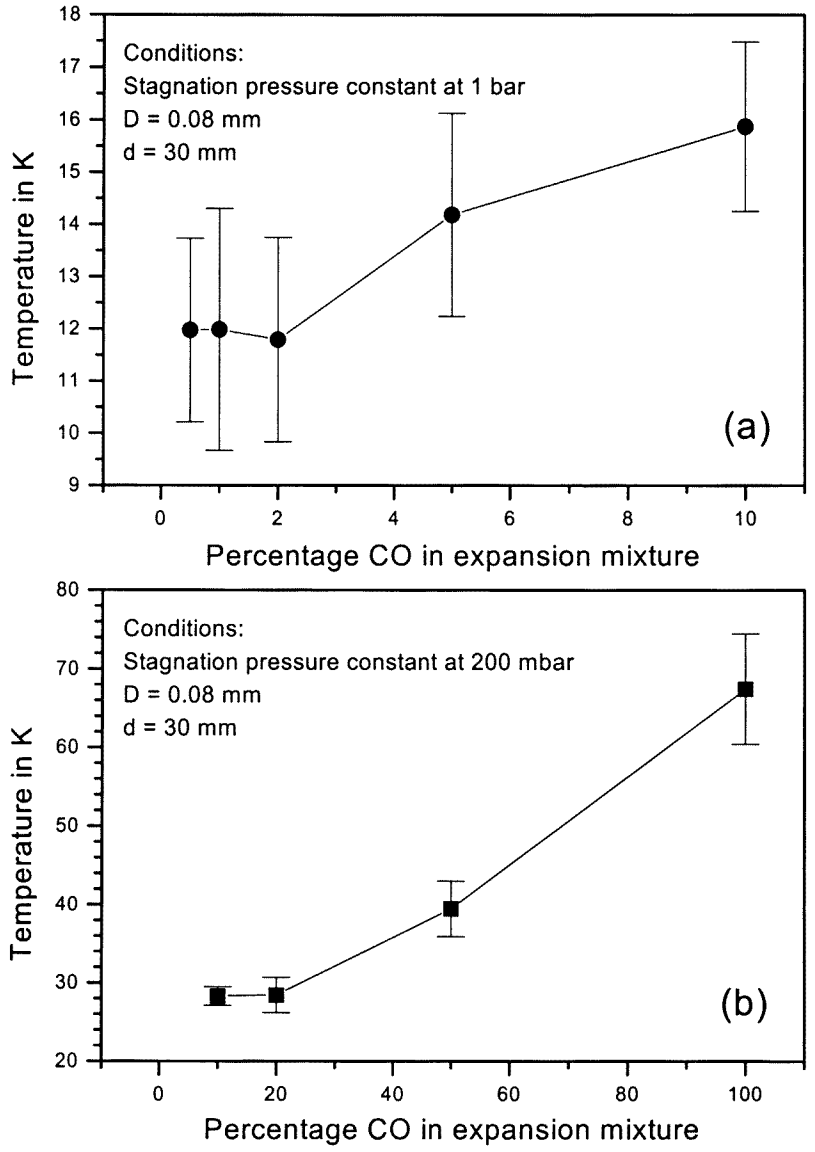

Figure 5-4: Plot of the rotational temperature of $^{12}C^{16}O$ in a flow-cooled CO sample in an argon jet as a function of the percentage of CO in the CO-Ar gas mixture for stagnation pressures of (a) 1 bar and (b) 200 mbar.

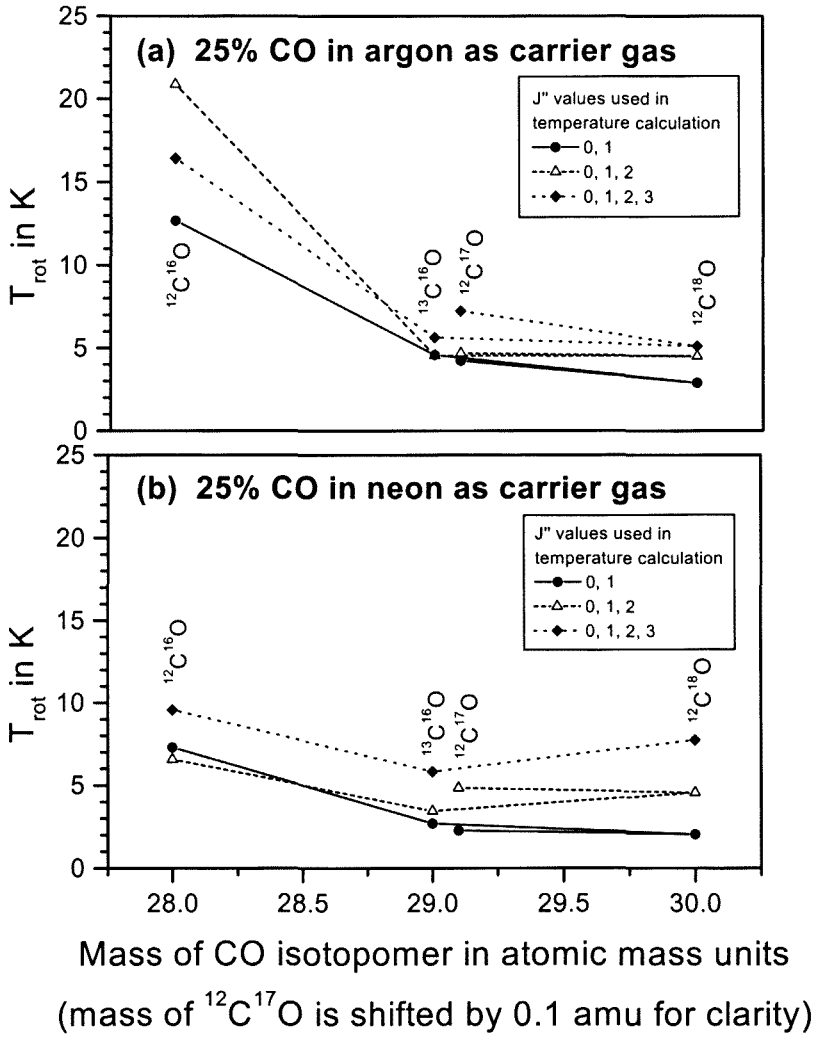

Figure 5-5: Rotational temperatures of the four observable CO isotopomers reached by flow-cooling in (a) an argon jet and (b) a neon jet, with 25 % CO in the gas mixture and a stagnation pressure of 4 bar.

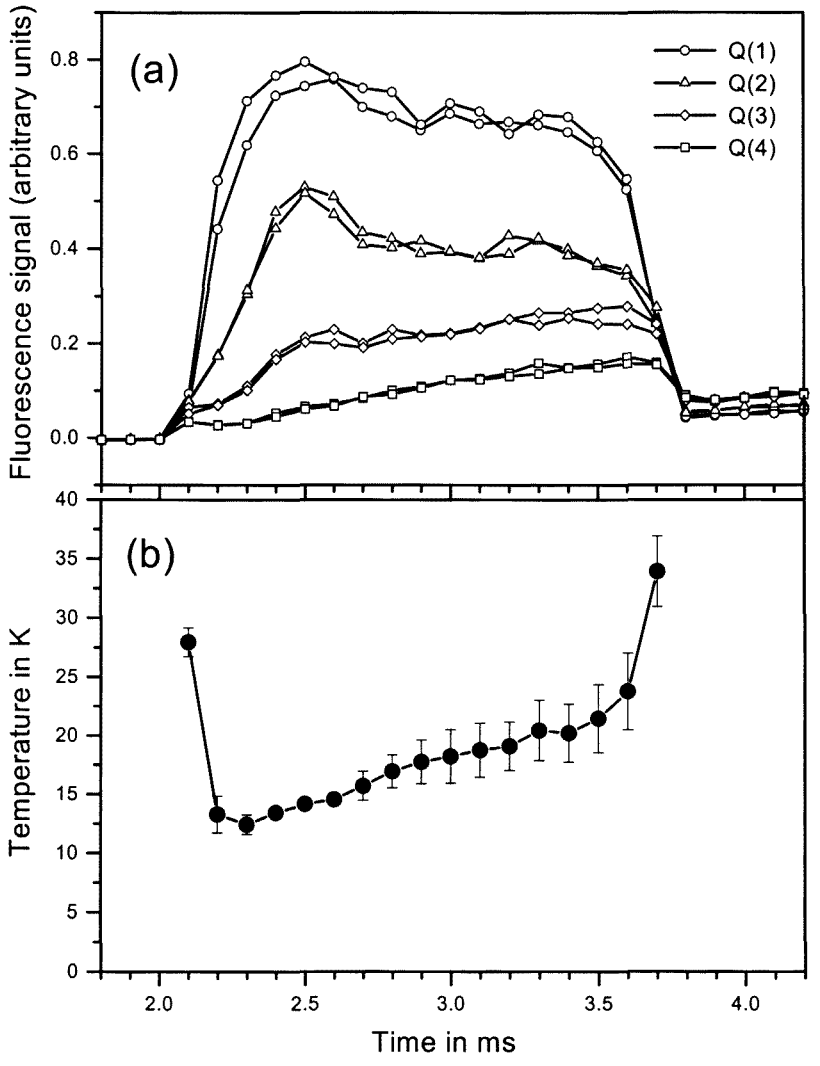

Figure 5-6: Delay scans (a) and the resulting temperature profile of a gas pulse (b) under the conditions of 4 bar stagnation pressure and gas mixture of 2.5 % CO in Ar. All four rotational lines show in the upper graph - $Q(1)$, $Q(2)$, $Q(3)$ and $Q(4)$ - were used to determine the rotational temperature profile plotted in the lower graph.

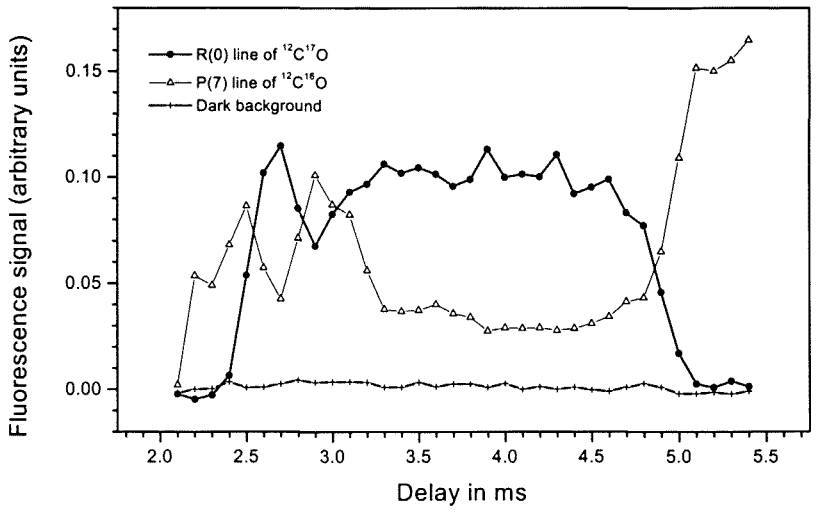

Figure 5-7: Delay scans over the $R(0)$ line of $^{12}C^{17}O$ and the neighbouring $P(7)$ line of $^{12}C^{16}O$. The difference between the delay scan profiles of the relatively "hot" $P(7)$ line - showing high intensity in the hot background gas after the gas pulse has passed - and the "cold" $R(0)$ line - showing maximum fluorescence in the flow-cooled gas pulse - facilitated the identification of the lines.

the end of the gas pulse. The gradual increase in the rotational temperature during the gas pulse is generally considered to be caused by an increase in the background pressure in the vacuum chamber on that time scale. For most experiments, where low temperatures and minimal disturbance in the jet were the desired conditions, the delay was chosen to work at that point in the beginning of the gas pulse where the rotational temperature reaches its minimum value. Under some experimental conditions, the delay scans showed disturbance of the rotational level populations during the gas pulse, as will be discussed in section 5.4.

Delay scans could be used as a valuable diagnostic tool, simply by distinguishing between "cold" and "hot" spectral features. "Cold" spectral features have larger intensities in the flow-cooled jet than in the background gas and "hot" spectral features have larger intensities in the room temperature background gas filling the sample volume after the pulsed valve has closed again than in the cooled gas pulse. Figure 5-7 shows delay scans over two weak spectral features near 144.84 nm that helped in identifying these features as the "cold" $R(0)$ line of $^{12}C^{17}O$ and the relatively "hot" neighbouring $P(7)$ line of $^{12}C^{16}O$.

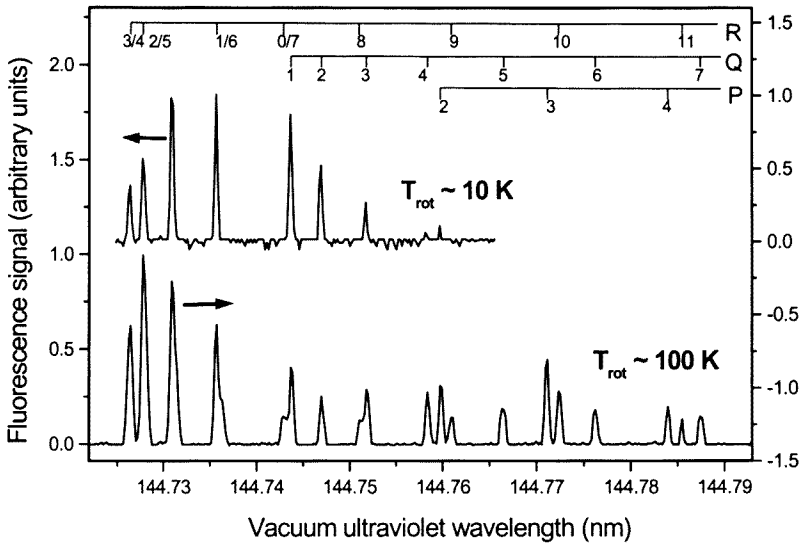

Figure 5-8: Compilation of two experimental spectra of the $A(v' = 3) - X(v'' = 0)$ band of $^{12}C^{16}O$ at two different rotational temperatures, ca. 10 K and 100 K respectively, in a supersonic jet. Note that the relatively large noise seen in the background spectrum of the top spectrum is not typical.

By using the experimentally determined rotational temperatures and the delay scan method, the experimental conditions in the free supersonic jet were characterised and optimised. Experimental conditions using a stagnation pressure of $3-4$ bar, a gas mixture of $0.5-1$ % CO in the carrier gas, an orifice diameter of 0.8 mm and nozzle-to-laser distance of 20 or 30 mm yielded flow-cooling to temperatures of a few Kelvin for the recording of low temperature laser-induced fluorescence spectra.

5.2 Laser-induced fluorescence excitation spectrum of flow-cooled CO

Rotationally resolved spectra of the $A(v' = 3) - X(v'' = 0)$ band of $^{12}C^{16}O$ at low rotational temperatures, from room temperature down to a few kelvin, were obtained by laser-induced fluorescence excitation spectroscopy of a natural CO sample in the supersonic jet. Two such spectra measured at different temperature conditions are illustrated in figure 5-8. The low noise

level of the spectra and characteristic (non-equilibrium) population distribution over rotational levels in the flow-cooled gas (as mentioned in the previous section) allowed the detection of the rotational lines of $^{12}C^{16}O$ up to $J'' = 19$ in the R branch, $J'' = 15$ in the Q branch and $J'' = 12$ in the P branch even at rotational temperatures as low as ca. 10 K. The only rotational lines in this range that could not be resolved are the $R(4 \leq J'' \leq 9)$ lines, due to overlap with the stronger $R(J'' = 0 - 3)$ and $Q(J'' = 1 - 3)$ lines.

Excellent signal to noise ratios were obtained for the strong $^{12}C^{16}O$ lines, often in excess of 100 and up to 500 for the $J'' \leq 1$ lines. The peak heights of the lines are dependent on the vacuum ultraviolet intensity, the partial CO pressure in the jet, as well as on the temperature that determines the population of individual levels. Low temperature was clearly observed to enhance the peak height of the $J'' \leq 1$ lines with the effect that a very low detection limit for $^{12}C^{16}O$ was achieved, easily 50 parts per million. The lowest concentration of any of the CO isotopomers in the gas mixture that could still be detected by its $R(0)$ line in this experimental setup was estimated to be about 3 parts per million for $^{12}C^{17}O$.

The second-most dominant feature of the spectra was the $A(v' = 3) - X(v'' = 0)$ band of the $^{13}C^{16}O$ isotopomer shifted by 85.4 cm^{-1} towards the longer wavelengths relative to the $^{12}C^{16}O$ band (see figure 5-9). Of the $^{13}C^{16}O$ band the lines of the R branch up to $J'' = 3$, the Q branch up to $J'' = 5$ and the P branch up to $J'' = 2$ could be detected clearly.

The $^{12}C^{16}O$ and $^{13}C^{16}O$ spectral lines were used as standard lines for the calibration of the experimental spectra. The non-equilibrium population of the higher J'' rotational levels had the advantage that a large number of $^{12}C^{16}O$ lines, distributed over the whole wavelength range that was investigated, were available to use for calibration of the spectra. To improve the accuracy of the calibration towards longer wavelengths, where the $^{12}C^{16}O$ lines are more widely spaced, the lines of $^{13}C^{16}O$ were also used as standard lines. The wavelength data of $^{12}C^{16}O$ and $^{13}C^{16}O$ published by Morton and Noreau [11] and Tilford and Simmons [36] were used. When the wavelengths of the $A(v' = 3) - X(v'' = 0)$ band of $^{12}C^{16}O$ published by Tilford and Simmons are compared to those published by Morton and Noreau the wavelengths of Tilford and Simmons are shifted by 4.5×10^{-4} nm on average. For calibration of our spectra the wavelengths of Morton and Noreau (which include the $^{13}C^{16}O$ transitions) were used as standards as far as possible. For the higher rotational lines of $^{12}C^{16}O$, not given by Morton and

Table 5.1: Experimental wavelength data of $^{12}C^{17}O$ and $^{12}C^{18}O$.

A$(v' = 3) - $**X**$(v'' = 0)$ **Transition**	**Experimental** λ **(nm)**	**Signal to noise ratio**	**Line width (nm)**
	$^{12}C^{18}O$		
$R(1)$	$144.9249 \pm (2 \times 10^{-4})$	20	...
$R(0)$	$144.9295 \pm (2 \times 10^{-4})$	60	4×10^{-4}
$Q(1)$	$144.9373 \pm (2 \times 10^{-4})$	19	4×10^{-4}
$Q(2)$	$144.9404 \pm (2 \times 10^{-4})$	3	6×10^{-4}
	$^{12}C^{17}O$		
$R(3)$	$144.8283 \pm (4 \times 10^{-4})$	~ 1	...
$R(4)$	$144.8297 \pm (4 \times 10^{-4})$	~ 1	...
$R(0)$	$144.8375 \pm (2 \times 10^{-4})$	20	5×10^{-4}
$Q(1)$	$144.8453 \pm (2 \times 10^{-4})$	7	5×10^{-4}
$Q(2)$	$144.8484 \pm (4 \times 10^{-4})$	~ 1	...
$Q(3)$	$144.8532 \pm (4 \times 10^{-4})$	~ 1	...

Note - The $R(1)$ line of $^{12}C^{17}O$ and the $R(2)$ line of $^{12}C^{18}O$ were not detected due to overlap with the stronger $P(7)$ line of $^{12}C^{16}O$ and the $Q(1)$ line of $^{13}C^{16}O$ respectively.

Noreau, the wavelengths of Tilford and Simmons were used after correction for the apparent shift.

Additional to the already well-studied $^{12}C^{16}O$ and $^{13}C^{16}O$ rotational lines, the spectra yielded spectral data on the naturally rare isotopomers $^{12}C^{18}O$ and $^{12}C^{17}O$ as discussed in more detail in the following section.

5.3 Detection of rare isotopomers of CO

Six individual rotational lines of the $A(v' = 3) - X(v'' = 0)$ vibronic band of $^{12}C^{17}O$, as well as four lines of the $^{12}C^{18}O$ band were detected. A typical spectrum containing these lines is illustrated in figure 5-9. In table 5.1 the wavelength data obtained from these measurements are

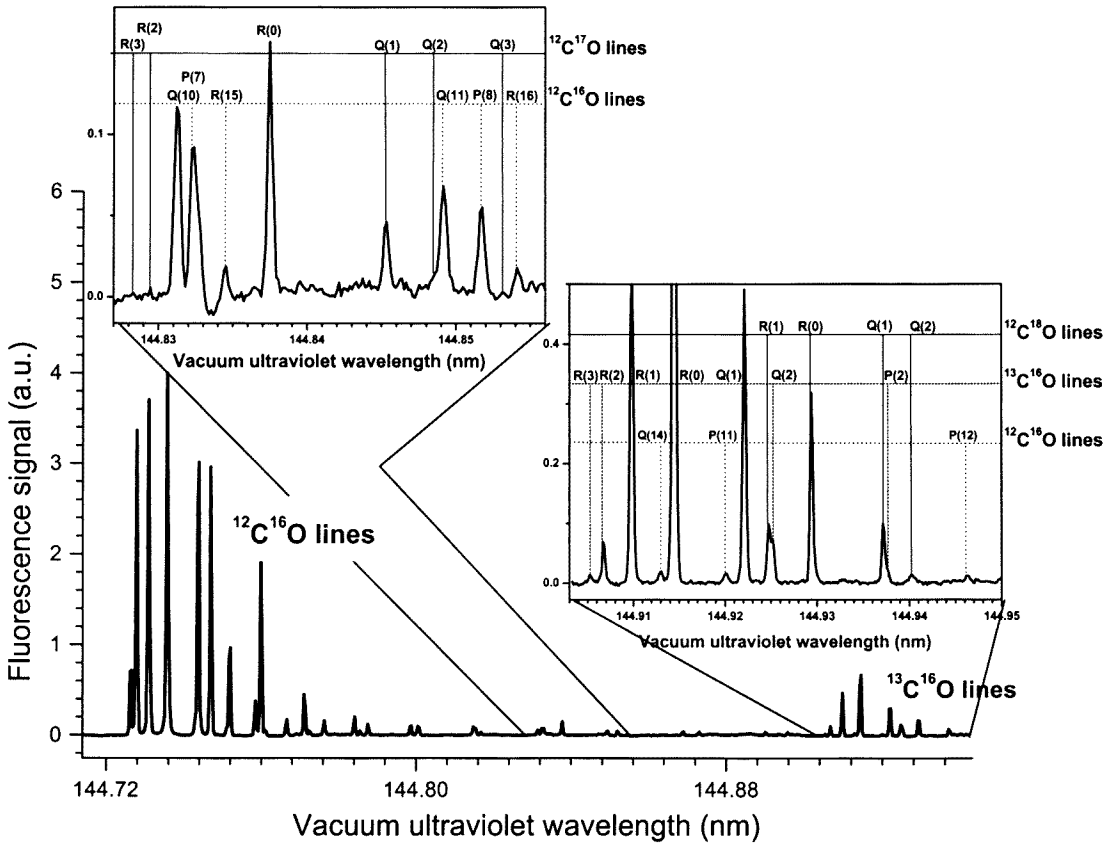

Figure 5-9: Overview of the complete experimental laser induced fluorescence excitation spectrum of the $A(\upsilon' = 3) - X(\upsilon'' = 0)$ band of four CO isotopomers. The enlarged inserts show the observable $^{12}C^{18}O$ and $^{12}C^{17}O$ lines.

Table 5.2: Calculated and experimental values of the vibrational isotopic shift of $^{13}C^{16}O$, $^{12}C^{18}O$ and $^{12}C^{17}O$.

Isotopomer	Calculated value (cm^{-1})	Experimental value (cm^{-1})
$^{12}C^{17}O$	48.3	48.7 ± 0.2
$^{13}C^{16}O$	84.7	85.4 ± 0.2
$^{12}C^{18}O$	91.9	92.6 ± 0.2

Note - The vibrational isotopic shift is the energy difference in wavenumbers between the band origin of the CO isotopomer and that of $^{12}C^{16}O$.

summarised. In general it was possible to detect the $Q(J'')$ and $R(J'')$ transitions that originate from rotational levels with $J'' \leq 3$; the $J'' = 0$, 1 transitions with good signal to noise ratio due to the low temperature. The temperature associated with the line intensity ratios of these lines is ca. 4 ± 1 K. The $R(1)$ line of $^{12}C^{17}O$ and the $R(2)$ line of $^{12}C^{18}O$ were not detected due to overlap with the stronger $P(7)$ line of $^{12}C^{16}O$ and the $Q(1)$ line of $^{13}C^{16}O$ respectively. The $R(0)$ and $R(1)$ lines of $^{12}C^{18}O$ overlap with the $Q(3)$ and $Q(2)$ lines of $^{13}C^{16}O$ respectively, but their wavelengths could be obtained from the spectrum. The $R(1)$ line of $^{12}C^{18}O$ and $Q(2)$ line of $^{13}C^{16}O$ are of the same intensity and were therefore resolved in the spectrum, whereas the intensity of the $R(1)$ line of $^{12}C^{18}O$ is so much larger than that of the $Q(3)$ line of $^{13}C^{16}O$ at the low temperature that the contribution of $Q(3)$ to the spectral feature could be neglected. The hyperfine splitting of the $^{12}C^{17}O$ lines [112] is not observable in the spectra since the splitting is much smaller than the experimental line widths of the rovibronic transitions.

The spectral lines of the $^{13}C^{16}O$, $^{12}C^{18}O$ and $^{12}C^{17}O$ isotopomers were positively identified and assigned by comparing the experimental wavelength positions of these lines with calculations of the isotopic shift using the equations from Herzberg [35, p. 141]. The agreement between the calculated and experimental values of the vibrational isotope shifts of $^{13}C^{16}O$, $^{12}C^{18}O$ and $^{12}C^{17}O$, as given in table 5.2, verified the assignment of the isotopomeric spectra.

The data of four different spectra, all similar to that of figure 5-9, and each containing the observable lines of both $^{12}C^{17}O$ and $^{12}C^{18}O$, were combined to obtain the experimental wavelengths data in table 5.1. The wavelength scales of these spectra were calibrated using the

wavelength data of $^{12}C^{16}O$ and $^{13}C^{16}O$ published by Morton and Noreau [11] and Tilford and Simmons [36] as discussed in the previous section. The bandwidth of the vacuum ultraviolet radiation is the physical factor determining the line widths and therefore the precision of the measured wavelengths. The errors to the wavelength values indicated in table 5.1 are equal to the average standard deviation of the least squares calibration fits on the four spectra, with the exception of the weakest lines where the uncertainty was estimated to be larger.

It was not attempted in this experiment to observe lines of the $^{13}C^{17}O$ and $^{13}C^{18}O$ isotopomers. The possibility to do such measurements is discussed in section 7.2.

5.4 Evidence for condensation in the flow-cooled gas mixture

The experimental investigation regarding CO van der Waals complexes was aimed at the detection of the electronic excitation spectrum of CO-Ar (or CO-Ne) complexes when exciting an $A(v' = 3, J') - X(v'' = 0, J'')$ transition of the CO component of the complex (also see discussion in section 2.4). The first crucial step towards the detection of the spectral features of the complex is to obtain and optimise the experimental conditions in the supersonic jet in order to obtain extensive formation of CO van der Waals complexes. To do this optimisation, a (semi-)quantitative measure of the concentrations of van der Waals complexes present in the jet is necessary. Since the spectral features of these complexes were not readily detectable, an indirect measure of the extent of complex formation had to be used.

The optimal conditions for the formation of CO van der Waals complexes in our experimental setup were investigated using indirect detection methods that made use of the readily detectable CO monomer signals and provided semi-quantitative evidence for the formation of CO van der Waals complexes in the jet. The methods involved the assumption that, under the condition that the CO number density in the sample volume is the limiting quantity determining the intensity of the fluorescence (i.e. with low percentage CO in the gas mixture), extensive formation of CO van der Waals complexes will lead to a decrease in the CO monomer population in the jet and therefore to a decrease in the CO monomer fluorescence signal.

The observation that is considered most direct evidence for extensive complex formation is the strong overall decrease in the $^{12}C^{16}O$ fluorescence signal observed in a neon jet at high

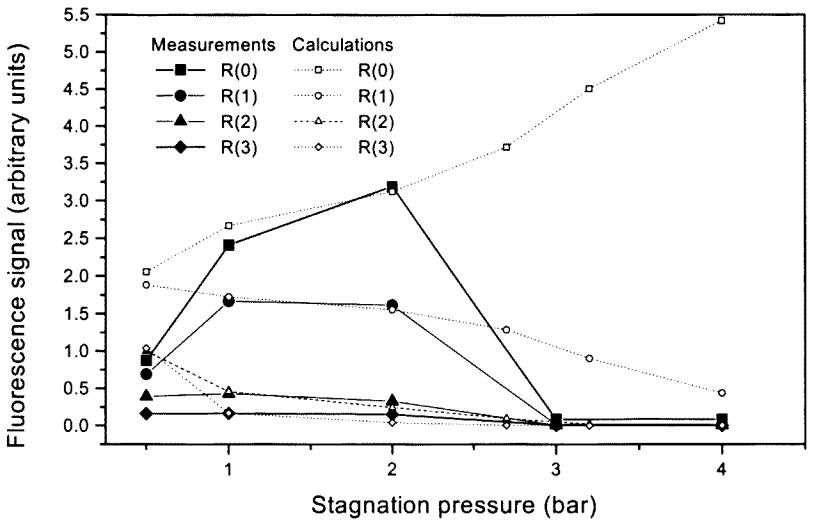

Figure 5-10: Fluorescence signals of the $R(J'' = 0 - 4)$ lines of $^{12}C^{16}O$ as a function of the stagnation pressure. The experimental measurements were done in a gas mixture of 1 % CO in neon. Note the dramatic decrease in all signals at pressures higher than 2 bar. The calculated values reflect the signal vs. stagnation pressure curve that would be expected from the experimentally determined rotational temperature at each stagnation pressure.

stagnation pressure with a low percentage CO in the gas mixture. The experiment of which the results are illustrated by figure 5-10 involved a series of spectra of the $R(J'' = 0 - 4)$ lines of $^{12}C^{16}O$ with a gas mixture of 1 % CO in neon. The stagnation pressure was decreased stepwise from 4 bar to 0.5 bar, recording a spectrum at each stagnation pressure. It was observed in a reproducible manner that the overall intensity of the CO spectrum increased by about an order of magnitude as the stagnation pressure was decreased from 4 bar to 2 bar. In the curves plotted in figure 5-10 the discontinuous decrease occurs in a pressure range between 3 and 2 bar already; in other similar experiments it took place in a pressure range slightly higher than 3 bar. The discontinuity in the signal intensity could not be explained by a change in the vacuum ultraviolet intensity or by a temperature related effect. In the series of scans, the temperature increases gradually with decreasing stagnation pressure in spite of the discontinuity in the overall intensities. No other artificial cause for the observation could be established.

The second interesting but more speculative evidence for condensation in the supersonic jet is the observation of a "dip" in the delay scan under certain conditions. The dip in the

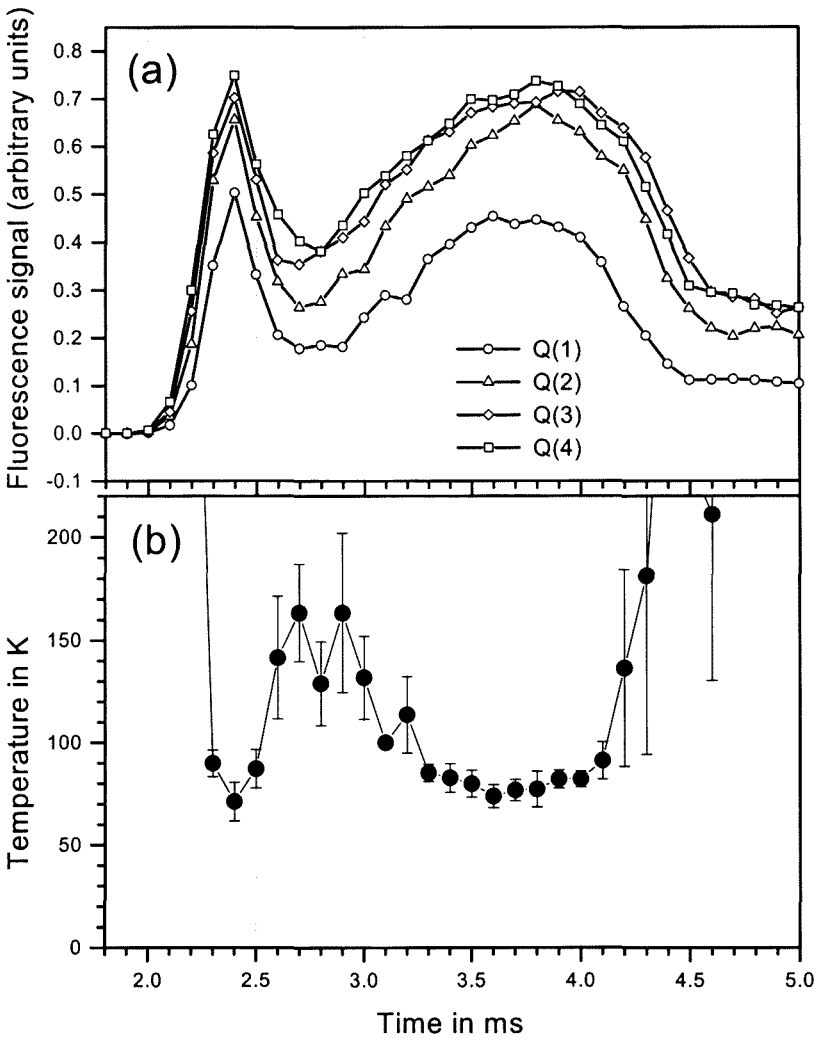

Figure 5-11: Delay scans (a) and the resulting temperature profile of a gas pulse (b) when allowing pure CO gas to expand into vacuum from a stagnation pressure of 100 mbar.

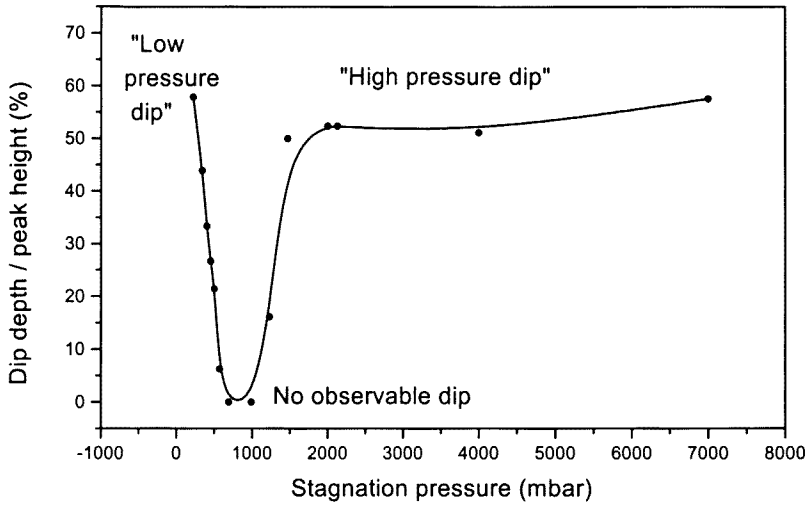

Figure 5-12: Qualitative illustration of the change of the depth of the observed dip in the delay scans as the stagnation pressure is increased by the addition of argon gas. The partial CO pressure in the gas mixture is constant at 20 mbar.

delay scan was most pronounced when expanding pure CO from a low stagnation pressure. Figure 5-11 illustrates an example of a delay scan with a pronounced dip. (Compare it with the profile in figure 5-6.) The fluorescence signals of all lines show a significant dip at about $0.7 - 0.9$ ms after the valve started to open (at delay values of $2.7 - 2.9$ ms in figure 5-11). In the temporal region of the dip, the calculated rotational temperature values are higher, as well as large uncertainties. This clearly indicates disturbance in the equilibrium conditions in the jet. The same type of dip was observed under different experimental conditions of stagnation pressure and percentage CO in the jet, given that the fluorescence line that was observed did not show saturation. Saturation of the sensitive detection system, yielding in the delay scans a flat topped profile and the loss of detail, occurred easily when observing a low rotational line (such as the $R(0)$ line).

The occurrence of the dip under different conditions of stagnation pressures and gas mixtures was investigated systematically in an attempt to identify the cause of the dip. If a constant CO partial pressure of 20 mbar was used but the total stagnation pressure was increased by adding more argon to the expansion mixture, the dip showed interesting behaviour as illustrated in figure 5-12. It showed a local maximum value when 20 mbar pure CO was expanded. As argon

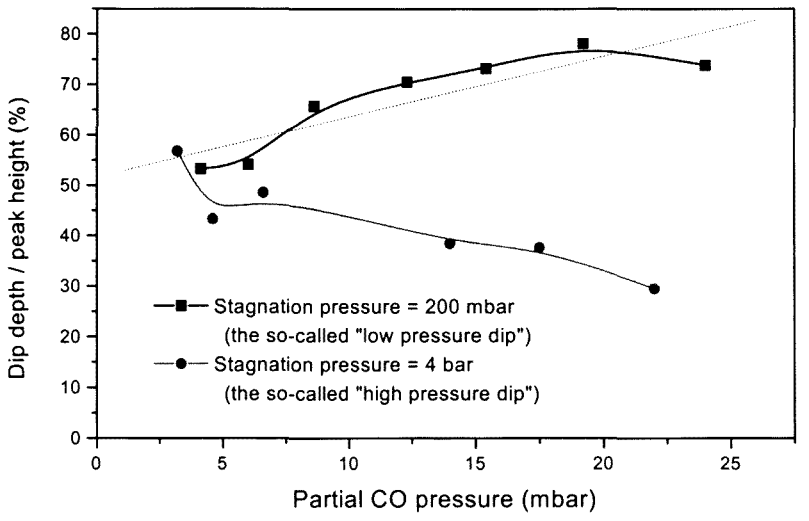

Figure 5-13: Qualitative illustration of the influence of the partial CO pressure in the gas mixture (approximately proportional to the CO concentration in the sample volume) on the depth of the observed dip in the delay scans at stagnation pressures of 200 mbar and 4 bar.

is added to increase the stagnation pressure, the dip depth (measured relative to the maximum signal height) decreases until the dip vanishes completely at about 600 mbar stagnation pressure. As the stagnation pressure is increased beyond 1 bar, a dip becomes observable again, remaining observable up to the maximum applied pressure of 7 bar.

The response of the "low pressure dip" at 200 mbar stagnation pressure and the "high pressure dip" respectively to the percentage CO in the gas mixture at 4 bar stagnation pressure was subsequently investigated. In this experiment the stagnation pressure was constant but the Ar-CO ratio in the gas mixture and therefore the partial CO pressure was adjusted. The results illustrated in figure 5-13 show that the dips at the two different stagnation pressure ranges did respond slightly differently to a change in the partial CO pressure in the mixture. The "low pressure dip" increased in depth as the CO pressure was increased whereas the "high pressure dip" decreased slightly in depth. Note that the data plotted in figures 5-12 and 5-13 are qualitative of nature since the quantities "dip depth" and "peak height" cannot be determined in a rigorous way. The "peak height" should actually be the maximum height that the signal would have in the absence of a dip, but since this cannot be determined, the signal height at the highest point in the delay scan, usually the peak at the beginning of the gas pulse before

the dip, is used. The "dip depth" values are obtained by subtracting the signal height at the lowest point in the dip from this "peak height" value.

Although these results suggest rather than prove the formation of CO-containing van der Waals complexes in the supersonic jet, they strongly indicate that some form of condensation does occur in the sample. The dip in the delay scans suggested that the optimal timing when searching for signals from the condensation products is $0.5 - 0.9$ ms after the valve started opening. The conditions under which evidence of condensation was observed in our experiments, as well as the optimum conditions reported in literature for the formation of CO-Ar complexes in a supersonic jet were considered in choosing the conditions to be used in searching for the electronic excitation spectrum of CO-Ar.

5.5 Search for the electronic excitation spectrum of CO-Ar

Extensive spectra were recorded in search of features of the electronic excitation spectrum of CO-Ar or CO-Ne van der Waals complexes. The spectra were taken under conditions that are very similar to the optimal conditions for formation of the CO-Ar complex reported in literature (as compared in section 6.3): stagnation pressure of $3 - 4$ bar, gas mixture containing $25 - 30$ % CO, nozzle orifice diameter of 0.8 mm, nozzle to laser source of 20 mm, 1 Hz repetition rate. Spectra were recorded over a large wavelength region around the $A^1\Pi(v' = 3) - X^1\Sigma^+(v'' = 0)$ band of $^{12}C^{16}O$ using argon and neon as carrier gas in respective scans. The spectral ranges that were investigated are given in table 5.3. The laser was timed to probe the gas pulse ca. $0.5 - 0.6$ ms after the valve started opening, as suggested by the dip observed in the delay scans.

Typical spectra measured in this spectral range are illustrated by the examples in figure 5-14. No distinct reproducible spectral features apart from those of the isotopomers of CO could be detected. The background signal showed some broad features, but repeated scans showed that this slow variation of the background signal was not reproducible. The slow variation appears to be an artifact of the data acquisition system - probably due to the drift of the boxcar output signal.

The laser-induced fluorescence excitation spectra were found to have a good detection limit for fluorescing species producing distinct narrow fluorescent lines. For comparison, a few lines

Table 5.3: Spectral ranges investigated for spectral features of CO van der Waals complexes.

Gas mixture	**Range in nm**	**Range in cm^{-1}**	**Range in cm^{-1} relative to $^{12}C^{16}O$ band head**
25 % CO in argon	144.61 - 145.09	68922.4 - 69151.8	−167 - +62.2
25 % CO in neon	144.61 - 145.05	68942.9 - 69151.8	−146 - +62.2

of $^{12}C^{17}O$ are show in figure 5-14. From the intensity of the $^{12}C^{17}O$ lines and the natural abundance of ^{17}O in nature (4.22×10^{-4} % - see table 2.1) the detection limit of the system for fluorescing species could be estimated. It was found to be about 3 parts per million[2]. With this detection limit, the detection system should be sufficiently sensitive for the detection of small populations of CO van der Waals complexes in a supersonic jet if the complexes have fluorescence lines of the same nature in this region. However, if the fluorescence of the complex is quenched by alternative relaxation channels or if the excitation lines of the complexes would be significantly broadened by a factor of 5 or more, these broadened lines will vanish in the fluctuation of the background signal. This will be discussed in more detail in section 6.3.

[2]A detection limit of 3 parts per million in this setup is equal to a partial pressure of 0.012 mbar of the particular species in 4 bar of stagnant gas prior to expansion.

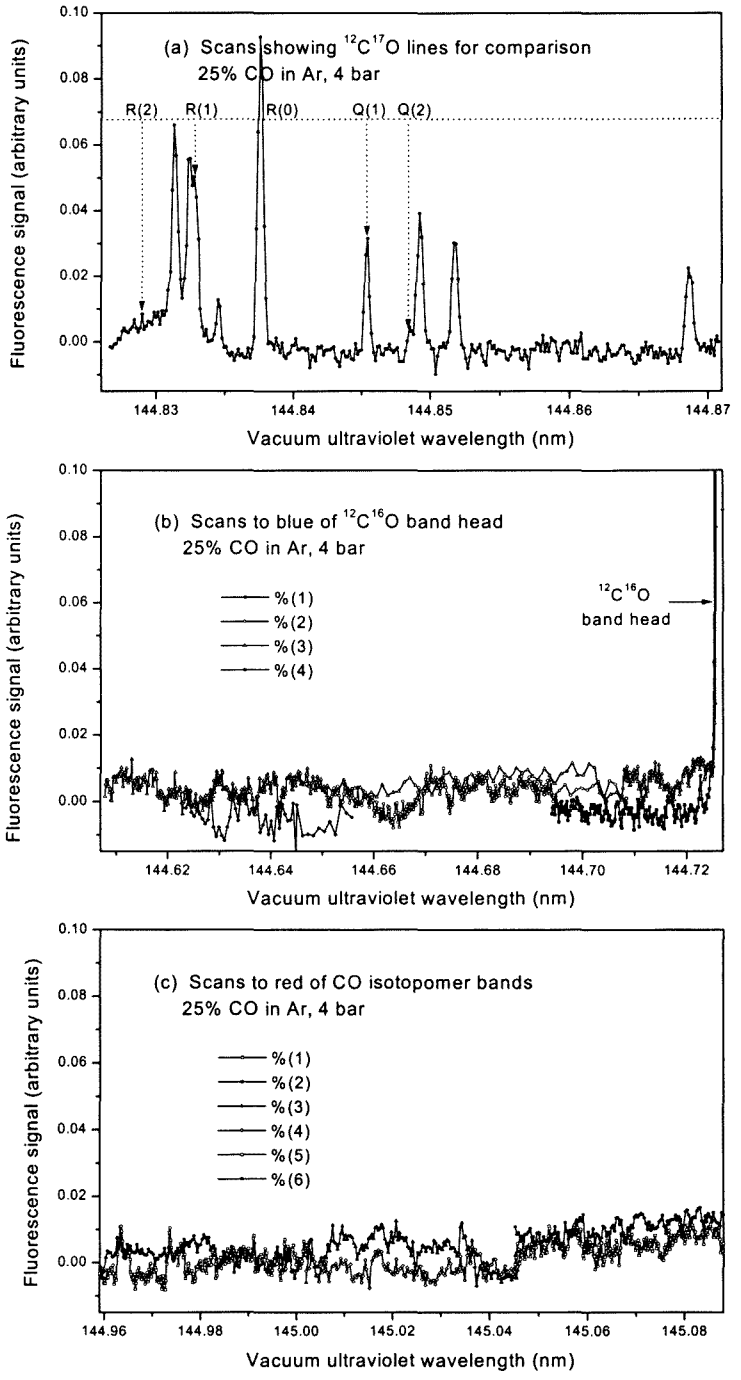

Figure 5-14: Examples of the results of scans over regions (b) blue and (c) red from the $^{12}C^{16}O$ band, i.e. regions free of CO monomer bands but where spectral features of CO-Ar could be expected. No spectral features were observed. For comparison of the vertical scale, a scan over the $^{12}C^{17}O$ lines is shown in (a).

Chapter 6

Discussion

The experimental results on the band structure of the $A^1\Pi(v' = 3) - X^1\Sigma^+(v'' = 0)$ band of CO, that were obtained in the present experiment, correspond well to general theory of diatomic molecules [35]. R, Q and P branches were observed, with the P branch of lower intensity than the R branch, as expected from the Hönl-London factors for a $^1\Pi - ^1\Sigma$ transition with $\Delta\Lambda = +1$ [35, p. 207]. The theoretical prediction that the Q branch should have approximately double the intensity of the other branches is not observed in our experimental spectra where the Q and R branches have similar intensities.

The $A^1\Pi(v' = 3) - X^1\Sigma^+(v'' = 0)$ band was chosen for its scientific relevance, as well as technical considerations. The $A^1\Pi - X^1\Sigma^+$ transition is a dominant and well-studied spectral system of $^{12}C^{16}O$ of which the $A^1\Pi(v') - X^1\Sigma^+(v'' = 0)$ progression in particular has astrophysical relevance [11]. The need for laboratory wavelengths of these lines for the interpretation of astrophysical observations served as a strong motivation for investigating the $A^1\Pi(v') - X^1\Sigma^+(v'' = 0)$ progression in search of the rarer isotopomer lines. In this progression the $A^1\Pi(v' = 3) - X^1\Sigma^+(v'' = 0)$ band is a strong, less perturbed band [14] lying in a suitable vacuum ultraviolet region in which the vacuum ultraviolet source employed in this experiment has high efficiency [97].

The experiment clearly demonstrated the advantages of combining our source of narrow bandwidth vacuum ultraviolet radiation and a pulsed free supersonic jet for high-resolution molecular spectroscopy with a high sensitivity for detection of trace species. The vacuum ultraviolet radiation is generated as a well collimated beam, which is ideal for probing only the

central part of the free supersonic jet, where optimal low temperature collision-free conditions and a relatively high gas density are found. The narrow bandwidth of the tunable vacuum ultraviolet radiation facilitates high spectral resolution that is essential to the analysis of molecular spectra, particularly of overlapping bands of different isotopomers. This high spectral resolution is well matched with the practically collision-free conditions in the jet that circumvent pressure broadening of the molecular spectral lines. The sensitivity of the method to detect trace amounts of molecular species is advanced by both the relatively high peak photon flux of the vacuum ultraviolet pulses, compared with alternative sources such as a D_2 lamp, and the relatively high gas density in the jet. The flow-cooling in the jet further contributes to the detection limit by enhancing the absolute intensities of the low rotational lines of trace isotopomeric species.

Individual rovibrational lines of the $A^1\Pi(v' = 3) - X^1\Sigma^+(v'' = 0)$ band of the isotopomers $^{12}C^{16}O$, $^{13}C^{16}O$, $^{12}C^{18}O$ and $^{12}C^{17}O$ were observed, illustrating the large intensity range of the measurements. The spectral data of $^{12}C^{17}O$ presented here are to my knowledge the first rotationally resolved laboratory measurement reported on the $A^1\Pi - X^1\Sigma^+$ band system of this isotopomer. The relevance of these newly measured $^{12}C^{17}O$ transition wavelengths to the interpretation of astrophysical data is discussed in section 6.2.

The two other topics that have emerged in the experimental work are the flow-cooling of different isotopomers of CO in a noble gas jet discussed in section 6.1 and the possibilities on the formation and detection of CO-Ar/CO-Ne van der Waals complexes in our experiment in section 6.3.

6.1 Flow-cooling of CO isotopomers seeded into a pulsed supersonic noble gas jet

The relative populations of the rotational levels of $^{12}C^{16}O$ as determined from the peak intensities in the spectra provide a measure of the rotational temperature of the molecules in the jet, as described in section 5.1, but they also exhibit the unique characteristics of the flow-cooling process.

The assumption made throughout the experiment, that the fluorescence excitation spectra

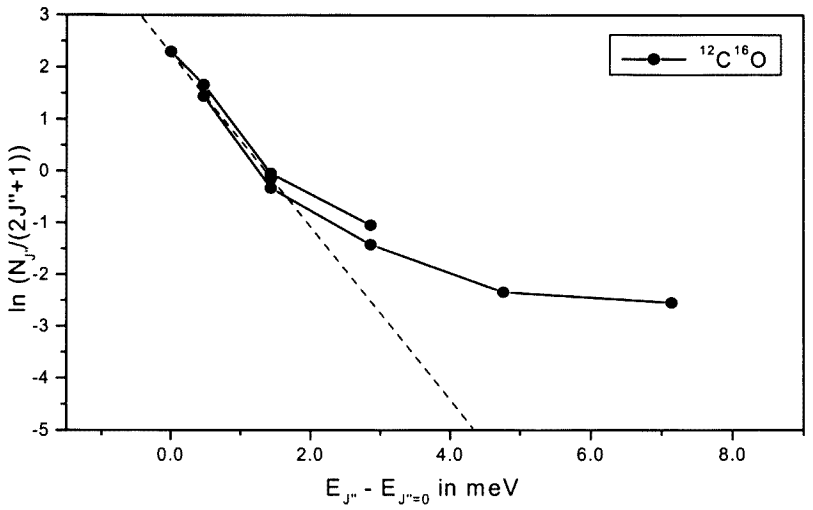

Figure 6-1: Experimental population distribution of the rotational levels of the $A(v' = 3) - X(v'' = 0)$ band of $^{12}C^{16}O$ (dots) compared to the Boltzmann distribution expected under equilibrium conditions (dashed line). When fitting the Boltzmann equation to the lowest few rotational levels, the populations observed in the higher rotational levels are much larger than expected from the Boltzmann distribution.

can be considered identical to the corresponding absorption spectra, is based on a number of experimental considerations, as discussed by Demtröder [106, p. 386]. Firstly the total spectral range investigated in the present experiment covers only about 200 cm^{-1} over which the quantum efficiency of the photomultiplier tube can be taken as constant. Secondly the fluorescence lifetimes of the rotational levels in the $A^1\Pi(v' = 3)$ band are similar, ensuring that the geometrical collection efficiency should be the same for all measured lines. Thirdly the fluorescence quantum yield of the $A^1\Pi(v' = 3)$ band of CO under the practically collision-free conditions in the supersonic expansion can considered to be approximately equal to 1.

In our spectra the population distribution over the rotational levels deviates from the Boltzmann distribution expected under equilibrium conditions. As clearly illustrated in figure 6-1 the populations of the higher J'' levels are significantly larger than expected from the Boltzmann distribution (see also figure 5-1 and the discussion in section 5.1). The excessive population in the high J'' levels as observed in our spectra confirms the observations of Smalley et al. in spectroscopic investigations of I_2 in He [113] and NO_2 in Ar [91] and of Kukolich et al. in a pure OCS gas expansion [114]. Both groups reported the population in the higher rotational levels to

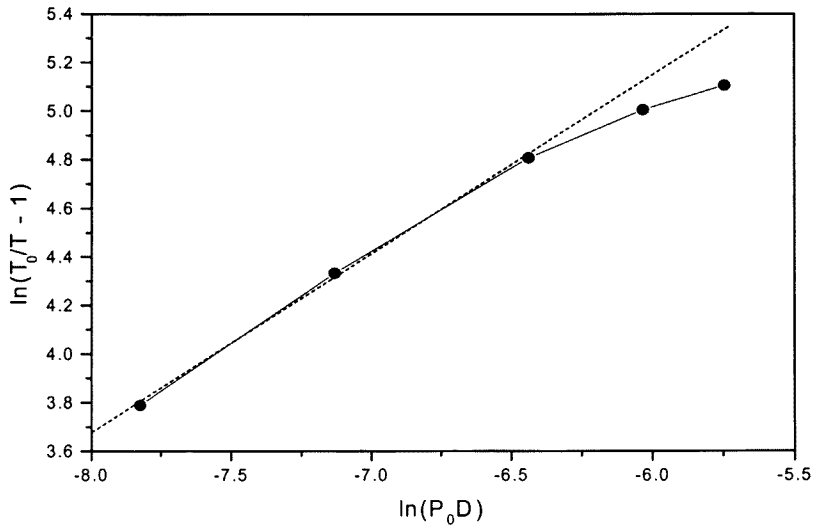

Figure 6-2: Linearised plot of the rotational temperature (calculated from $J'' = 0, 1$ data) versus stagnation pressure P_0 for a mixture of 0.5 % CO in Ne. The gradient of the line fitted through the data points taken at the three lowest stagnation pressures is 0.74.

be in excess to the population expected when extrapolating the Boltzmann distribution of the lowest few rotational levels, as illustrated in figure 6-1. This observation indicates that the rate of translation-rotation relaxation is the largest for the lowest rotational states and decreases as the value of J'' increases. The deviation of the populations of the rotational states from the Botzmann distribution also indicates that the rotation-rotation relaxation rates are relatively slow under the conditions of the supersonic jet, so that complete relaxation to an equilibrium population distribution has not taken place at the point of observation in the jet.

These results - showing that the system has not come to a state of thermal equilibrium in the rotational degrees of freedom - mean that, strictly speaking, no true rotational temperature can be assigned to the system. The experimental rotational temperatures used in the present work were assigned using a specific set of rovibrational lines as discussed in section 5.1, to the example of Smalley et al. [85]. These experimental rotational temperature values must be considered relative measures of the degree of cooling, useful for comparison of conditions in the jet, but not as absolute temperatures in a rigorous sense.

The dependence of the rotational temperature on the stagnation pressure yielded further qualitative indications of the relaxation rates under different conditions. In figure 6-2 the

relation between the experimentally determined rotational temperatures in the jet T_{rot} and the stagnation pressure P_0 for a gas mixture of 0.5 % CO in neon (the same data as shown in figure 5-3) is plotted in a logarithmic form that can easily be compared with the theoretical equation 3.4 (p. 22) describing the relation between the terminal translational temperature T_{tr} in the jet and the stagnation pressure. A logarithmic plot of equation 3.4 - $\ln(T_0/T_{tr} - 1)$ versus $\ln(P_0 D)$, where T_0 is the temperature in the stagnant gas and D the orifice diameter, is a straight line with gradient of 0.8. The experimental plot cannot be expected to correspond exactly with equation 3.4 that holds for the terminal translational temperature. Firstly the thermal equilibrium in the jet is not complete causing the rotational cooling to lag behind the translational cooling and therefore the measured rotational temperature is not an absolute measure of the terminal translational temperature. Secondly the theoretical equation holds for a pure noble gas expansion whereas our measurements are taken with a gas mixture. However, the plot of the natural logarithms of $T_0/T_{rot} - 1$ versus $P_0 D$ as illustrated in figure 6-2 is linear in the low stagnation pressure region, deviating at higher stagnation pressures. The smaller gradient of 0.74 of the linear fit through the low pressure data of figure 6-2 is indicative of a decrease in the value of γ as more degrees of freedom (the rotational degrees of freedom) are taken into account. The deviation of the plot from linearity at suggests the incomplete relaxation of the rotational degrees of freedom.

A second trend that was observed was an increase in the lowest temperature reached in the jet when the percentage CO in the gas mixture is increased. This is understood in terms of the fact that CO molecules, in contrast to argon atoms, store additional thermal energy in rotational and vibrational degrees of freedom that needs to be dissipated, retarding the cooling process. Seen in another way, the addition of a significant fraction of CO to the expanding gas changes the ratio of specific heats, γ, of the gas mixture to a lower value than for argon (see the γ values in table 3.1, page 21) and therefore changes the relation between the terminal temperature and the stagnation pressure as expressed theoretically in equation 3.4.

As discussed in section 3.1 and illustrated in figure 3-1 neon and argon are the two noble gases that should be the most efficient for collisional cooling of CO isotopomers according to simple momentum conservation considerations. Our results offer a comparison of the flow-cooling efficiency of the different CO isotopomers in Ar and in Ne as carrier gases. The trends

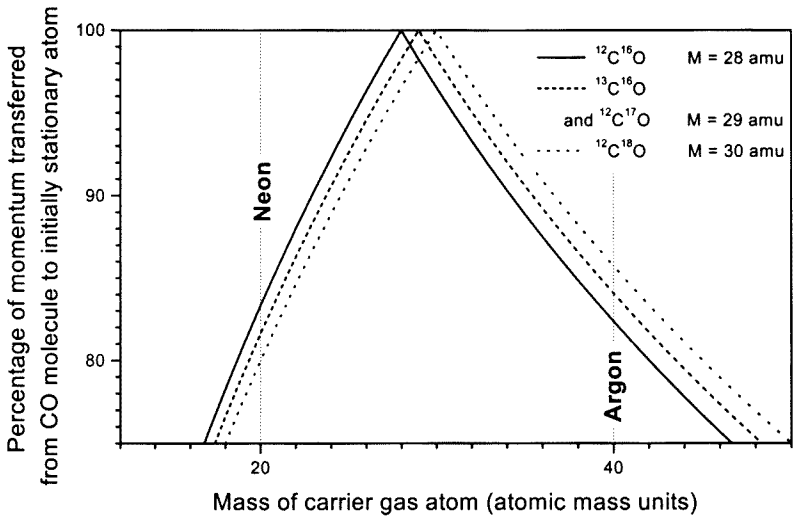

Figure 6-3: Illustration of the efficiency of momentum transfer in collisions between different CO isotopomers and argon or neon atoms, as relevant to the flow-cooling process. The curve was obtained by calculating the percentage of momentum transferred from the CO molecule to an initially stationary noble gas atom during an elastic two-body collision.

observed for the different isotopomers reflect qualitatively the momentum transfer consideration mentioned at the end of section 3.1. Assuming that the cooling of the rotational degrees of freedom of a CO isotopomer in a noble gas jet is caused (via translational-rotational relaxation) mainly by two-body collisions with the noble gas atoms and that the collision cross sections for collisions of different CO isotopomers with the atoms of a specific noble gas are similar (a reasonable assumption for isotopomers), then the momentum transfer in such a two-body collision depends on the mass ratio $M_{CO}/M_{noble\ gas}$ which differs for the different isotopomers.

This effect is illustrated in figure 6-3[1]. From the calculated values in this illustration it can be seen that in an Ar expansion $^{12}C^{16}O$ should be cooled less efficiently than the heavier CO isotopomers. In a Ne expansion the opposite should hold. $^{12}C^{16}O$ should be cooled more efficiently in Ne than in Ar and opposite for the heavier isotopomers, although this statement relies on the rough estimate that the collisional cross section with different noble gas atoms are the same. In our experimental results, as illustrated in figure 5-5, page 60, the following

[1] Again the model used is a simple "billiard-ball" model considering head-on collisions. The results are to be taken as a qualitative illustration only.

trends can be observed. $^{12}C^{16}O$ is cooled to a lower rotational temperature in Ne than in an Ar expansion as expected from the momentum considerations. In an Ar expansion it is observed that the heavier the isotopomer, the lower the rotational temperature that it reaches in the expansion, whereas the results in a Ne expansion suggest a reversal of this trend for the heavier three isotopomers - also as expected. The $^{12}C^{16}O$ rotational temperature in the Ne expansion remains higher than that of $^{13}C^{16}O$ and $^{12}C^{17}O$ contrary to what is expected. This might be due to saturation of the strongest low-J'' lines of $^{12}C^{16}O$ at these low temperatures.

The characteristics of the flow-cooling process in the free supersonic jet had definite advantages in our experimental endeavour to detect rare isotopomers in a natural CO gas sample. The low rotational temperature facilitated the detection of the spectral lines of the rare $^{12}C^{17}O$ and $^{12}C^{18}O$ isotopomers by increasing the intensities of the low rotational lines of these isotopomers and decreasing the intensities of the neighbouring higher rotational lines of the more abundant isotopomers. At the same time, however, the high rotational lines of $^{12}C^{16}O$ and $^{13}C^{16}O$ did not vanish completely so that numerous lines were available for wavelength calibration of the spectra. In this way the previously unknown excitation wavelengths of $^{12}C^{17}O$ could be determined accurately.

A last consideration mentioned in the literature regarding the use of supersonic expansion in spectroscopy is the warning that line profiles and even line positions measured in supersonic jets show anomalies due to Doppler shifts. However, when the specific conditions in the jet-discharge experiments where the anomalies were observed [115, 116] are studied, it is evident that those conditions are not applicable to the present experiment. With laser excitation, unlike discharge excitation, the probe volume is extremely localised and by eliminating stray light it is possible to gather fluorescence from the cold and practically parallel flowing core of the expansion only, thereby minimising the influence of the Doppler effect.

6.2 Astrophysical application of experimental $^{12}C^{17}O$ and $^{12}C^{18}O$ wavelength data

The astrophysical importance of the observations of the rare $^{12}C^{18}O$ and $^{12}C^{17}O$ isotopomers, as well as the necessity of accurate laboratory measured wavelength data for these species,

is evident from the discussion in section 2.3. The first rotationally resolved measurements of vacuum ultraviolet absorption lines of interstellar $^{12}C^{17}O$ and $^{12}C^{18}O$ were recently reported by Sheffer et al. [4], having observed individual rovibronic lines in the $A^1\Pi(v' = 2-5) - X^1\Sigma^+(v'' = 0)$ bands of $^{12}C^{18}O$ and $^{12}C^{17}O$ in spectra measured by the Space Telescope Imaging Spectrograph aimed toward the star X Persei. When publishing these results in June 2002, spectroscopic data for the $v' = 0-9$ bands of $^{12}C^{18}O$ as published by Beaty et al. [41] were at their disposal, but no laboratory measured rest wavelengths for the bands of $^{12}C^{17}O$ were available. The rest wavelengths are used to calculate the Doppler shift and subsequent heliocentric velocity of the interstellar gas relative to our solar system. Sheffer et al. [4] calculated rest wavelengths for $^{12}C^{17}O$ by applying appropriate isotopomeric corrections to the Dunham coefficients of $^{12}C^{16}O$. However, the use of these calculated rest wavelengths for $^{12}C^{17}O$ resulted in an apparent difference between the heliocentric velocity obtained from the $^{12}C^{17}O$ data and that obtained from the $^{12}C^{18}O$ data measured in the same interstellar cloud region. This raised concerns about the accuracy of the calculated $^{12}C^{17}O$ rest wavelengths and left an uncertainty regarding the heliocentric velocity of the interstellar gas cloud.

In the present work, laboratory measured vacuum ultraviolet transition wavelengths of the $A^1\Pi(v' = 3) - X^1\Sigma^+(v'' = 0)$ band of $^{12}C^{18}O$ and $^{12}C^{17}O$, one of the bands detected by Sheffer et al. [4], were obtained by recording laser-induced fluorescence excitation spectra in a natural CO gas sample flow-cooled in a supersonic jet. The low temperature in the supersonic jet and characteristics of the vacuum ultraviolet radiation facilitated the detection of the rare isotopic species. The band origins of the rare $^{12}C^{17}O$ and $^{12}C^{18}O$ isotopomers are found among higher rotational lines of the more abundant isotopomers $^{12}C^{16}O$ and $^{13}C^{16}O$, as seen in figure 5-9 (page 66). A low rotational temperature enhances the intensities of the low rotational lines of the heavier isotopomers while reducing the intensities and widths of the neighbouring higher rotational lines of the more abundant isotopomers that tend to obscure them at room temperature. The narrow bandwidth and high spectral intensity of the vacuum ultraviolet radiation contributed to high sensitivity and high spectral resolution that facilitated the detection of the rare isotopomers' lines.

The low rotational temperature of about 4 ± 1 K of the CO sample in the jet corresponds roughly to the temperatures in diffuse interstellar clouds [11] allowing the detection of the same

Table 6.1: Comparison of the rest wavelengths from present experiment and data used by Sheffer et al. 2002 as well as resulting heliocentric velocities of interstellar CO towards X Persei.

	Data of Sheffer et al. [4]		Present Experiment	
Parameter	$^{12}C^{18}O$	$^{12}C^{17}O$	$^{12}C^{18}O$	$^{12}C^{17}O$
$A - X$ band	$3 - 0$	$3 - 0$	$3 - 0$	$3 - 0$
$\lambda_0[R(1)]$ (nm)	144.9248 [a]	144.8332 [b]	144.9249	... [c]
$\lambda_0[R(0)]$ (nm)	144.9294 [a]	144.8379 [b]	144.9295	144.8375
$\lambda_0[Q(1)]$ (nm)	144.9371 [a]	144.8458 [b]	144.9373	144.8453
v_{helio} (km/s) [d]	15.0	13.5	14.7 ± 0.4	14.4 ± 0.4

[a] Wavelengths calculated by Sheffer et al. [4] from term values of Beaty et al. [41].
[b] Wavelengths calculated by Sheffer et al. [4] from $^{12}C^{16}O$ data by correcting for the isotopic shift.
[c] The R(1) line of $^{12}C^{17}O$ was not detected due to overlap with the stronger P(7) line of $^{12}C^{16}O$.
[d] Heliocentric velocities of the interstellar CO toward X Persei calculated by using the corresponding λ_0 values.

rotational transitions as observed in the interstellar spectra, generally those originating from levels with $J'' \leq 3$. Each spectrum in our work covered the $A^1\Pi(v' = 3) - X^1\Sigma^+(v'' = 0)$ band of $^{12}C^{16}O$ and $^{13}C^{16}O$, as well as $^{12}C^{18}O$ and $^{12}C^{17}O$. This allowed accurate calibration of the wavelengths of the $^{12}C^{18}O$ and $^{12}C^{17}O$ lines using the known wavelengths of the lines of the more abundant isotopomers as standards. A typical spectrum, as illustrated in figure 5-9, shows the $^{12}C^{18}O$ and $^{12}C^{17}O$ lines among the $^{12}C^{16}O$ and $^{13}C^{16}O$ lines that were used as well distributed standard lines for the wavelength calibration of the spectrum. The calibrated wavelengths of the $^{12}C^{18}O$ and $^{12}C^{17}O$ lines have already been given in table 5.1 (page 65).

Our experimental wavelength data on the $A^1\Pi(v' = 3) - X^1\Sigma^+(v'' = 0)$ band of $^{12}C^{18}O$ and $^{12}C^{17}O$ were applied successfully [117] to resolve the discrepancy in the interpretation of the spectra of Sheffer et al. [4]. In table 6.1 our experimental wavelength data are compared to the corresponding rest wavelength data used by Sheffer et al. in their paper [4]. Whereas the $^{12}C^{18}O$ wavelengths obtained in the present experiment correspond well (within 0.0001 nm)

with the values of Beaty et al. [41] as used by Sheffer, a difference of ca. 0.0005 nm exists between the calculated $^{12}C^{17}O$ rest wavelengths used by Sheffer et al. [4] and our experimental wavelengths. The effect of this systematic shift is clearly seen in the heliocentric velocities calculated using these rest wavelengths. As reported by Sheffer et al. [4] and seen in table 6.1 a discrepancy of 1.5 km/s is found in the heliocentric velocities calculated for the interstellar CO when using the rest wavelengths of $^{12}C^{18}O$ and $^{12}C^{17}O$ which Sheffer et al. had at their disposal. It is, however, physically improbable to observe two different Doppler shifts for two isotopomer spectra measured from the same sample volume in interstellar space. Using our experimental rest wavelengths the difference in heliocentric velocity calculated from the two sets of data is reduced to 0.3 km/s, which is smaller that the uncertainty of 0.4 km/s on the values [117]. As anticipated by Sheffer et al. [4], the correction of the systematic shift in the $^{12}C^{17}O$ rest wavelength values contributed most to equalise the calculated heliocentric velocities. The average heliocentric velocity obtained from the data of the present experiment is 14.5 ± 0.4 km/s which is slightly lower than the 15.0 km/s obtained by Sheffer et al. [4] from their $^{12}C^{18}O$ data.

There is definitely a need for more accurate laboratory wavelength data of the $A - X$ bands of $^{12}C^{17}O$ that are of astrophysical interest [11, 4].

6.3 Possibilities regarding the formation and detection of CO-Ar and CO-Ne van der Waals complexes in this experiment

The conclusive proof for the presence of CO van der Waals complexes in the spectroscopic sample is the detection of characteristic spectral features associated with such a complex. In the present experiment it was the detection of fluorescence following the laser excitation of the CO-Ar (or CO-Ne) complex from its CO($X^1\Sigma^+, v'' = 0, J''$)-Ar($X^1S$) ground state to its CO($A^1\Pi, v' = 3, J'$)-Ar(X^1S) excited state. The vibronic bands of the electronic excitation spectrum of the $^{12}C^{16}O$-noble gas complex are expected to lie close to the corresponding bands of the $^{12}C^{16}O$ monomer in the vacuum ultraviolet region of the spectrum.

The two conditions for the detection of characteristic spectral features of a complex are (i) that the gas conditions and dynamics in the gas sample (supersonic jet in most cases)

must result in the formation of a sufficiently large concentration of the complex species in the sample volume to be detectable and (ii) that the spectroscopic method of detection, with its fundamental and technical limitations, must be suitable to detect such a concentration of the specific complex. In the case of CO-Ar complexes, the suitability of a supersonic jet for the formation and spectroscopic study of this complex has already been demonstrated by numerous experiments [9, 58, 60, 61]. However, our spectroscopic method - the spectroscopic detection of the vacuum ultraviolet electronic excitation spectrum of the CO-Ar complex by measuring laser-induced fluorescence - has to my knowledge never been reported before.

In the present work, where characteristic features of the complex species were not observable right away, the first task was to establish whether and under which conditions an observable concentration of CO-Ar was formed in the supersonic jet. Indirect evidence for the occurrence of condensation, which should include the formation of simple van der Waals complexes as first step, were obtained from changes in the laser-induced fluorescence signal of the CO monomer (referring to $^{12}C^{16}O$). Two sets of results providing such evidence for the formation of CO-Ar/CO-Ne and CO-CO have been presented in section 5.4. The basic assumption in the interpretation of these results is that, in the case where the CO concentration is the factor limiting the fluorescence signal, significant complex formation will decrease the CO concentration and therefore the CO fluorescence signal, under conditions where this decrease cannot be explained by other experimental factors such as the intensity of the excitation radiation or the temperature.

The first result was the observation of a discontinuous decrease in the total fluorescence signal of the CO monomer at the highest stagnation pressures in a neon jet, as illustrated in figure 5-10. The most probable explanation for the observation is that under favourable conditions in the jet - at high stagnation pressure when the temperature becomes sufficiently low - the formation of CO van der Waals complexes reaches such an extent that it starts to deplete the CO concentration. This effect was not observed to such a dramatic extent in an argon expansion, probably due to a difference in the dynamics and the temperature reached in the argon jet. In a similar investigation, trying to detect the laser-induced fluorescence excitation spectrum of I_2-Ar van der Waals complexes, Smalley et al. [113] interpreted a result similar to this - a large reduction in the intensity of the uncomplexed molecular bands at the

highest nozzle pressures - as an indication of substantial complex formation, although no discrete fluorescence features of the complex could be observed. This supports the interpretation of the above mentioned results as being caused by the formation of CO-Ne van der Waals complexes.

The second set of results facilitating further interpretation concerns the observation of a dip in the delay scan profile, as illustrated in figure 5-11. This phenomenon was investigated under different experimental conditions. The observation that the dip is sensitive to the stagnation pressure and CO percentage indicates that the dip is not likely to be an artificial effect of the mechanical operation of the valve. A possible explanation for the dip would be that the dip is due to partial depletion of the CO monomer population due to complex formation in that temporal part of the gas pulse where conditions are suitable, i.e. starting some tenths of milliseconds after the beginning of the gas pulse when the expansion has developed fully and the cooling is optimal and ending as soon as gas particles rebounding from the chamber walls begin to interfere with the sample volume.

It can also be speculated that the "low pressure dip" and the "high pressure dip" (refer to figure 5-12) might have different complex formation processes as dominant cause. The "low pressure dip" that is observed with a high CO to Ar ratio in the gas mixture is possibly caused dominantly by the formation of CO-CO complexes. The high CO to Ar ratio would allow a high rate of three-body collisions involving two CO molecules. The "high pressure dip" that is observed under conditions of very low temperatures and CO percentages in the mixture would rather be caused by the formation of CO-Ar complexes. With CO percentages as low as 0.5 % in the gas mixture, the rate of three-body collisions involving one CO molecule and forming CO-Ar would be much higher than the rate of collisions that could lead to the formation of CO dimers.

Different condensation processes in the two different pressure regions could qualitatively explain the difference in the influence of the partial CO pressure in the mixture at constant stagnation pressure on the dip depth. The number of CO monomers removed by the formation of CO-Ar should be directly proportional to the CO concentration in the jet. The signal height used to normalise the "dip depth" is also proportional to the CO concentration, meaning that the "dip depth relative to the peak height" should not change significantly as the partial CO pressure is changed. In contrast, the formation rate of CO dimers should be proportional to

Table 6.2: Optimal experimental conditions for formation of CO-Ar van der Waals complexes.

Reference	[58] [a]	[60] [b]	[61] [b]	Present work
Gas mixture (% CO in Ar)	30	40	30	30
Stagnation pressure (bar)	4	5	5	4
Background pressure (mbar)	$< 10^{-1}$	...	5×10^{-2}	5×10^{-6}
Gas pulse period [c] (ms)	0.5	0.5	0.5	2.5
Orifice diameter (mm)	0.5	0.5	0.5	0.8
Nozzle to laser distance (mm)	10	...	...	20
Estimated temperature (K)	...	$5 - 10$	...	$2 - 10$

[a] Gated detection with boxcar.
[b] Double modulation technique used in detection.
[c] Solenoid valve (General Valves, series 9) used in all cases.

the square of the CO concentration and would remove two CO monomers from the sample so that a plot of "dip depth relative to the peak height" versus partial CO pressure should be a function increasing quadratically. The depth of the "low pressure dip" is observed to increase more with the partial CO pressure than the depth of the "high pressure dip", confirming these speculations in a qualitative sense.

Although a detailed interpretation of these results remains speculative, complex formation seems to be the most reasonable explanation for the observations.

The above mentioned results, interpreted as semi-quantitative evidence for the formation of complex formation in the jet, was used to guide the choice of the experimental conditions employed in our setup in the search for the spectral features of CO van der Waals complexes. Physical limitations of the apparatus and rules of thumb provided by the theory of a supersonic expansion (section 3.1) were also taken into account in the optimisation. The optimal conditions chosen on account of our experimental evidence agreed well with those conditions reported as successful for the formation and study of CO-Ar van der Waals complexes in literature. In table 6.2 the conditions used in the present work are compared to the conditions reported in literature on experimental CO-Ar studies. Hepp and coworkers [58, 60, 61] did successful millimeter-wave spectroscopy on CO-Ar using their supersonic expansion setups. No estimate

of the relative CO-Ar concentration in the jet is given in these papers, but the reproduced spectra of the measured CO-Ar lines in [58] have approximately the same signal to noise ratio as the $^{12}C^{17}O$ lines they measured by the same method, in spite of the fact that the complex has a smaller electronic dipole moment than $^{12}C^{17}O$. It would therefore be reasonable to assume that the relative concentration of the complex should be of the same order as that of $^{12}C^{17}O$ in natural abundance: about 0.04 % of the concentration of the $^{12}C^{16}O$, which equals 120 parts per million or 0.48 mbar in 4 bar of stagnant gas before expansion in their experiment. The small differences in the experimental parameters used in the present work compared to that of Hepp et al. [58, 60, 61] are not expected to change (reduce) the formation of complexes significantly. The longer gas pulse period used in the present work should not influence the probability of forming van der Waals complexes in the jet. The larger nozzle diameter in the present work should be of advantage to condensation in the jet according to the theory discussed in section 3.1.

Considering our experimental conditions in comparison with those reported in literature, the formation of a sufficiently large concentration of van der Waals complexes for detection could be expected in our setup. On account of our experimental evidence as discussed in section 5.4, I am of opinion that CO-Ar/CO-Ne van der Waals complexes, possibly together with CO-CO, are formed in our supersonic jet and that the concentration of these species should be high enough to allow spectroscopic detection.

The question remains why no clearly distinguishable features of the electronic excitation spectrum of CO-Ar (or CO-Ne or CO-CO) could be observed in the present work, in spite of the evidence that significant condensation does occur and in spite of a good detection sensitivity, as demonstrated by the detection of concentrations as low as 3 parts per million of $^{12}C^{17}O$ in the natural CO gas sample (equalling a pressure of 0.012 mbar in 4 bar of stagnant gas prior to expansion). As discussed in section 5.5 laser-induced fluorescence excitation spectra were recorded over a wide spectral region around the $A^1\Pi(v'' = 3) - X^1\Sigma^+(v' = 0)$ band of $^{12}C^{16}O$ without finding any distinct reproducible spectral features that could be associated with CO-Ar or CO-Ne van der Waals complexes. In the choice of the wavelength region to be scanned the results of preliminary theoretical calculations of Salazar and Hernández [80] on CO-Ar were considered and eventually an even larger wavelength region was investigated. The preliminary

results of Salazar and Hernández predicted 4 possibly observable bands of the CO-Ar complex within the range of 60 cm^{-1} from the band head of the CO monomer band.

It must be kept in mind that these wavelength positions predicted for the complex bands might not be very accurate. The calculations done up to date [81] were preliminary of nature and the model that was used involved the assumption that the geometry of the CO-Ar van der Waals complex of the ground and excited states are identical (see section 2.4). Therefore it is possible that the spectral features of the CO-Ar or CO-Ne van der Waals complexes are lying outside the wavelength range that was investigated and were not observed for this reason. The following discussion, however, is based on the assumption that the investigated wavelength range did cover some excitation wavelengths of CO-Ar or CO-Ne.

In order to understand the presence or absence of distinct spectral features of the CO-Ar complex in the laser-induced fluorescence excitation spectra the mechanisms of excitation, as well as relaxation and dissociation of the complex after excitation have to be known. The excitation and photodissociation dynamics have to my knowledge not been studied for the CO-Ar complex. However, for the I_2-noble gas complexes (in particular I_2-Ar) the photodissociation dynamics on electronic excitation has been studied in detail, by experimental as well as theoretical methods. The experimental and theoretical study of the dissociation of I_2-Ar, excited to the $I_2(B, v')$-Ar state, began in 1976 with the work of Smalley et al. [113] and continues to the present, as reviewed recently by Rohrbacher et al. [118], Burroughs et al. [119] and Roncero et al. [120]. There are a number of general results from this intensive study on I_2-Ar that are of general interest and possibly have relevance for the understanding of the CO-noble gas van der Waals complexes.

In its electronic ground state van der Waals complexes such as I_2-Ar and CO-Ar are stable under the low temperature conditions in a supersonic expansion. Due to the low temperature, the average energy of the collisions that the complex is subject to is significantly lower than the binding energy of the complex (the binding energy of $CO(X, v'' = 0)$-Ar is ca. 105 cm^{-1} [60]). However, electronic excitation of the complex, resulting from electronic excitation of the molecular component, usually leads to rapid dissociation of the complex.

The study of I_2-noble gas complexes illustrated firstly that while some van der Waals complexes, such as the T-shaped I_2-noble gas complexes, show discrete optical excitation transitions,

there are van der Waals complexes, such as the linear I_2-Ar [121] and Cl_2-Ar [118] isomers, that have diffuse continua as excitation spectra. This is attributed to the linear isomer not having favourable Franck-Condon factors to low-lying vibrational levels of the van der Waals bond in the excited state and vertical optical excitation consequently ending in highly excited levels or even the continuum of the upper state [121].

Secondly, even in the case of discrete excitation to a low-lying level in the excited state, the dissociation lifetimes of the I_2-noble gas complexes have been found to be much shorter than the radiative lifetime of the complex so that, if fluorescence is observed on excitation of the complex, this fluorescence comes from a fluorescing dissociation product and not from the complex itself [122]. There have been found to be two dominant competing dissociation mechanisms for I_2-Ar: vibrational predissociation and complex-induced electronic predissociation [120]. Vibrational predissociation can take place either directly or via intramolecular vibrational redistribution, as illustrated in figure 6-4 (a) and (b) respectively. In both cases a fluorescent dissociation product, the molecule PQ in its excited A state, is formed. In the case of direct vibrational predissociation, the rate of dissociation varies smoothly with the vibrational state v' of PQ(v') that has originally been excited - the dissociation lifetime decreasing as v' increases. This agrees with the theoretical "momentum gap" argument of Ewing [123]: that the lifetime of the complex is proportional to the square root of the excess energy (the energy difference between the I_2 molecular stretching vibration quantum and the van der Waals binding energy) that has to be converted to translational energy of the products during the dissociation. On the other hand the rate of dissociation via intramolecular vibrational redistribution will vary non-monotonically with v' due to strong influences of accidental near resonances between energy levels of the PQ(A, v')-R and the PQ($A, v'-1$)-R states [119]. In the case of I_2-Ar the second dissociation mechanism, complex-induced electronic predissociation (also called electronic quenching), is understood as a process similar to collisional quenching where the presence of the Ar atom causes coupling between the bound fluorescing $B^3\Pi(O_u^+)$ electronic state of I_2 and a dissociative electronic state of the I_2 molecule dissociating to I($^2P_{2/3}$) +I($^2P_{2/3}$). Electronic predissociation therefore causes dissociation of the excited I_2-Ar complex into non-fluorescing atomic products. The rate of the electronic predissociation varies non-monotonically with v'.

In the case of I_2 complexes with a small noble gas atom, as with I_2-He, the direct vibrational

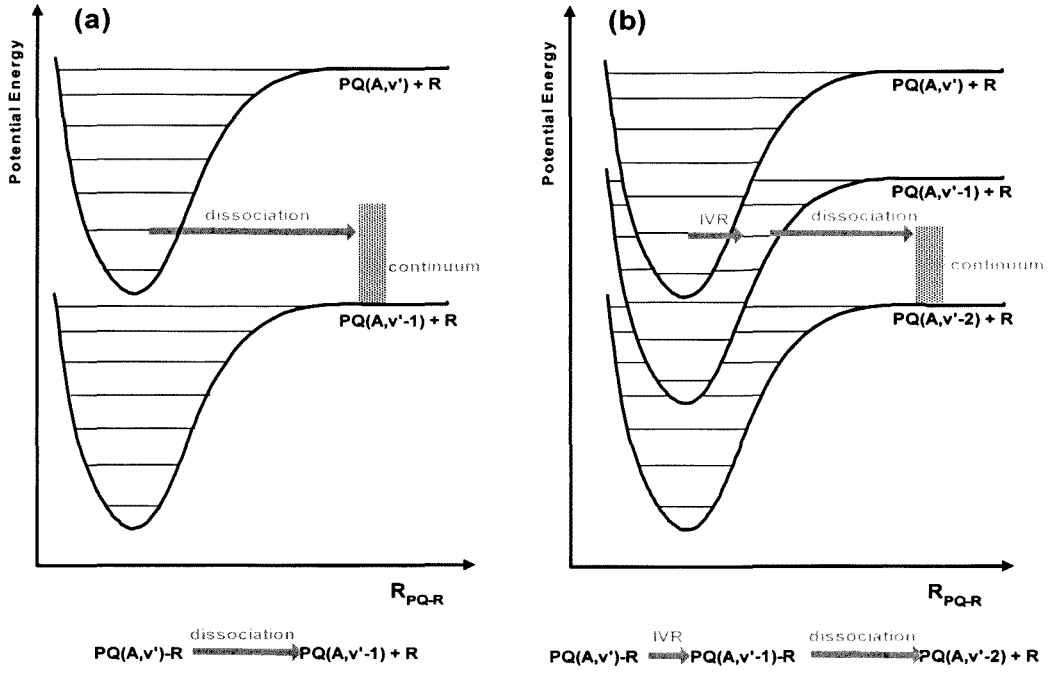

Figure 6-4: Schematic illustration of the two mechanisms of vibrational predissociation of a van der Waals complex PQ(A, v')-R, where PQ is a diatomic molecule (with an electronic ground state X and excited electronic state A) and R a noble gas atom. Direct vibrational dissociation is illustrated by (a), while (b) illustrates an example of vibrational predissociation via intramolecular vibrational relaxation.

predissociation mechanism dominates [124], while electronic predissociation becomes increasingly important the larger the noble gas atom. This agrees with the observation that larger atoms are more efficient collisional quenchers [124, 125]. Competition between these different dissociation processes was used to explain the failure to observe the laser-induced fluorescence excitation spectrum of T-shaped I_2-Ar upon excitation of the $I_2(B, v')$-Ar state of the complex with $0 \leq v' \leq 11$, as well as the oscillating intensities of the fluorescence observed upon excitations with $12 \leq v' \leq 26$ [124].

The extrapolation of these results to CO-noble gas van der Waals complexes is speculative, but it provides a basis for discussion. A T-shaped configuration has been found to be the most stable ground state configuration of all the CO-noble gas van der Waals complexes and a T-shaped configuration is also generally assumed for the excited states of CO-noble gas complexes. In the ab initio calculations of Salazar and Hernández, that have been discussed briefly in section 2.4, the optimised T-shaped geometry of the CO(X)-Ar ground state was used and a T-shaped geometry for the excited CO(A)-Ar state was assumed. These calculations predict the stability of the ground CO(X)-Ar state and excited CO(A)-Ar state to be similar, seen in the D_e values in table 2.2. Also the equilibrium bond lengths, R_e, of the ground and excited states are predicted to differ by less than 2 %, meaning that the Franck-Condon factors are favourable for optical excitation to low-lying vibrational levels of the van der Waals bond. Therefore, from the theoretical predictions, assuming a T-shaped geometry for the excited state, the excitation spectrum of CO-Ar is expected to be discrete and well-defined. Rapid dissociation of the complex upon excitation could however significantly broaden the features of the excitation spectrum.

Regarding the dissociation dynamics of the electronically excited CO($A, v' = 3$)-Ar complex[2] vibrational predissociation and different forms of complex induced electronic quenching must be considered as possible mechanisms of relaxation.

Vibrational predissociation via intramolecular vibrational redistribution is not probable in the case of CO-Ar due to energy considerations. The stretching vibrational quantum of the CO molecule ($E_{CO(A,v'=3)} - E_{CO(A,v'=2)} = 1412$ cm^{-1} [13]) is about an order of magnitude larger than the estimated binding energy of the van der Waals bond (115 cm^{-1} [81]). Therefore

[2] Similar arguments hold for CO-Ne.

the bound regions of the potential energy curves associated with CO($A, v' = 3$)-Ar and with CO($A, v' = 2$)-Ar do not overlap in energy (compare with figure 6-4).

Direct vibrational predissociation of CO-Ar should occur at a much slower rate than for the T-shaped I_2-Ar complex according to the "momentum gap" argument [123]. The large momentum difference results in a very weak coupling between the high-frequency C-O stretching vibration (ω_e of CO ~ 1500 cm^{-1}) and the low-frequency stretching vibration of the van der Waals bond (ω_e of CO-Ar < 30 cm^{-1}). The nearly rectangular T-shaped symmetry ($\theta_{O-Ar} = 93°$) of the CO-Ar complex would also contribute to a very weak coupling between these vibrational modes in the excited state, as has been found to be the case in the CO($X, v'' = 0$)-Ar ground state [63]. If vibrational predissociation does occur the CO molecule will be left after dissociation in the $A^1\Pi(v' = 2)$ state from which it will relax to the $X^1\Sigma^+$ ground state by the emission of vacuum ultraviolet fluorescence. This relaxation channel would therefore be detectable in our experimental setup.

Electronic quenching in the case of CO-Ar is not expected to follow the mechanism proposed for I_2-Ar. The $A^1\Pi(v' = 3)$ state of CO is too far below the dissociation energy of the electronic ground state of the molecule to allow coupling to a dissociative electronic state of CO leading to dissociation of the C-O bond (as with I_2-Ar). In the case of CO one possible mechanism of electronic quenching is internal conversion to a high vibrational level of the electronic ground state. Intersystem crossing is a second possibility that should be considered with CO-Ar due to the interaction between the singlet $A^1\Pi$ excited state and the triplet states with which it overlaps.

In the CO-Ar complex the perturbation of the van der Waals bond on the CO could possibly induce an internal conversion in the CO energy state - from the $A^1\Pi(v' = 3)$ state to that high vibrational level of the $X^1\Sigma^+$ ground state lying in energy just below the $A^1\Pi(v' = 3)$ energy level. The van der Waals bond would probably dissociate in this process due to strong coupling between different vibrational modes at the high vibrational energy. This will leave the CO molecule in a high vibrationally excited level of its ground state from which it will return to the lower vibrational levels of the ground state by infrared emission. Such infrared emission would not be detected in our experiment.

It is known for CO that the singlet $A^1\Pi$ excited state has strong spin-orbit interaction

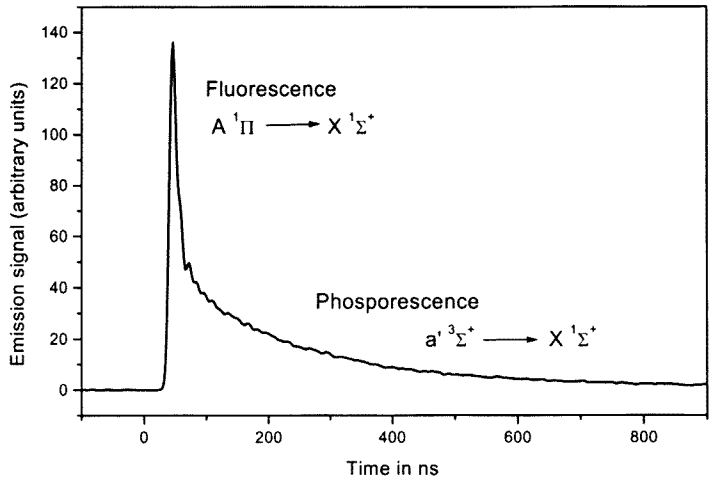

Figure 6-5: The superimposed decay curves of the vacuum ultraviolet laser induced emission from two excited states: the singlet $A^1\Pi(v' = 4, J' = 7)$ and the triplet $a'^3\Sigma^+(v' = 14, J' = 3, N' = 4)$ states. These states were populated simultaneously by pumping at ca. 141.950 nm with a ca. 15 ns laser pulse. The emission was measured by a solarblind photomultiplier. The initial peak ($\tau \sim 20$ ns) is due to the fast decaying $A^1\Pi$ state and slower decaying tail ($\tau > 200$ ns) to the longer lived $a'^3\Sigma^+$ state. (This measurement was made with a setup very similar to ours in the laboratory of Prof. C.R. Vidal at the Max Planck Institut für extraterrestrische Physik during my study visit in 1999.)

with the $a'^3\Sigma^+$, $d^3\Delta$, $e^3\Sigma^-$ and $a^3\Pi$ triplet excited states with which it overlaps in energy [14], facilitating intersystem crossings and intercombination transitions. A CO molecule in one of these triplet states may return directly to the singlet $X^1\Sigma^+$ ground state by emission of vacuum ultraviolet phosphorescence with a lifetime that depends on the specific singlet-triplet coupling [29]. The alternative channel is relaxation to the lowest meta-stable $a^3\Pi$ triplet state by the emission of visible or infrared photons (with a lifetime for this process of the order of microseconds [29]), from which the molecule returns to the singlet $X^1\Sigma^+$ ground state by emission of a vacuum ultraviolet photon with a lifetime in the order of milliseconds [126]. The intersystem crossing channel therefore also produces emission (phosphorescence) in the vacuum ultraviolet, but the emission lifetime is significantly longer than that of the fluorescence from the singlet $A^1\Pi$ excited state, as qualitatively illustrated in figure 6-5. The emission decay curve in figure 6-5 is a superposition of the short lived ($\tau \sim 20$ ns) fluorescence

from the $A^1\Pi(v' = 4, J' = 7)$ singlet state and the longer lived ($\tau > 200$ ns) phosphorescence originating from the $a'^3\Sigma^+(v' = 14, J' = 3, N' = 4)$ triplet state. Note firstly that this specific $a'^3\Sigma^+(v' = 14, J' = 3)$ triplet state has a relatively short radiative lifetime due to strong interaction with a singlet state, and secondly that this measurement was done in stagnant gas ($\sim 10^{-1}$ mbar pressure) meaning that the lifetime is further shortened by collisional relaxation. Under collision-free conditions the radiative lifetimes of the triplet states are longer.

The presence of the van der Waals bond could advance the intersystem crossing channel in excited CO-Ar complexes. If the triplet level to which the intersystem crossing is made would be less than circa 100 cm^{-1} (the estimated binding energy of the van der Waals bond) lower than the $A^1\Pi(v' = 3)$ level the complex could survive the intersystem crossing and, as example, the triplet state complex $CO(a'^3\Sigma^+, v' = 12)$-Ar could be formed. However, the estimated energy difference between the $A^1\Pi(v' = 3)$ level and the $a'^3\Sigma^+(v' = 12)$ level in CO as calculated from molecular constants [12] is 376 cm^{-1} meaning that the complex will probably dissociate in this process. Dissociation will leave the CO molecule in the $a'^3\Sigma^+(v' = 12)$ triplet state. This would mean that the vacuum ultraviolet emission originating from the excited complex or from the triplet CO after dissociation of the complex will decay slowly, spreading the total radiative energy coming from the CO-Ar complexes over a longer time. As a result, the measurement of the signal during the first 30 ns only, as has been shown to be very efficient to detect the fluorescence of the singlet-singlet CO transitions in the experiment, would be inefficient for the detection of the phosphorescence of the complexes. The phosphorescence due to intersystem crossing could therefore also contribute to the failure to detect vacuum ultraviolet emission from the excited CO-Ar complexes by the specific method of data acquisition that is applied. Delaying the time-gate during which the signal is measured by an appropriate period could make the detection method more sensitive to phosphorescence from the triplet states while discriminating against the strong singlet-singlet fluorescence. If complex induced intersystem crossing is occurring, this adjustment in the measuring conditions could be helpful in the detection of the phosphorescence of the complexes.

In conclusion, from ab initio calculations on CO-Ar and comparison with the results on I_2-noble gas complexes, it can be expected that the CO-Ar complex should have a discrete excitation spectrum and that its dissociation rate via direct vibrational predissociation should

be relatively slow. Consequently electronic predissociation channels such as complex-induced internal conversion or intersystem crossing mechanisms could be expected to play a dominant role in the relaxation of the CO($A, v' = 3$)-Ar state. In the case of complex-induced intersystem crossing, our detection system is inefficient in detecting the phosphorescence and in the case of complex-induced internal conversion the infrared emission that would result lies outside the sensitivity range of the photomultiplier tube used. These mechanisms could therefore be the reason for the failure to detect the CO($A, v' = 3$)-Ar$\longleftarrow$CO($X, v'' = 0$)-Ar excitation band of CO-Ar by laser-induced fluorescence.

Chapter 7

Conclusions and outlook

The following sections contain a concise summary of the main results and conclusions, as discussed in chapters 5 and 6, and the outlook towards continuation and extension of the research presented here.

7.1 Summary of results and conclusions

In the study presented here, the experimental setup that was developed in our laboratory was successfully used for high-resolution vacuum ultraviolet laser spectroscopy of a natural CO gas sample under conditions of flow-cooling to rotational temperatures as low as 2 ± 1 K in a pulsed free supersonic jet, with argon or neon as carrier gas.

The experimental parameters that were found to influence the degree of flow-cooling in the jet most are the stagnation pressure, the percentage of CO in the gas mixture that is expanded and the choice of the carrier gas. The effects of these parameters were investigated and used to control the experimental conditions in the jet. Optimal cooling (measured by the $^{12}C^{16}O$ rotational temperature) was obtained in our setup with a stagnation pressure of 4 bar, a gas mixture containing ca. 1 % CO in neon, a gas pulse period of 2.5 ms, nozzle orifice diameter of 0.8 mm and nozzle-to-laser distance of 20 mm. For larger signals and the search of CO van der Waals complexes 25 – 30 % of CO in the gas mixture was used, resulting in a rotational temperature still typically below 10 K.

The typical non-equilibrium characteristics of flow-cooling in a supersonic jet were clearly

observed in our experiment. The rotational relaxation lags behind the translational relaxation, and even among the rotational levels the relaxation of the higher rotational levels lags behind that of the lower rotational levels. The rotational temperatures that the different CO isotopomers reached by flow-cooling in the jet are found to agree roughly with trends expected from collisional momentum transfer.

Laser-induced fluorescence excitation spectroscopy was demonstrated in this study as a sensitive method to obtain low-noise high-resolution excitation spectra of $^{12}C^{16}O$ and its isotopomers. The total undispersed fluorescence was measured upon excitation of individual rotational lines in the $A(v' = 3) - X(v'' = 0)$ vibronic band. Under the low rotational temperature conditions the detection limit for CO isotopomers (especially seen with the rare $^{12}C^{17}O$) was 3 parts per million (equal to a partial pressure of 0.012 mbar in 4 bar stagnant gas prior to expansion). The spectral resolution of the spectra is approximately 0.25 cm^{-1} (0.5 pm at 144.7 nm).

The low rotational temperature of the sample facilitated the spectroscopic detection of rare CO isotopomers in a natural CO gas sample. Six individual rotational lines of $^{12}C^{17}O$, as well as four of $^{12}C^{18}O$, were detected in the $A(v' = 3) - X(v'' = 0)$ vibronic band. The wavelengths of these lines were determined, with an accuracy of ca. 2×10^{-4} nm, using the large number of $^{12}C^{16}O$ and $^{13}C^{16}O$ lines in the spectrum as standard lines for wavelength calibration. The spectral results on $^{12}C^{17}O$ are to my knowledge the first rotationally resolved laboratory measurements reported on the $A^1\Pi - X^1\Sigma^+$ band of this isotopomer. The newly measured $^{12}C^{17}O$ wavelengths were immediately applicable to a recent problem in astrophysics [4] and resulted in the calculation of consistent Doppler shift and heliocentric velocity values [117].

The conditions in a supersonic jet also facilitate the formation and study of van der Waals complexes. In our experimental investigation evidence of complex formation has been found in the decrease of the CO monomer signal under suitable conditions. Evaluating this evidence as well as reports on successful experimental studies of CO-Ar van der Waals complexes, complex formation (CO-Ar/CO-Ne and CO-CO) is considered to occur in our seeded supersonic jet. However, in the spectral region around the $A(v' = 3) - X(v'' = 0)$ band of $^{12}C^{16}O$ that was investigated, no distinct spectral features that could be associated with these complexes were

observed. Although the possibility must be considered that the excitation wavelengths are not lying as predicted inside the wavelength region that was investigated, there are a number of other possible reasons for not observing the complexes' spectral features that are more fundamental of nature. Studies on the excitation and dissociation dynamics of I_2-noble gas van der Waals complexes show that either a continuum excitation spectrum [121] or vibrational and electronic predissociation processes [124] could contribute to a weak or not detectable excitation spectrum of van der Waals complexes. Based on theoretical calculations on the excited CO(A)-Ar complex [81] the excitation spectrum of CO-Ar is expected to be discrete. Complex-induced internal conversion or intersystem crossing, both probably leading to dissociation of the complex, are considered as possible reasons for the failure to detect the excitation spectrum of CO-Ar or CO-Ne complexes by laser-induced fluorescence in the present experiment.

This experimental study on CO has fully exploited the advantages of the combination of a narrow band vacuum ultraviolet laser source and the extreme flow-cooling of the spectroscopic sample in a free supersonic jet. The results obtained with a sample of natural CO gas contributed new wavelengths to the spectral data on the rare $^{12}C^{17}O$ isotopomer. The study also made the first modest contribution of experimental evidence in the previously uninvestigated topic of the electronic excitation and dissociation dynamics of CO-noble gas van der Waals molecules.

The results presented here clearly demonstrate the potential of our experimental setup for vacuum ultraviolet laser spectroscopy and opened the way for further investigation of not only CO isotopomers and complexes, but any other molecular species with distinct spectroscopic features in the vacuum ultraviolet.

7.2 Outlook

As mentioned in the introduction of this dissertation, the study presented here must be considered a pioneer project opening the way for further application of vacuum ultraviolet laser spectroscopy - employing the narrow band tunable vacuum ultraviolet source in combination with supersonic jet techniques - in our laboratory.

Of immediate interest would be continuation of the measurements of the spectral lines

of $^{12}C^{17}O$. These spectral data that can be measured with high sensitivity and calibrated accurately with our experimental setup are of immediate relevance in the field of astrophysical research of the interstellar medium. In this field of research there is a definite need for more extensive laboratory measurements characterising the $A(v') - X(v'' = 0)$ progression of $^{12}C^{17}O$, in particular the bands with $v' = 2-5$ that have been observed already in the vacuum ultraviolet spectrum of the interstellar medium [11, 4]. The present study provided data for the $v' = 3$ band. Similar results for the other bands should be obtainable without significant changes to the experimental setup.

It might be possible to detect the strongest lines of the even rarer $^{13}C^{18}O$ isotopomer in natural abundance with this setup if the fluorescence collection is improved. The $R(0)$ line of $^{12}C^{18}O$ was measured with a signal to noise ratio of 60. At present the fluorescence that is collected comes from a small solid angle of about 0.04 steradians. If the solid angle from which the fluorescence is collected is doubled, for example by placing a collecting mirror behind the gas jet, the detection of the $R(0)$ line of the 100 times less abundant $^{13}C^{18}O$ should be possible. Detection of the $^{13}C^{17}O$ isotopomer that would by the same argument require at least a 5 fold increase in the sensitivity would be more difficult to achieve. The detection of CO isotopomers containing ^{14}C is not possible due to the low natural abundance (^{14}C:$^{13}C \sim 1 : 10^{13}$) of the unstable ^{14}C atom. Operation of our apparatus with isotope enriched samples is not possible due to technical, cost and safety considerations.

Continuation of the search for the excitation spectrum of the CO-noble gas van der Waals complexes might be a bigger experimental challenge, but would contribute valuable results to the fundamental understanding of the CO-noble gas complex as prototype van der Waals complex. In view of the ongoing theoretical work on CO-Ar employing state of the art ab initio methods [63, 81], results on the excitation spectrum of CO-Ar will be most valuable as a test case for these studies. The present study did not yield enough results to clearly indicate the best strategy for the continuation of the investigation, but the following speculative conclusions can be offered. If intersystem crossing and the resulting phosphorescence would be the dominant channel in the dynamics of the excited complex, then delaying the measurement window by an appropriate time interval after the laser pulse could help to detect the phosphorescence associated with the complexes, while discriminating against the strong fluorescence from the

excited singlet states of the uncomplexed CO. It might also be recommended to investigate other v' bands in the $A(v') - X(v'' = 0)$ progression because the probability for intersystem crossing and internal conversion should vary non-monotonically with v'. If electronic predissociation channels were the dominant reason for the failure to observe the spectral features of the CO-Ar complex, it might be recommended to investigate excitations of the complex to CO(A, v')-Ar states with high v' values. The higher the v' level, the more strongly vibrational predissociation competes with electronic quenching and the more probable it becomes to observe fluorescence upon excitation of the complex.

It could also be helpful to make use of other detection methods, such as measurement of absorption or ion-current, to find the features of the excitation spectrum of the CO-Ar and CO-Ne. To obtain good quality absorption spectra would require separation of the sum-frequency beam from all other vacuum ultraviolet radiation that is generated, and careful pulse-to-pulse normalisation of the transmitted vacuum ultraviolet pulse energy with respect to the incident vacuum ultraviolet pulse energy. Ionisation measurements will require designing electrodes for efficient electron and ion collection.

Confirmation of the predicted excitation wavelengths of the CO-Ar and CO-Ne complexes would be helpful in future experiments. We would like to propose to Salazar and Hernández that in future models optimised geometries (regarding the CO bond length, van der Waals bond angle and van der Waals bond length) be used for both the ground and excited state of the complex. To our knowledge such calculations are planned.

In the long term the application of the experimental setup for vacuum ultraviolet laser spectroscopy to new analytical problems is also envisaged. Applications related to the study of CO are the investigations of CO-dimers, metal carbonyls or the adsorption of CO on catalyst surfaces. Another field that is considered is the spectroscopic investigation of selected Si-O containing molecules with ring-structures that are fundamentally related to the structures in technologically important solid silicon-oxide materials, like fused silica. Investigation of these molecules by vacuum ultraviolet spectroscopy might lead to a better understanding of the degradation processes in ultra-pure fused silica during prolonged exposure to ultraviolet radiation. Other possibilities that are currently envisaged are the investigation of the interaction of vacuum ultraviolet radiation with solid state materials such as ultraviolet-transparent crystals

and diamond-like carbon.

For future work, the setup for high-resolution vacuum ultraviolet laser spectroscopy will be complemented by a conventional vacuum spectrometer (McPherson, model 255) fitted with optics and a detector for the analysis of light in the vacuum ultraviolet region. This spectrometer setup will have a lower resolution, but will allow fast and easy recording of absorption spectra of samples over larger spectral regions than can be scanned with a single laser dye in the laser source. It will also be possible to connect the spectrometer to the laser-induced fluorescence setup for recording of dispersed fluorescence spectra emitted upon vacuum ultraviolet laser excitation, as discussed at the end of section 3.3. Additionally the ability of the spectrometer will facilitate further refinement and optimisation of the two-photon resonant four-wave sum-frequency mixing process generating the tunable vacuum ultraviolet radiation as it will facilitate the separate measurement of the sum-frequency and the accompanying third-harmonic signals. Some further recommendations on technical improvements to the current experimental setup are given in appendix 8.2.

The vacuum ultraviolet laser excitation could in future be used in combination with the time-of-flight mass spectrometer that is currently being developed in our group. This will allow employment of laser-induced ionisation as detection method for non-fluorescing species.

Laser spectroscopy in the vacuum ultraviolet has more experimental challenges and is not as widely applicable as some other spectroscopic methods. However, since a tunable narrow bandwidth vacuum ultraviolet laser source is a relatively scarce asset, it is hoped that this setup will be used for further investigation on scientifically and technologically relevant topics in this niche area in spectroscopy.

Chapter 8

Appendices

8.1 Theory of sum-frequency generation in a gaseous medium

The process of four-wave mixing in gases has been discussed in general in numerous publications of which Hanna et al. [101], Shen [127] and Vidal et al. [128, 95] are only a few examples. However, detailed descriptions are usually limited to the case of third harmonic generation. My M.Sc. thesis [102] contains a comprehensive discussion of the theoretical descriptions of four-wave mixing with specific reference to third-harmonic generation, as well as sum-frequency generation in a magnesium-krypton medium. The purpose of the following discussion is to provide a coherent outline of the theoretical description of the specific sum-frequency generation process $\omega_s = 2\omega_1 + \omega_2$, in an atomic gas medium. This should serve as background to the discussion in sections 3.2 and 4.1 where results from this theory are used explicitly or implicitly.

In the framework of the relevant theory on the nature of light and matter, an analysis of the interaction of light with a material medium involves the simultaneous solution of the Schrödinger equation, as description of the response of the atoms or molecules of the material medium to electromagnetic perturbation, and Maxwell's equations describing the response of the electromagnetic wave to the local properties of the medium. This means that the material medium is treated as a quantum mechanical system whereas the electromagnetic radiation is treated classically, as appropriate for strong radiation fields. The Schrödinger equation is solved either by density matrix theory [129] or by a perturbation approach to the density matrix [130] to yield expressions for the linear and nonlinear susceptibilities that characterise

the field dependent properties of the medium completely. In this discussion, the results of the perturbation approach as implemented by Puell and collaborators [130, 131] will be used.

The second part of the problem is to solve the Maxwell equations for the appropriate conditions. In a charge-free, current-free, non-magnetic gaseous medium, the four equations of Maxwell reduce to the Maxwell wave equation (in cgs units),

$$\nabla^2\mathbf{E} - \frac{1}{c^2}\frac{\partial^2\mathbf{E}}{\partial t^2} = \frac{4\pi}{c^2}\frac{\partial^2\mathbf{P}}{\partial t^2}. \tag{8.1}$$

This equation shows that any time dependent polarisation in the medium serves as a source term to an electromagnetic field. Without any loss of generality, the polarisation of a material medium can be separated into a linear and a nonlinear component, $\mathbf{P}^{[L]}$ and $\mathbf{P}^{[NonL]}$ respectively, and the nonlinear component further into contributions of different orders (n),

$$\mathbf{P} = \mathbf{P}^{[L]} + \mathbf{P}^{[NonL]} = \mathbf{P}^{[L]} + \sum_{n=2}^{\infty}\mathbf{P}^{(n)}.$$

Applying this formalism to the Maxwell wave equation for a medium subjected to a continuous plane wave electromagnetic field ($\widehat{E}_j$, propagating in the z direction), assuming that the amplitudes of both the electromagnetic field and the resulting polarisation ($\widehat{P}_j$) of the medium vary slowly on the spatial and temporal scales of the wavelength and period of the electromagnetic wave, equation 8.2 - the so-called fundamental equation of nonlinear optics [128] - is obtained:

$$\begin{aligned}\frac{d\widehat{E}_j}{dz} &= i\frac{2\pi\omega_j}{n_j c}P_j^{[NonL]}e^{-ik_j z} - \frac{\sigma_j^{(1)}}{2}N\widehat{E}_j \\ &= i\frac{2\pi\omega_j}{n_j c}\sum_{n=2}^{\infty}P_j^{(n)}e^{-ik_j z} - \frac{\sigma_j^{(1)}}{2}N\widehat{E}_j.\end{aligned} \tag{8.2}$$

In this equation N is the number density and $\widehat{E}_j$ and $P_j^{(n)}$ are the Cartesian components of the electric field and the n^{th} order nonlinear polarisation at frequency ω_j defined by the Fourier

series

$$\begin{aligned}\mathbf{E}(z,t) &= \frac{1}{2}\sum_j \left[\widehat{\boldsymbol{\varepsilon}}_j \widehat{E}(z,\omega_j)\, e^{-i(\omega_j t - k_j z)} + cc\right] \qquad (8.3)\\ &= \frac{1}{2}\sum_j \left[\widehat{\boldsymbol{\varepsilon}}_j E(r,\omega_j)\, e^{-i\omega_j t} + cc\right] \text{ with } E(r,\omega_j) = \widehat{E}(r,\omega_j)\, e^{ik_j z}\\ \text{and } \mathbf{P}^{(n)}(z,t) &= \frac{1}{2}\sum_j \left[\widehat{\boldsymbol{\varepsilon}}_j P^{(n)}(z,\omega_j)\, e^{-i\omega_j t} + cc\right]. \qquad (8.4)\end{aligned}$$

n_j is the complex index of refraction at frequency ω_j; a scalar quantity in an isotropic gaseous medium. The wave vector k_j of the field at frequency ω_j is related to the real index of refraction $\overline{n}_j$ of the medium at that frequency, which is a direct function of the real part of the linear susceptibility $\overline{\chi}^{(1)}(\omega_j)$. Under the assumption that $n_j \approx 1$ the relation is given by

$$k_j = \frac{\omega_j}{c}\overline{n}_j \approx \left[1 + 2\pi N \overline{\chi}^{(1)}(\omega_j)\right]. \qquad (8.5)$$

The last term of equation 8.2 incorporates one-photon absorption of the field at frequency ω_j. The absorption cross section $\sigma_j^{(1)}$ is related to the imaginary part of the linear susceptibility $\widetilde{\chi}^{(1)}(\omega_j)$ as well as to the real index of refraction of the medium[1] by

$$\sigma_j^{(1)} \approx \frac{4\pi\omega_j}{c\overline{n}_j}\widetilde{\chi}^{(1)}(\omega_j). \qquad (8.6)$$

To model a nonlinear optical process, the fundamental equation of nonlinear optics has to be combined with the results from the Schrödinger equation, namely the definition of the n^{th} order nonlinear susceptibility in terms of the nonlinear polarisation $P_{\alpha_s}^{(n)}$, as well as the explicit quantum mechanical expression for each nonlinear susceptibility tensor $\chi^{(n)}_{\alpha_s\alpha_1\ldots\alpha_n}$. The n^{th} order nonlinear susceptibility is defined by the following most general relation[2] between the

[1] The index of refraction in the denominator of equation 8.6 is often neglegted in literature under the assumption that $\overline{n}_j \approx 1$. See appendix C of reference [102] for a discussion of the different ways this approximation is applied to yield different expressions.

[2] The numerical factor in this relation depends on the convention used. The specific factor $\frac{n!}{2^{n-1}}$ holds for a widely used convention for defining nonlinear susceptibilities (see [102, p. 41]) if no two of the frequencies $\omega_1\ldots\omega_n$ are identical.

polarisation and the electric fields [101, equation 2.7]

$$P_{\alpha_s}^{(n)}(z,\omega_s) = \frac{n!N}{2^{n-1}} \sum_{\alpha_1 \ldots \alpha_n} \chi_{\alpha_s \alpha_1 \ldots \alpha_n}^{(n)} (-\omega_s; \omega_1 \ldots \omega_n) E_{\alpha_1}(z,\omega_1) \ldots E_{\alpha_n}(z,\omega_n)$$

where $\omega_s = \omega_1 + \omega_2 + \ldots + \omega_n$ and α_s, $\alpha_1 \ldots \alpha_n$ each describe the "polarisation orientation"[3] of the component. The general quantum mechanical expression for the n^{th} order nonlinear susceptibility is a tensor of rank $n+1$, according to Hanna et al. [101, equation 2.15] given by the expression

$$\chi_{\alpha_s \alpha_1 \alpha_2 \ldots \alpha_n}^{(n)} (-\omega_s; \omega_1 \ldots \omega_n) = \tag{8.7}$$

$$\frac{S_T}{n!\hbar^n} \sum_{g, b_1 \ldots b_n} \rho(g) \frac{\langle g| \mu_{\alpha_s}(\omega_s) |b_1\rangle \langle b_1| \mu_{\alpha_1}(\omega_1) |b_2\rangle \ldots \langle b_n| \mu_{\alpha_n}(\omega_n) |g\rangle}{(\omega_{b_1 g} - \omega_1 - \omega_2 \ldots - \omega_n)(\omega_{b_2 g} - \omega_2 \ldots - \omega_n) \ldots (\omega_{b_n g} - \omega_n)}$$

where

$$\mu_{nm}^{\alpha} = \langle n| \mu_{\alpha}(\omega) |m\rangle \tag{8.8}$$

is the expectation value of the transition electric dipole moment and

$$\omega_{nm} = \Omega_{nm} - i\Gamma_{nm}. \tag{8.9}$$

is the complex transition frequency of the transition between states n and m. The sum over all atomic (or molecular) states $b_1 \ldots b_n$ as well as over all the possible initial states g weighted by their unperturbed population densities $\rho(g)$ must be calculated. S_T is a permutation operator indicating that summation must be carried out over all permutations of the $n+1$ interacting waves and therefore all permutations of the parameter pairs $\alpha_s \omega_s$, $\alpha_1 \omega_1$, ..., $\alpha_n \omega_n$.

A general solution that involves solving the fundamental equation 8.2 simultaneously for every relevant frequency present in the nonlinear medium, each potentially including nonlinear

[3]The "polarisation orientation" refers to the transverse polarisation of the electromagnetic field that is propagating in the z direction, for example left or right hand circular polarisation or linear polarisation in the x or y direction.

contributions of several orders, is not possible. However, analytical solutions can be obtained for specific physical conditions. Considering only the case relevant to our experimental setup, extensive simplifications can be made. For a gaseous nonlinear medium showing inversion symmetry only odd order nonlinear contributions to the polarisation exist[4]. Working with moderate dye laser powers as in our work it is safe to assume that only third order nonlinear processes will be significant. The fundamental equation 8.2 can therefore be simplified to

$$\frac{d\widehat{E}_j}{dz} = i\frac{2\pi\omega_j}{n_j c}P_j^{(3)}e^{-ik_j z} - \frac{\sigma_j^{(1)}}{2}N\widehat{E}_j. \tag{8.10}$$

The next consideration is which frequencies ω_j will be significant in the medium. In our experimental setup there are two incident laser beams at frequencies ω_1 and ω_2. The conditions are optimised to enhance the generation of the sum-frequency $\omega_s = 2\omega_1 + \omega_2$. The processes of third-harmonic generation $\omega_{TH} = 3\omega_1$ and difference frequency generation $\omega_s = 2\omega_1 - \omega_2$ are also possible, although discriminated against by the experimental conditions. However, in the small signal limit the different nonlinear processes should be approximately independent and the sum-frequency generation process can be considered separately. Considering only the sum-frequency generation process equation 8.10 must be solved for ω_1 and ω_2 and $\omega_s = 2\omega_1 + \omega_2$. In the small signal limit, quantified as $|E_s| \ll |E_1|$ or $|E_2|$, it can be assumed that the incident field amplitudes are only attenuated by one-photon absorption and not by the nonlinear process itself. Thus $\widehat{E}_1$, $\widehat{E}_2$ can be expressed as

$$\begin{aligned}
\widehat{E}_1(z) &= \widehat{E}_1(z=0)\exp\left(-\frac{N\sigma_1^{(1)}}{2}\right) \\
\widehat{E}_2(z) &= \widehat{E}_2(z=0)\exp\left(-\frac{N\sigma_2^{(1)}}{2}\right)
\end{aligned}$$

with the incident light entering the medium at position $z = 0$. The propagation of the sum-

[4]This can be seen by inspection from the expression 8.12 for the nonlinear susceptibility. The electric dipole moment factors $\langle n|\,\mu_{\alpha_j}(\omega_j)\,|m\rangle$ in the numerator of $\chi^{(n)}$ obey the selection rule for electric dipole transitions, being only non-zero if the states n and m have opposite parity. In non-hydrogenic gaseous media where all states have definite parity, a non-zero numerator is not possible for even orders. In solid state optical media where states of different parity are mixed, this selection rule breaks down allowing even order processes.

frequency field is defined by the differential equation

$$\frac{d\widehat{E}_s}{dz} = i\frac{2\pi\omega_s}{n_s c}P^{(3)}(z,\omega_s)\,e^{-ik_s z} - \frac{\sigma_s^{(1)}}{2}N\widehat{E}_s \tag{8.11}$$

The definition of the nonlinear polarisation in terms of susceptibilities can also be simplified. In the quantum mechanical expression for $\chi^{(n)}_{\alpha_s\alpha_1\alpha_2\ldots\alpha_n}(-\omega_s;\omega_1\ldots\omega_n)$ application of the permutation operator yields a number of terms of which all but the dominant one can generally be neglected. The expression for the appropriate third order nonlinear susceptibility $\chi^{(3)}_{\alpha_s\alpha_1\alpha_1\alpha_2}(-\omega_s;\omega_1,\omega_1,\omega_2)$ can be approximated by

$$\chi^{(3)}_{\alpha_s\alpha_1\alpha_1\alpha_2}(-\omega_s;\omega_1,\omega_1,\omega_2) = \tag{8.12}$$

$$\frac{1}{\hbar^3}\sum_{g,l,m,n}\rho(g)\frac{\langle g|\,\mu_{\alpha_s}(\omega_s)\,|l\rangle\,\langle l|\,\mu_{\alpha_1}(\omega_1)\,|m\rangle\,\langle m|\,\mu_{\alpha_1}(\omega_1)\,|n\rangle\,\langle n|\,\mu_{\alpha_2}(\omega_2)\,|g\rangle}{(\omega_{lg}-\omega_1-\omega_1-\omega_2)(\omega_{mg}-\omega_1-\omega_1)(\omega_{ng}-\omega_1)}.$$

The sum over the different states g can be neglected in the atomic magnesium medium at circa 750 $^\circ C$ as the population densities $\rho(g)$ and therefore the contributions of all but the lowest energy ground state of the atoms are very small. Using the two-photon resonance of ω_1 with the $m-g$ transition for resonant enhancement, the expression for the nonlinear susceptibility for the sum-frequency process becomes:

$$\chi^{(3)}_{\alpha_s\alpha_1\alpha_1\alpha_2}(-\omega_s;\omega_1,\omega_1,\omega_2) = \tag{8.13}$$

$$\frac{1}{\hbar^3}\frac{1}{(\omega_{mg}-\omega_1-\omega_1)}\sum_l\frac{\langle g|\,\mu_{\alpha_s}(\omega_s)\,|l\rangle\,\langle l|\,\mu_{\alpha_1}(\omega_1)\,|m\rangle}{(\omega_{lg}-\omega_1-\omega_1-\omega_2)}\sum_n\frac{\langle m|\,\mu_{\alpha_1}(\omega_1)\,|n\rangle\,\langle n|\,\mu_{\alpha_2}(\omega_2)\,|g\rangle}{(\omega_{ng}-\omega_1)}.$$

The sum over the polarisation orientations in the expression for $P_j^{(3)}$ can be simplified as well by applying the angular momentum selection rules governing $\chi^{(3)}_{\alpha_s\alpha_1\ldots\alpha_n}$ and taking into account the polarisations of the incident laser beams in the experiment. In the four electric dipole moment factors $\langle a|\,\mu_{\alpha_j}(\omega_j)\,|b\rangle$ in the numerator of $\chi^{(3)}_{\alpha_s\alpha_1\alpha_1\alpha_2}$ both states $|a\rangle$ and $|b\rangle$ are

atomic angular momentum eigenstates characterised by magnetic quantum numbers m_a and m_b respectively. The Wigner-Eckart theorem [132] is applicable to them yielding the selection rule

$$\triangle m_1 + \triangle m_1 + \triangle m_2 + \triangle m_s = 0 \tag{8.14}$$

where $\triangle m_j$ is the change in the magnetic quantum number associated with the electric dipole moment operator dependent on its polarisation orientation α_j. When using for example circularly polarised incident laser beams, this selection rule allows the generation of the sum-frequency $\omega_s = \omega_1 + \omega_1 + \omega_2$ only if the beams of frequencies ω_1 and ω_2 are polarised circularly in opposite ways ($\triangle m$ is $+1$ and -1 respectively). The generation of the third harmonic of ω_1 is then theoretically forbidden. Thus only one term remains in the expression for the third order nonlinear polarisation given by

$$P^{(3)}_{\alpha_{-1}}(z,\omega_s) = \frac{3N}{4}\chi^{(3)}_{\alpha_{-1}\alpha_{+1}\alpha_{+1}\alpha_{-1}}(-\omega_s;\omega_1,\omega_1,\omega_2)\left[E_{\alpha_{+1}}(z,\omega_1)\right]^2 E_{\alpha_{-1}}(z,\omega_2)$$

or simply written as

$$P^{(3)}(z,\omega_s) = \frac{3N}{4}\chi^{(3)}(-\omega_s;\omega_1,\omega_1,\omega_2)\left[E(z,\omega_1)\right]^2 E(z,\omega_2)\,. \tag{8.15}$$

When these simplifications are substituted into equation 8.11 and the expression is integrated over a medium length L (assuming a rectangular density profile of the medium in the region $0 \leq z \leq L$) an expression is obtained for the amplitude of the generated sum-frequency field at the end of the medium (position $z = L$):

$$\begin{aligned}\widehat{E_s}(L) \;=\; & i\frac{\pi\omega_s}{2cn_s}\frac{3N}{2}L\chi^{(3)}(-\omega_s;\omega_1,\omega_1,\omega_2)\left(\widehat{E_1}(0)\right)^2\left(\widehat{E_2}(0)\right) \\ & \frac{\exp(-\Gamma_s/2)}{\frac{\Gamma_s-\Gamma_i}{2}-i\triangle kL}\left(\exp\left(\frac{\Gamma_s-\Gamma_i}{2}-i\triangle kL\right)-1\right)\end{aligned} \tag{8.16}$$

The absorption cross sections have been rewritten here as optical depths (opacities):

$$\Gamma_s = \sigma^{(1)}(\omega_s)NL$$

is the optical depth of the medium for the sum-frequency wave and

$$\Gamma_i = 2\Gamma_1 + \Gamma_2 = \left(2\sigma^{(1)}(\omega_1) + \sigma^{(1)}(\omega_2)\right) NL$$

is the total optical depth for the incident waves. The wave vector difference $\triangle k$ is defined as

$$\triangle k = k_s - (2k_1 + k_2)$$

Taking the modulus squared and using the relation between intensity and amplitude $I_j(z) = \frac{n_j c}{8\pi}\left|\widehat{E_j}(z)\right|^2$ equation 8.16 can be rewritten in terms of intensities

$$I_s(L) = \frac{144\pi^4\omega_s^2}{c^4 n_s (n_1)^2 n_2} N^2 L^2 \left|\chi^{(3)}(-\omega_s;\omega_1,\omega_1,\omega_2)\right|^2 [I_1(0)]^2 [I_2(0)]\, F(\triangle kL, \Gamma_i, \Gamma_s) \qquad (8.17)$$

$F(\triangle kL, \Gamma_i, \Gamma_s)$ is the phase matching factor, containing the dependence of the process on the wave vector mismatch $\triangle k$. The phase matching factor is generally maximised by minimising the value of $\triangle k$, which corresponds to the conservation of linear momentum in the interaction between the four electromagnetic fields. In the case of collinear laser beams, this requirement of $\triangle k = 0$ for optimal conversion can be expressed as a relation between the indices of refraction of the medium at the incident and generated frequencies: $2\omega_1 n_1 + \omega_2 n_2 = \omega_s n_s$.

The specific form of the expression for the phase matching factor is influenced by the optical depths Γ_i and Γ_s, the density profile of the medium and the focussing conditions of the incident laser beams. It is given in general by the expression

$$F(\triangle kL, \Gamma_i, \Gamma_s) = \frac{\exp(-\Gamma_i) + \exp(-\Gamma_s) - 2\exp(-\frac{\Gamma_s - \Gamma_i}{2})\cos(\triangle kL)}{\left(\frac{\Gamma_s - \Gamma_i}{2}\right)^2 + (\triangle kL)^2} \qquad (8.18)$$

In a magnesium vapour medium the incident frequencies can be chosen to minimise the value of Γ_i, but the absorption of the vacuum ultraviolet sum-frequency wave is often associated with

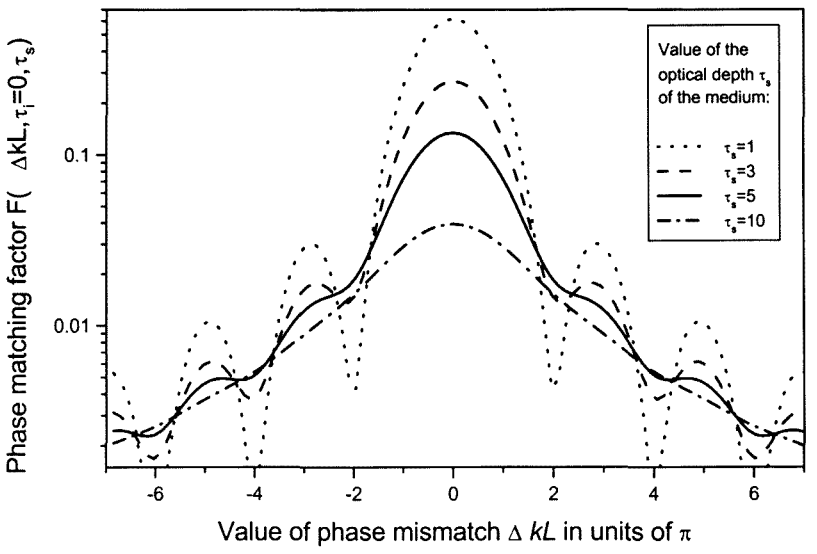

Figure 8-1: Theoretical phase matching curves calculated for different values of the optical depth Γ_s. A logarithmic scale is used on the vertical axis to make the oscillatory structure clearly observable.

auto-ionisation of the medium that cannot be avoided. In this case the phase matching factor is given by

$$F(\triangle kL, \Gamma_i \ll 1, \Gamma_s) \approx F(\triangle kL, \Gamma_s) = \frac{1 + \exp(-\Gamma_s) - 2\exp(-\frac{\Gamma_s}{2})\cos(\triangle kL)}{\left(\frac{\Gamma_s}{2}\right)^2 + (\triangle kL)^2} \tag{8.19}$$

Figure 8-1 illustrates theoretical phase matching curves for different values of the optical thickness of the medium Γ_s. Experimental phase matching curves show an asymmetry dominantly due to the magnesium vapour medium in the heat pipe not being perfectly uniform (having density gradient on both sides) and to a lesser extent due to the slight focussing of the laser beams in our setup [133, 128].

Equation 8.17 with phase matching factor 8.19 is appropriate to describe sum-frequency generation in the magnesium vapour medium used in the present work under conditions of moderate laser intensities (i.e. in the small signal limit). These equations show the intensity of the sum-frequency light generated to be dependent on:

- the square of the number density of the medium N and the medium length L (within

certain limits since a denser or longer medium also contributes to greater opcity of the medium),

- the intensities of the incident beams $[I_1(0)]^2\,[I_2(0)]$, therefore (to first approximation) to the cube of the average incident laser intensity,
- the square of the nonlinear susceptibility $\chi^{(3)}\left(-\omega_s;\omega_1,\omega_1,\omega_2\right)$ which in turn is influenced by angular momentum selection rules and can be enhanced by appropriate resonances,
- the phase matching factor $F(\triangle kL,\Gamma_s)$ that is influenced most by the value of the wave number mismatch $\triangle kL$ and the optical thickness of the medium for the sum-frequency wave Γ_s,
- other conditions influencing the peak position and symmetry of the phase matching factor, namely the deviation of the true density profile of the medium from the assumed rectangular profile and the focussing of the incident laser beams[5].

8.2 Technical recommendations for future work

Regarding the experimental setup a few suggestions for future modifications and improvement can be made.

The first recommended modification is the implementation of a mechanism to separate the wavelengths entering the sample volume from the vacuum ultraviolet source. As discussed in section 4.1 no attempt was made in the present work to separate the tunable vacuum ultraviolet sum-frequency from the fixed vacuum ultraviolet third-harmonic frequency or the visible frequencies that are all present in the beam. The elimination of the third-harmonic and visible frequencies will be essential for future spectroscopy on molecules where the presence of additional frequencies (visible or vacuum ultraviolet) might influence the spectroscopic process. The separation of the sum-frequency beam from the third-harmonic is also necessary for quantitative measurements of the power of the incident vacuum ultraviolet sum-frequency radiation.

[5]The discussion up to here has strictly been for plane waves which holds approximately for laser beams in the parallel beam limit. When the incident laser beams are focussed in the nonlinear medium as would normally be done in an experimental setup, the phase matching factor becomes dependent on the focussing condition. However in our experiment the incident beams are relatively weakly focussed and the parallel beam limit remains a good first order approximation.

Separation of the different wavelengths could be done using a suitable lens [134] or a customised prism as used by Yamanouchi et al. [99] with a small apex angle and carefully aligned baffles to block the unwanted frequency components.

For quantitative fluorescence measurements the setup should also be modified to measure the sum-frequency power by splitting off a few percent of the beam after the frequency separation, before the experimental volume. These measurements of the sum-frequency power can then be used to normalise the fluorescence signal of each laser pulse with respect to the vacuum ultraviolet sum-frequency power generated by that pulse. This should improve the signal to noise ratio of the scans and will yield fluorescence measurements that are not only of qualitative but also of quantitative significance.

The slow random drift in the baseline of the integrated signal coming from the boxcar integrators was a problem in the present work (see the last paragraph of section 4.3). This could be reduced by investigating the use of higher repetition rates in the scans so that the drift will have a longer time scale relative to the scan rate. An improvement could be obtained by changing the control programme of the data acquisition system in such a way that the boxcar acquires an additional background data point between each two laser shots. When the thus acquired background spectrum is (automatically) subtracted from the fluorescence spectrum the electronic drift should be eliminated. The ideal would be the recording of a complete emission decay curve in digital form for each laser shot. From such data the decay rate constant, emission amplitude, as well as emission quantum yield can be obtained shot-to-shot. This however requires fast recording and processing of large volumes of data.

In the present work the pulsed gas valve was controlled by a home-built controller, providing voltage pulses at only about 75 % of the voltage specified for the valve (see section 4.2). This was probably the cause of some technical difficulties in working with the valve and the failure to obtain shorter gas pulses. I would recommend the replacement of the home-built controller with the commercial Iota One valve driver of General Valves Corporation which has in the mean time become available.

Bibliography

[1] E.F. Van Drieshoek and J.H. Black (1988). "The photodissociation of interstellar CO", *The Astrophysical Journal* **334**, 771-802.

[2] C. Letzelter, M. Eidelsberg, F. Rostas, J. Breton and B. Thieblemont (1987). "Photoabsorption and photodissociation cross sections of CO between 88.5 and 115 nm", *Chemical Physics* **114**, 273-288.

[3] H.G. Kim and S.S. Hong (2002). "Carbon monoxide observations of small dark globules. I. Internal structure", *The Astrophysical Journal* **567**, 376-390.

[4] Y. Sheffer, D.L. Lambert and S.R. Federman (2002). "Ultraviolet detection of interstellar $^{12}C^{17}O$ and the CO isotopomeric ratios toward X Persei", *The Astrophysical Journal* **574**, L171-L174.

[5] D.S. Balser, J.P. McMullin and T.L. Wilson (2002). "CO isotopes in planetary nebulae", *The Astrophysical Journal* **572**, 326-334.

[6] P.H. Krupenie (1966). "The band spectrum of carbon monoxide", *National Standard Reference data Series - National Bureau of Standards* **5**, Washington D.C..

[7] P. Bergamaschi, R. Hein, C.A.M. Brenninkmeijer and P.J. Crutzen (2000). "Inverse modeling of the global CO cycle, 2, Inversion of $^{13}C/^{12}C$ and $^{18}O/^{16}O$ isotope ratios", *Journal of Geophysical Research - Atmospheres* **105** (D2), 1929-1945.

[8] P. Quay, S. King, D. White, M. Brockington, B. Plotkin, R. Gammon, S. Gerst, J. Stutsman (2000). "Atmospheric (CO)-^{14}C: A tracer of OH concentration and mixing rates", *Journal of Geophysical Research - Atmospheres* **105** (D12), 15147-15166.

[9] Y. Xu and A.R.W. McKellar (1996). "The infrared spectrum of the Ar-CO complex. Comprehensive analysis including van der Waals stretching and bending states", *Molecular Physics* **88**, 859-874.

[10] Atomic Masses and Abundances (1996-1997). In D.R. Lide (Eds.), *Handbook of Chemistry and Physics*, 77th edition, p. 1-10, CRC Press, Boca Raton.

[11] D.C. Morton and L. Noreau (1994). "A compilation of electronic transitions in the CO molecule and the interpretation of some puzzling interstellar absorption features", *The Astrophysical Journal Supplement Series* **95**, 301-343.

[12] K.P. Huber and G. Herzberg (1979). "*Molecular spectra and molecular structure. IV. Constants of diatomic molecules*". Van Nostrand Reinhold company, New York.

[13] A. Mellinger (1995). "*Untersuchung hochangeregter Triplettzustände des CO-Moleküls*", Ph.D. dissertation, Technische Universität München and Max Planck Institut für extraterrestrische Physik, Garching, Germany.

[14] J.D. Simmons, A.M. Bass and S.G. Tilford (1969). "The fourth positive system of carbon monoxide observed in absorption at high resolution in the vacuum ultraviolet region", *The Astrophysical Journal* **155**, 345-358.

[15] A.E. Glassgold, P.J. Huggins and W.D. Langer (1985). "Shielding of CO from dissociating radiation in interstellar clouds", *The Astrophysical Journal* **290**, 615-626.

[16] A. Mellinger, E.G. Rohwer and C.R. Vidal (2001). "Carbon monoxide triplet Rydberg series in the f complex region", *Journal of Molecular Spectroscopy* **206**, 126-134.

[17] T. Ebata, N. Hosoi and M. Ito (1992). "Rotational analysis of $v = 1$ level of $n = 8 - 10$ Rydberg states of CO by triple resonant multiphoton spectroscopy", *Journal of Chemical Physics* **97**, 3920-3930.

[18] M. Eidelsberg, A. Jolly, J.L. Lemaire, W.-ÜL. Tchang-Brillet, J. Breton and F. Rostas (1999). "Experimental determination of the band oscillator strengths of the CO $A^1\Pi(11 \leq v' \leq 23) - X^1\Sigma^+(v'' = 0)$ made at the LURE-SuperACO synchrotron facility", *Astronomy and Astrophysics* **346**, 705-712.

[19] J. Baker, F. Launay, M. Eidelsberg and F. Rostas (2000). "A reinvestigation of the $c^3\Pi - X^1\Sigma(0-0)$ absorption band of carbon monoxide", *Journal of Molecular Spectroscopy* **203**, 314-319.

[20] S. Sekin, Y. Adachi and C. Hirose (1989). "Optogalvanic observation of the CO $W^1\Pi$-$B^1\Sigma^+$ transition", *Journal of Chemical Physics* **90**, 5346-5348.

[21] S. Sekin, T. Masaki, Y. Adachi and C. Hirose (1988). "Optogalvanic spectrum of CO. II. The rotational structure of the $L^1\Pi$ state", *Journal of Chemical Physics* **89**, 3951-3954.

[22] M. Drabbels, J. Heinze, J.J. ter Meulen and W. Leo Meerts (1993). "High resolution double-resonance spectroscopy on Rydberg states of CO", *Journal of Chemical Physics* **99**, 5701-5711.

[23] M. Komatsu, T. Ebata, T. Maeyama and N. Mikami (1995). "Rotational structure and dissociation of the Rydberg states of CO investigated by ion-dip spectroscopy", *Journal of Chemical Physics* **103**, 2420-2435.

[24] M. Komatsu, T. Ebata and N. Mikami (1993). "Rotational analysis of $n = 4-7$ Rydberg states of CO observed by ion-dip spectroscopy", *Journal of Chemical Physics* **99**, 9350-9365.

[25] A. Fujii, T. Ebata and M. Ito (1989). "Production of rotationally state selected ions by resonant enhanced multiphoton ionization of CO in a supersonic free jet", *Chemical Physics Letters* **161**, 93-97.

[26] J. Baker, J.L. Lemaire, S. Couris, A. Vient, D. Malmasson and F. Rostas (1993). " A 2+1 REMPI study of the E-X transition in CO. Indirect predissociations in the $E^1\Pi$ state", *Chemical Physics* **178**, 569-579.

[27] M.A. Hines, H.A. Michelsen and R.N. Zare (1990). "2+1 resonantly enhanced multiphoton ionization of CO via the $E^1\Pi$-$X^1\Sigma^+$ transition: From measured ion signals to quantitative population distributions", *Journal of Chemical Physics* **93**, 8557-8564.

[28] A. Mellinger and C.R. Vidal (1994). "Laser-reduced fluorescence spectroscopy on predissociated CO triplet states", *Journal of Chemical Physics* **101**, 104-110.

[29] K.H. Strobl and C.R. Vidal (1987). "Radiative lifetimes of selected rovibronic triplet levels of the CO molecule", *Journal of Chemical Physics* **86**, 62-70.

[30] P. Klopotek and C.R. Vidal (1985). "Two-step vacuum-ultraviolet visible excitation spectroscopy on the CO molecule", *Journal of the Optical Society of America B* **2**, 869-876.

[31] K.S.E. Eikema, W. Hogervorst and W. Ubachs (1994). "Predissociation rates in carbon monoxide: dependence on rotational state, parity and isotope", *Chemical Physics* **181**, 217-245.

[32] P.F. Levelt, W. Urbachs and W. Hogervorst (1992). "Extreme ultraviolet laser spectroscopy on CO in the 91-100 nm range", *Journal of Chemical Physics* **97**, 7160-7166.

[33] F. Merkt and T.P. Softley (1990). "Resonance-enhanced sum-frequency generation of XUV radiation in CO", *Chemical Physics Letters* **165**, 477-486.

[34] K. Tsukiyama, M. Momose, M. Tsukakoshi and T. Kasuya (1990). "Generation of XUV radiation by four-wave mixing in CO", *Optics Communications* **79**, 88-92.

[35] G. Herzberg (1950). "*Molecular spectra and molecular structure. I. Spectra of diatomic molecules*". Van Nostrand Reinhold company, New York.

[36] S.G. Tilford and J.D. Simmons (1972). "Atlas of the observed absorption spectrum of carbon monoxide between 1060 and 1900 Å", *Journal of Physical and Chemical Reference Data* **1**, 147-187.

[37] D.S. Meier and J.L. Turner (2001). "Molecular gas and star formation in the nucleus of IC 342: $C^{18}O$ and millimeter continuum imaging", *The Astrophysical Journal* **551**, 687-701.

[38] A.M. Smith and T.P. Stecher (1971). "Carbon monoxide in the interstellar spectrum of Zeta Ophiuchi", *The Astrophysical Journal* **164**, L43-L47.

[39] A.M. Smith, F.C. Bruhweiler, D.L. Lambert, B.D. Savage, J.A. Cardelli, D.C. Ebbets, C.-H. Lyu and Y. Sheffer (1991). "First results from Goddard High-Resolution Spectrograph: C_I, S_I and CO toward ζ Persei and the physical conditions in diffuse clouds", *The Astrophysical Journal* **377**, L61-L64.

[40] Y. Sheffer, S.R. Federman, D.L. Lambert and J.A. Cardelli (1992). "Fractionation of CO in the diffuse clouds toward ζ Ophiuchi", *The Astrophysical Journal* **397**, 482-491.

[41] L.M. Beaty, V.D. Braun and K.P. Huber (1997). "A high-resolution ^{18}O isotope study in the vacuum ultraviolet of the $A^1\Pi \rightarrow X^1\Sigma^+$ 4th positive system of CO", *The Astrophysical Journal Supplement Series* **109**, 269-277.

[42] M. Rytel (1970). "Ångström system of the $^{12}C^{18}O$ molecule", *Acta Physica Polonica* **A38**, 299-308.

[43] M. Rytel (1970). "The Ångström system of the $^{13}C^{16}O$ molecule", *Acta Physica Polonica* **A37**, 559-568.

[44] Z. Malak, M. Rytel, J.D. Janjić and D.S. Pešić (1984). "Ångström system of the $^{13}C^{18}O$ molecule", *Acta Physica Hungarica* **55**, 85-95.

[45] M. Eidelsberg, J.-Y. Roncin, A. Le Floch, F. Launay, C. Letzelter and J. Rostas (1987). "Reinvestigation of the vacuum ultraviolet spectrum of CO and isotopic species: the $B^1\Sigma^+ \longleftrightarrow X^1\Sigma^+$ transition", *Journal of Molecular Spectroscopy* **121**, 309-336.

[46] A.C. Le Floch, F. Launay, J. Rostas, R.W. Field, C.M. Brown and K. Yoshino (1987). "Reinvestigation of the CO $A^1\Pi$ state and its perturbations: the $v = 0$ level", *Journal of Molecular Spectroscopy* **121**, 337-379.

[47] C. Haridass and K.P. Huber (1994). "A high-resolution ^{13}C isotope study in the vacuum ultraviolet of spectra of CO($A \longleftarrow X$), C I and C II", *The Astrophysical Journal* **420**, 433-438.

[48] C. Haridass, S. Paddi Reddy and A.C. Le Flocht (1994). "The Fourth Positive ($A^1\Pi \rightarrow X^1\Sigma^+$) system of $^{12}C^{18}O$ and $^{13}C^{18}O$: Perturbations in the $A^1\Pi$ state", *Journal of Molecular Spectroscopy* **167**, 334-352.

[49] M. Eidelsberg and F. Rostas (1990). "Spectroscopic, absorption and photodissociation data for CO and isotopic species between 91 and 115 nm", *Astronomy and Astrophysics* **235**, 472-489.

[50] J. Baker and F. Launay (2000). "First observation of the forbidden $k - X$ transition of $^{13}C^{16}O$", *Journal of Molecular Spectroscopy* **203**, 196-199.

[51] W. Ubachs, I. Velchev and P. Cacciani (2000). "Predissociation in the $E^1\Pi$, $v = 1$ state of the six natural isotopomers of CO", *Journal of Chemical Physics* **113**, 547-560.

[52] C. Chakravarty, D.C. Clary, A. Degli Esposti and H.-J. Werner (1990). "Calculation of the electronic spectrum for Ar-OH", *Journal of Chemical Physics* **93** (5), 3367-3378.

[53] S. Bauerecker and M. Taraschewski (2001). "Liquid-helium temperature long-path infrared spectroscopy of molecular clusters and supercooled molecules", *Review of Scientific Instruments* **72**, 3946-3955.

[54] M.C. Salazar, J.L. Paz, A.J. Hernández (1998). "Test study on the excitation spectra of the CO-H_2 van der Waals molecule", *Journal of Molecular Structure (Theochem)* **426**, 53-58.

[55] M.D. Brookes and A.R.W. McKellar (1999). "Infrared spectra of the Kr-CO and Xe-CO van der Waals complexes", *Molecular Physics* **97**, 127-137.

[56] R.R. Toczylowski and S.M. Cybulski (2000). "An ab initio study of the potential energy surface and spectrum of Ar-CO", *Journal of Chemical Physics* **112**, 4604-4612.

[57] A.R.W. McKellar (2000). "Infrared spectrum of the Ar-CO complex: observation of the $v_{CO} = 2 \longleftarrow 0$ band at 4260 cm^{-1}", *Molecular Physics* **98**, 111-115.

[58] M. Hepp, W. Jäger, I. Pak and G. Winnewisser (1996). "Absorption measurements of Ar-CO b-type rotational transitions with a supersonic jet millimeter-wave spectrometer", *Journal of Molecular Spectroscopy* **176**, 58-63.

[59] M. Hepp, R. Gendriesch, I. Pak, F. Lewen, G. Winnewisser (1997). "Submilllimeter-wave absorption spectroscopy of the Ar-CO complex: detection of the van der Waals bending vibration", *Journal of Molecular Spectrscopy* **183**, 295-299.

[60] M. Hepp, R. Gendriesch, I. Pak, Y.A. Kuritsyn, F. Lewen, G. Winnewisser, M. Brookes, A.R.W. McKellar, J.K.G. Watson and T. Amano (1997). "Millimetre-wave spectrum of

the Ar-CO complex: the $K = 2 \leftarrow 1$ and $3 \leftarrow 2$ subbands", *Molecular Physics* **92**, 229-236.

[61] R. Gendriesch, I. Pak, F. Lewen, L. Surin, D.A. Roth and G. Winnewisser (1999). "Sub-millimeter Detection of the van der Waals Stretching Vibration of the Ar-CO Complex", *Journal of Molecular Spectroscopy* **196**, 139-145.

[62] G. Jansen (1996). "The rovibrational spectrum of the ArCO complex calculated from a semiempirically extrapolated coupled pair functional potential energy surface", *Journal of Chemical Physics* **105**, 89-103.

[63] F.A. Gianturco and F. Paesani (2001). "The rovibrational structure of the Ar-CO complex from a model interaction potential", *Journal of Chemical Physics* **115**, 249-256.

[64] T.B. Pedersen, J.L. Cacheiro, B. Fernandez and H. Koch (2002). "Rovibrational structure of the Ar-CO complex based on a novel three-dimensional ab initio potential", *Journal of Chemical Physics* **117**, 6562-6572.

[65] A.R.W. McKellar, Y. Xu, W. Jäger and C. Bissonnette (1999). "Isotopic probing of very weak intermolecular forces: Microwave and infrared spectra of CO-He isotopomers", *Journal of Chemical Physics* **110**, 10766-10773.

[66] R.W. Randall, A.J. Cliffe, B.J. Howard and A.R.W. McKellar (1993). "The infrared spectrum of Ne-CO: Analysis of combined jet and statistic cell data for ^{20}Ne and ^{22}Ne" *Molecular Physics* **79**, 1113-1126.

[67] A.R.W. McKellar and M.-C. Chan (1998). "Infrared spectrum of the CO-Ne complex: long-path diode laser observations of higher excited states", *Molecular Physics* **93**, 253-262.

[68] K.A. Walker, T. Ogata, W. Jäger, M.C.L. Gerry and I. Ozier (1997). "Pure rotational spectra of the van der Waals complexes Ne-CO, Kr-CO, and Xe-CO", *Journal of Chemical Physics* **106**, 7519-7530.

[69] G. Winnewisser, B.S. Dumesh, I. Pak, L.A. Surin, F. Lewen, D.A. Roth and F.S. Rusin (1998). "Novel intracavity jet millimeter wave spectrometer: Detection of b-type rotational transitions of Ne-CO", *Journal of Molecular Spectroscopy* **192**, 243-246.

[70] L.A. Surin, B.S. Dumesh, F. Lewen, D.A. Roth, V.P. Kostromin, F.S. Rusin, G. Winnewisser and I. Pak (2001). "Millimeter-wave intracavity-jet ORTRON-spectrometer for investigation of van der Waals complexes", *Review of Scientific Instruments* **72**, 2535-2542.

[71] R. Moszynski, T. Korona, P.E.S. Wormer and A. van der Avoird (1997). "Ab initio potential energy surface and infrared spectrum of the Ne-CO complex", *Journal of Physical Chemistry A* **101**, 4690-4698.

[72] G.C. McBane and S.M. Cybulski (1999). "An ab initio pontential energy surface for Ne-CO", *Journal of Chemical Physics* **110**, 11734-11741.

[73] K.A. Walker and A.R.W. McKellar (2001). "Millimeter-wave spectroscopy of Kr-CO and Xe-CO using a coaxial jet spectrometer", *Journal of Molecular Spectroscopy* **205**, 331-337.

[74] Y. Xu and W. Jäger (1999). "Direct observation of rotational transitions of the CO-CO dimer", *Journal of Chemical Physics* **111**, 5754-5756.

[75] M.C. Brookes and A.R.W. McKellar (1999). "Infrared spectrum and energy levels of the CO dimer: evidence for two almost isoenergetic isomers", *Journal of Chemical Physics* **111**, 7321-7328.

[76] K.A. Walker and A.R.W. McKellar (2001). "Millimeter-wave spectra of the CO dimer: observation and assignment of 20 new transitions", *Journal of Molecular Spectroscopy* **208**, 209-212.

[77] M.C. Salazar, J.L. Paz and A.J. Hernández (1999). "Ab initio basis set study of the CO$\cdots$He van der Waals interaction", *Journal of Molecular Structure (Theochem)* **493**, 133-137.

[78] M.C. Salazar, J.L. Paz, A.J. Hernández and H.F. Castejón (2001). "Test study on the excitation spectra of the CO-He van der Waals molecule", *Journal of Molecular Structure (Theochem)* **539**, 119-126.

[79] M.C. Salazar and A.J. Hernández, private communication, 2002.

[80] M.C. Salazar and A.J. Hernández, unpublished results, June 2002. These are the results of ab initio calculations of the potential energy curves (as function of the van der Waals bond length) for the $CO(X^1\Sigma^+)-Ar(X^1S)$ ground as well as $CO(A^1\Pi)-Ar(X^1S)$ excited state of CO-Ar in a supermolecular approach using the Hartree-Fock energy as reference state and Møller-Plesset perturbation theory to the second order of approximation to calculate the interaction energy.

[81] M.C. Salazar and A.J. Hernández, unpublished results, March 2003. These results are potential energy curves (as function of the van der Waals bond length) of the $CO(X^1\Sigma^+)-Ar(X^1S)$ ground state and $CO(A^1\Pi)-Ar(X^1S)$ excited state of CO-Ar obtained by ab initio calculations. Coupled cluster theory with iterative treatment of single and double excitations and non-iterative treatment of triple excitations (the CCSD(T) method) has been used to calculate the interaction energies.

[82] A. Kantrowitz and J. Grey (1951). "A High Intensity for the Molecular Beam. Part I. Theoretical", *The Review of Scientific Instruments* **22**, 328-332.

[83] H. Stafast and J.R Huber (1984). "Kalte Moleküle und schmalbandige Laser", *Chimia* **38**, 1-8.

[84] K.L. Saenger and J.B. Fenn (1983). "On the time required to reach fully developed flow in pulsed supersonic free jets", *Journal of Chemical Physics* **79**, 6043-6045.

[85] R.E. Smalley, L. Wharton and D.H. Levy (1977). "Molecular Optical Spectroscopy with Supersonic Beams and Jets", *Accounts of Chemical Research* **10**, 139-145.

[86] J.B. Anderson and J.B. Fenn (1965). "Velocity distributions in molecular beams from nozzle sources", *The Physics of Fluids* **8**, 780-787.

[87] H. Ashkenas and F.S. Sherman (1966). "Experimental methods in rarefied gas dynamics". In J.H. de Leeuw (Ed.), *Advances in Applied Mechanics - Rarefied Gas Dynamics Supplement 3, Vol II*, pp. 84-105, Academic Press, New York.

[88] "Thermodynamische Eigenschaften von Gasen, Dämpfen, Flüssigkeiten und festen Stoffen" (1967). In H. Borchers, H. Hausen, K.-H. Hellwege, K.L. Schäfer and E. Schmidt (Eds.), *Landolt-Börnstein Zahlenwerte und Functionen aus Physik, Chemie, Astronomie, Geophysik, Technik*, 6th edition, Volume IV, Part 4a, Springer-Verlag, Berlin.

[89] Airliquide homepage (21 May 2003). Address www.airliquide.com/en/business/products/gases/gasdata/index.asp

[90] J.B. Anderson, R.P. Andres and J.B. Fenn (1965). "Supersonic nozzle beams". In D.R. Bates and I. Estermann (Eds.), *Advances in Atomic and Molecular Physics*, pp. 275-317, Academic Press, New York.

[91] R.E. Smalley, L. Wharton and D.H. Levy (1975). "The fluorescence excitation spectrum of rotationally cooled NO_2", *Journal of Chemical Physics* **63**, 4977-4989.

[92] F.M. Behlen and S.A. Rice (1981). "Intersystem crossing in cold isolated molecules of naphtalene", *Journal of Chemical Physics* **75**, 5672-5684.

[93] O.F. Hagena (1974). "Cluster Beams from Nozzle Sources". In P.P. Wegener (Ed.), *Molecular Beams and Low Density Gasdynamics*, p. 93-181, Marcel Dekker Inc., New York.

[94] J.B. Anderson and R.P. Andres (1966). "Studies of low density supersonic jets". In J.H. de Leeuw (Ed.), *Advances in Applied Mechanics - Rarefied Gas Dynamics Supplement 3, Vol II*, pp. 106-127, Academic Press, New York.

[95] C.R. Vidal (1987). "Four-wave frequency mixing in gases". In L.F. Molenauer and J.C. White (Eds.), *Topics in Applied Physics* **59** - "Tunable lasers", pp. 57-113, Springer Verlag, Heidelberg.

[96] W. Ubachs, K.S.E. Eikema and W. Hogervorst (1993). "Narrow-band extreme-ultraviolet laser radiation tunable in the range 90.5 – 95 nm", *Applied Physics B* **57**, 411-416.

[97] S.C. Wallace and G. Zdasiuk (1976). "High-efficiency four-wave sum mixing in magnesium at 140 nm", *Applied Physics Letters* **28**, 449-451.

[98] T.J. McKee, B.P. Stoicheff and S.C. Wallace (1978). "Tunable, coherent radiation in the Lyman-α region (1210-1290 Å) using magnesium vapor", *Optics Letters* **3**, 207-208.

[99] K. Yamanouchi and S. Tsuchiaya (1995). "Tunable vacuum ultraviolet laser spectroscopy: excited state dynamics of jet-cooled molecules and van der Waals complexes", *Journal of Physics B: Atomic Molecular and Optical Physics* **28**, 133-165.

[100] H. Junginger, H.B. Puell, H. Scheingraber and C.R. Vidal (1980). "Resonant third-harmonic generation in a low-loss medium", *IEEE Journal of Quantum Electronics* **QE-16**, 1132-1137.

[101] D.C. Hanna, M.A. Yuratich and D. Cotter (1979). "*Nonlinear Optics of Free Atoms and Molecules*", Chapters 1-4, Springer Verlag, Heidelberg.

[102] C.M. Steinmann (1999). "*Development and characterisation of a tunable laser source in the vacuum ultraviolet*", M.Sc. thesis, University of Stellenbosch, Stellenbosch, South Africa.

[103] H. Scheingraber and C.R. Vidal (1981). "Heat pipe oven of well-defined column density", *Review of Scientific Instruments* **52**, 1010-1012.

[104] B. Steffes, X. Li, A. Mellinger and C.R. Vidal (1996). "Heat pipe oven for large column densities with a well-defined optical path length", *Applied Physics B* **62**, 87-90.

[105] D.H. Levy (1980). "Laser spectroscopy of cold gas-phase molecules", *Annual Reviews of Physical Chemistry* **31**, 197-225.

[106] W. Demtröder (1996). "*Laser Spectroscopy. Basic Concepts and Instrumentation*", Second Enlarged Edition, Springer Verlag, Berlin.

[107] W.R. Gentry and C.F. Giese (1978) "Ten-microsecond pulsed molecular beam source and a fast ionization detector", *Review of Scientific Instruments* **49**, 595-600.

[108] H.J. Heger (1999). "*On-line Spurenanalytik aromatischer Verbindungen aus komplexen Proben: Entwicklung und Feldanwendung eines Lasermassenspektrometers für Untersuchungen am Rauchgas von Abfallverbrennungsanlagen*", Ph.D. dissertation, Technische Universität München, München, Germany.

[109] J.E.M. Goldsmith and J.E. Lawler (1981). "Optogalvanic Spectroscopy", *Contemporary Physics* **22**, 235-248.

[110] S.H. Ashworth and J.M. Brown (1991). "*An Atlas of Optogalvanic Transitions in Neon*", Rutherford Appleton Laboratory, Report RAL-91-069, Chilton DIDCOT Oxon OX11 0QX, United Kingdom of Britain.

[111] H. Bitto, I.-C. Chen and C.B. Moore (1986). "Rotational state distribution of CO photofragments from triplet ketene", *Journal of Chemical Physics* **85**, 5101-5106.

[112] F.J. Lovas and P.H. Krupenie (1974). "Microwave spectra of molecules of astrophysical interest VII. Carbon monoxide, carbon monosulphide, and silicon monoxide", *Journal of Physical and Chemical Reference Data* **3**, 245-257.

[113] R.E. Smalley, L. Wharton and D.H. Levy (1976). "The fluorescence excitation spectrum of the HeI_2 van der Waals complex", *Journal of Chemical Physics* **64**, 3266-3276.

[114] S.G. Kukolich, D.E. Oates and J.G.S. Wang (1974). "Rotational energy distribution in a nozzle beam", *Journal of Chemical Physics* **61**, 4686-4689.

[115] K.P. Huber and T.J. Sears (1985). "Emission spectra in a supersonic expansion: the quartet system of NO and the Schüler band of ND_4", *Chemical Physics Letters* **113**, 129-134.

[116] K.P. Huber and M. Vervloet (1992). "High-resolution Fourier transform spectroscopy of supersonic jets: The $C''^5\Pi_{ui} \longrightarrow A'^5\Sigma_g^+$ Herman infrared bands of $^{14}N_2$", *Journal of Molecular Spectroscopy* **153**, 17-25.

[117] C.M. Steinmann, E.G. Rohwer and H. Stafast (2003). "Accurate laboratory wavelengths of the vacuum ultraviolet $A(v' = 3) - X(v'' = 0)$ band of $^{12}C^{17}O$ and $^{12}C^{18}O$", *The Astrophysical Journal* **590**, L123-L126. Erratum: *The Astrophysical Journal* **591**, L167.

[118] A. Rohrbacher, N. Halberstadt and K.C. Janda (2000). "The dynamics of noble gas-halogen molecules and clusters", *Annual Review of Physical Chemistry* **51**, 405-433.

[119] A. Burroughs and M.C. Heaven (2001). "Dissociation dynamics of $I_2(B)$-Ar: Rotational population distributions of $I_2(B, v)$ fragments from the T-shaped and linear complexes", *Journal of Chemical Physics* **114**, 7027-7035.

[120] O. Roncero, B. Lepetit, J.A. Beswick, N. Halberstadt and A.A. Buchachenko (2001). "$ArI_2(X) \longrightarrow Ar+I_2(B)$ photodissociation: Comparison between linear and T-shaped isomers dynamics", *Journal of Chemical Physics* **115**, 6961-6973.

[121] M.L. Burke and W. Klemperer (1993). "The one-atom cage effect: continuum processes in I_2-Ar below the B-state dissociation limit", *Journal of Chemical Physics* **98**, 1797-1809.

[122] W. Klemperer, C.-C. Chuang, K.J. Higgins, A.E. Stevens Miller and H.C. Fu (2001). "Spectroscopy of van der Waals molecules: Isomers and vibrational predissociation", *Canadian Journal of Physics* **79**, 101-108.

[123] G.E. Ewing (1979). "A guide to the lifetimes of vibrationally excited van der Waals molecules: The momentum gap", *Journal of Chemical Physics* **71**, 3143-3144.

[124] G. Kubiak, P.S.H. Fitch, L. Wharton and D.H. Levy (1978). "The fluorescence excitation spectrum of the ArI_2 van der Waals complex", *Journal of Chemical Physics* **68**, 4477-4480.

[125] A.E. Stevens Miller, C.-C. Chuang, H.C. Fu, K.J. Higgins and W. Klemperer (1999). "Dynamics of linear and T-shaped Ar-I_2 dissociation upon $B \longleftarrow X$ optical excitation: A dispersed fluorescence sutdy of the linear isomer", *Journal of Chemical Physics* **111**, 7844-7856.

[126] T. Sykora (1999). "*Zeemaneffektstudie an Interkombinationsbanden sowie rotationsselektive Messung metastabiler Lebensdauern im CO-Molekül*", Ph.D. thesis, Technische Universität München, München, Germany.

[127] Y.R. Shen (1984). "*The Principles of Nonlinear Optics*", Chapter 14. John Wiley and Sons, New York.

[128] C.R. Vidal (1980). "Coherent VUV sources for high resolution spectroscopy", *Applied Optics* **19**, 3897-3903.

[129] A.T. Georges, P. Lambropoulos and J.H. Marburger (1977). "Theory of third-harmonic generation in metal vapors under two-photon resonance conditions", *Physical Review A* **15**, 300-307.

[130] H. Puell and C.R. Vidal (1976). "Nonlinear polarisations and excitations and their time dependence in discrete multilevel systems", *Physical Review A* **14**, 2225-2239.

[131] H. Puell, H. Scheingraber and C.R. Vidal (1980). "Saturation of resonant third-harmonic generation in phase-matched systems", *Physical Review A* **22**, 1165-1178.

[132] J.J. Sakurai (1995). In S.F. Tuan (Ed.), *Modern Quantum Mechanics*, Chapter 3. Addison-Wesley Publishing Company, Reading, Massachusetts.

[133] H. Puell, K. Spanner, W. Falkenstein, W. Kaiser and C.R. Vidal (1976). "Third-harmonic generation of mode-locked Nd:glass laser pulses in phase-matched Rb-Xe mixtures", *Physical Review A* **14**, 2240-2257.

[134] F. Mühlberger, R. Zimmermann and A. Kettrup (2001). "A mobile mass spectrometer for comprehensive on-line analysis of trace and bulk components of complex gas mixtures: parallel application of the laser-based ionization methods vuv single-photon ionization, resonant multiphoton ionization, and laser-induced electron impact ionization", *Analytical Chemistry* **73**, 3590-3604.